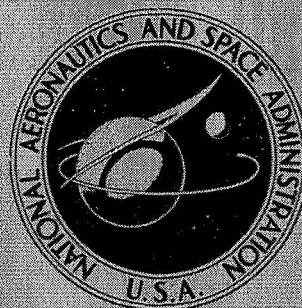


N71-36426

NASA TECHNICAL  
MEMORANDUM



NASA TM X-2325

NASA TM X-2325

CASE FILE  
COPY



SUBSONIC CHARACTERISTICS OF  
A TWIN-JET SWEEP-WING FIGHTER MODEL  
WITH LEADING-EDGE KRUEGER FLAPS

by

*Julian G. Carmichael, Jr.*

*McDonnell Douglas Corporation*

*St. Louis, Mo. 63166*

*and*

*Edward J. Ray*

*Langley Research Center*

*Hampton, Va. 23365*

1. Report No. NASA TM X-2325	2. Government Accession No.	3. Recipient's Catalog No.	
4. Title and Subtitle SUBSONIC CHARACTERISTICS OF A TWIN-JET SWEEP-WING FIGHTER MODEL WITH LEADING-EDGE KRUEGER FLAPS		5. Report Date October 1971	6. Performing Organization Code
		8. Performing Organization Report No. L-7804	10. Work Unit No. 136-63-02-37
7. Author(s) Julian G. Carmichael, Jr. (McDonnell Douglas Corporation) and Edward J. Ray (Langley Research Center)		11. Contract or Grant No.	
		13. Type of Report and Period Covered Technical Memorandum	
9. Performing Organization Name and Address  NASA Langley Research Center Hampton, Va. 23365		14. Sponsoring Agency Code	
		12. Sponsoring Agency Name and Address  National Aeronautics and Space Administration Washington, D.C. 20546	
15. Supplementary Notes			
16. Abstract  An investigation has been conducted at Mach numbers of 0.60 and 0.90 to determine the effects of various combinations of leading-edge Krueger flaps, inboard plain flaps, and outboard slats on the static aerodynamic characteristics of a twin-jet, swept-wing fighter-airplane model. The angle-of-attack range was varied from $-2^{\circ}$ to $24^{\circ}$ and the angle-of-sideslip range was varied from about $4^{\circ}$ to $-15^{\circ}$ . The results of the investigation indicated that the addition of Krueger flaps caused significant improvements in maximum lift coefficient and in drag coefficient at high lift coefficients.			
17. Key Words (Suggested by Author(s))  Leading-edge flaps Twin-jet swept-wing fighter airplane High subsonic Krueger application		18. Distribution Statement  Unclassified - Unlimited	
19. Security Classif. (of this report) Unclassified	20. Security Classif. (of this page) Unclassified	21. No. of Pages 69	22. Price* \$3.00

# SUBSONIC CHARACTERISTICS OF A TWIN-JET SWEEP-WING FIGHTER MODEL WITH LEADING-EDGE KRUEGER FLAPS

By Julian G. Carmichael, Jr.  
McDonnell Douglas Corporation  
and  
Edward J. Ray  
Langley Research Center

## SUMMARY

An investigation has been conducted in the Langley high-speed 7- by 10-foot tunnel to assess the static aerodynamic characteristics of a 5-percent-scale twin-jet swept-wing fighter configuration with leading-edge Krueger flaps at Mach numbers of 0.60 and 0.90 with particular regard to improved maneuvering. The longitudinal aerodynamic characteristics were determined for various deflections of leading-edge Krueger flaps and several combinations of Krueger flaps, outboard slats, and inboard plain flaps.

The results of the investigation indicated that the addition of Krueger flaps caused significant improvements in maximum lift coefficient and in drag coefficient at high lift coefficients. Generally, the Krueger flap configurations reduced the static longitudinal stability. Several combinations of leading-edge slats with Krueger flaps brought about similar improvements in maximum lift coefficient and in the drag coefficient at high lift but with a lesser reduction in longitudinal stability.

## INTRODUCTION

Recent aerodynamic research has been conducted on a twin-jet swept-wing fighter configuration to investigate wing leading-edge devices for improving transonic maneuverability. Previous McDonnell Douglas and NASA investigations have shown that the installation of wing leading-edge slats significantly improves the transonic trimmed lift and drag characteristics of the airplane. The slats also improve the wind-tunnel-determined transonic buffet characteristics as discussed in reference 1. These improvements were substantiated in a flight-test investigation discussed in references 2 and 3.

Based on low-speed experience, Krueger flaps are generally more adaptable to thin wings than are leading-edge slats. Accordingly, an investigation was made in the Langley high-speed 7- by 10-foot tunnel to investigate the effectiveness of the Krueger flap as a

maneuvering device. The aerodynamic characteristics of several Krueger flap and flap-slat configurations were determined. Tests were made through a range of angle of attack from  $-2^{\circ}$  to  $24^{\circ}$  and through a range of angle of sideslip from  $4^{\circ}$  to  $-15^{\circ}$  at angles of attack of approximately  $0^{\circ}$ ,  $4^{\circ}$ ,  $12^{\circ}$ , and  $18^{\circ}$ . The various configurations were tested at Mach numbers of 0.60 and 0.90.

## SYMBOLS AND ABBREVIATIONS

All the data contained herein are referred to the stability-axis system, with the exception of the  $C_{n\beta, \text{dyn}}$  derivatives and the axial-force coefficient  $C_A$  which are referred to the body-axis system. Reference dimensions used in the reduction of these data are indicated in this section. The moment reference point was at 33-percent wing mean aerodynamic chord. (See fig. 1.)

Measurements and calculations were made in the U.S. Customary Units. They are presented herein in the International System of Units (SI) with the equivalent values given parenthetically in the U.S. Customary Units.

b wing reference span, 58.522 centimeters (23.04 inches)

c local chord of airfoil section

$\bar{c}$  mean aerodynamic chord of wing, 24.445 centimeters (9.624 inches)

c.g. assumed center of gravity

$C_A$  axial-force coefficient,  $\frac{\text{Axial force}}{qS}$

$C_D$  drag coefficient,  $\frac{\text{Drag}}{qS}$

$C_L$  lift coefficient,  $\frac{\text{Lift}}{qS}$

$C_{L\alpha}$  lift-curve slope per degree,  $\frac{\partial C_L}{\partial \alpha}$

$C_l$  rolling-moment coefficient,  $\frac{\text{Rolling moment}}{qSb}$

$C_{l\beta}$  rolling moment due to sideslip per degree,  $\frac{\partial C_l}{\partial \beta}$

$C_m$  pitching-moment coefficient,  $\frac{\text{Pitching moment}}{qS\bar{c}}$

$C_{m_{CL}}$	static margin, $\frac{\partial C_m}{\partial C_L}$
$C_n$	yawing-moment coefficient, $\frac{\text{Yawing moment}}{qSb}$
$C_{n\beta}$	yawing moment due to sideslip per degree, $\frac{\partial C_n}{\partial \beta}$
$C_{n\beta, \text{dyn}}$	dynamic directional-stability parameter per degree, $\left( \frac{\partial C_n}{\partial \beta} - \frac{I_Z}{I_X} \frac{\partial C_l}{\partial \beta} \tan \alpha \right) \cos \alpha$
$C_Y$	side-force coefficient, $\frac{\text{Side force}}{qS}$
F.S.	fuselage station, centimeters (inches)
$i_t$	horizontal-tail incidence, degrees (positive with leading edge up)
$I_X$	rolling moment of inertia, 34 984.8 kg-m <sup>2</sup> (25 800 slug-ft <sup>2</sup> )
$I_Z$	yawing moment of inertia, 204 213.6 kg-m <sup>2</sup> (150 600 slug-ft <sup>2</sup> )
L/D	lift-to-drag ratio
$(L/D)_{\text{MAX}}$	maximum lift-to-drag ratio
L.E.	leading edge
M	Mach number
q	dynamic pressure, newtons/meter <sup>2</sup> (pounds/foot <sup>2</sup> )
R	Reynolds number
S	wing reference area including body intercept, 1231.0 centimeters <sup>2</sup> (190.8 inches <sup>2</sup> )
W.S.	wing station, centimeters (inches)
$\alpha$	wing angle of attack, degrees
$\beta$	angle of sideslip, degrees
$\delta$	flap or slat deflection

### Model designations:

Basic	basic model
$F_{K_2}$	inboard leading-edge Krueger flap
$F_{K_3}$	midboard leading-edge Krueger flap
$F_{K_4}$	outboard leading-edge Krueger flap
$F_N$	inboard leading-edge plain flap
$S_{17}$	outboard leading-edge slat

### MODEL

Drawings of the complete model and of the various model components are shown in figures 1 and 2, respectively, and photographs of the model are presented in figure 3. The model which was studied represented a twin-jet swept-wing fighter airplane having a discontinuous wing leading edge. It employed an all-movable horizontal tail (stabilator) which incorporated  $23.25^\circ$  negative dihedral. Most of the tests were made with a stabilator incidence angle of  $0^\circ$ ; however, a limited study was made with a negative deflection of  $8^\circ$  to indicate longitudinal trim effects. The wing had  $0^\circ$  dihedral inboard of the discontinuity and  $12^\circ$  dihedral outboard of the discontinuity.

All of the leading-edge devices were attached by means of fixed brackets. The Krueger flaps varied in deflection from  $20^\circ$  to  $70^\circ$ . The fixed inboard leading-edge flaps were formed so that there was no gap between the flap and the fuselage. For the outboard leading-edge slats there was a converging gap between the slat and wing. (See fig. 2(c).)

### TESTS AND CORRECTIONS

The investigation was conducted in the Langley high-speed 7- by 10-foot tunnel which is a continuous-flow facility. The unit Reynolds number (based on the average temperature) and dynamic pressure at each of the test Mach numbers are shown in the following table:

M	R per meter	R per foot	q, kN/m <sup>2</sup>	q, lb/ft <sup>2</sup>
0.60	$10.92 \times 10^6$	$3.33 \times 10^6$	20	422
.90	12.79	3.90	34	715

Boundary-layer transition was effected by applying strips of No. 100 carborundum grit 1.3 mm (0.05 inch) wide at the following positions:

- (1) 19 mm (0.75 inch) behind the fuselage nose
- (2) 6.3 mm (0.25 inch) behind the inlet duct lip
- (3) 5-percent chord (both surfaces) of horizontal and vertical tails
- (4) 40-percent chord (both surfaces) of wing without Krueger flaps or slats

No transition strip was used on the wing when the Krueger flaps or slats were employed since two comparison tests showed the effect of the strips to be negligible.

Aerodynamic forces and moments were measured by means of a sting-supported six-component strain-gage balance housed within the model fuselage. The angles of attack shown herein have been corrected for the combined bending of the sting and balance system due to aerodynamic loading. Balance cavity pressures were monitored throughout the investigation by means of differential pressure gages, and axial-force and drag-coefficient data have been adjusted to correspond to a condition of free-stream static pressure at the base of the model. No corrections were made to the base drag or internal drag through the simulated engine nacelles. Jet-boundary and blockage corrections were applied to the results as prescribed in references 4 and 5.

## PRESENTATION OF RESULTS

The results of the investigation are presented in the following figures:

<u>Longitudinal characteristics</u>	<u>Figure</u>
Basic configuration:	
M = 0.60 . . . . .	4
M = 0.90 . . . . .	5
Effect of deflecting the $F_{K_3} F_{K_4}$ Krueger flaps:	
M = 0.60 . . . . .	6
M = 0.90 . . . . .	7
Effect of deflecting the $F_{K_3} F_{K_4}$ Krueger flaps with $\delta F_{K_2} = 30^\circ$ :	
M = 0.60 . . . . .	8
M = 0.90 . . . . .	9
Effect of deflecting the $F_{K_3} F_{K_4}$ Krueger flaps with $\delta F_N = 15^\circ$ :	
M = 0.60 . . . . .	10
M = 0.90 . . . . .	11
Effect of deflecting the $F_{K_3}$ Krueger flaps with $S_{17}$ extended:	
M = 0.60 . . . . .	12
M = 0.90 . . . . .	13

<u>Longitudinal characteristics</u>	<u>Figure</u>
Effect of deflecting the $F_{K_3}$ Krueger flaps with $S_{17}$ extended and $\delta F_N = 15^\circ$ :	
$M = 0.60$ . . . . .	14
$M = 0.90$ . . . . .	15
Effect of horizontal-tail incidence with $\delta F_{K_3}, \delta F_{K_4} = 20^\circ$ :	
$M = 0.60$ . . . . .	16
$M = 0.90$ . . . . .	17
Summary figure: Basic configuration and basic with $\delta F_{K_3}, \delta F_{K_4} = 20^\circ$ . . . . .	18
<u>Lateral-directional characteristics</u>	
Basic configuration . . . . .	19
Basic configuration with $\delta F_{K_3}, \delta F_{K_4} = 20^\circ$ . . . . .	20
Summary figure: Basic configuration and basic with $\delta F_{K_3}, \delta F_{K_4} = 20^\circ$ . . . . .	21

## DISCUSSION

### Longitudinal Stability Characteristics

In the present study emphasis was placed on Krueger flaps since they appeared to offer a relatively simple maneuvering device which might be incorporated within the confines of thin wings. The following discussion, therefore, is limited primarily to the characteristics determined with one of the more promising Krueger flap arrangements.

The effects of midboard and outboard Krueger devices on the static longitudinal characteristics of the basic configuration are shown in figure 6. Figure 6(a) shows that, at a Mach number of 0.60 with the Kruegers deflected to  $30^\circ$ , the maximum lift coefficient was increased from 0.94 to 1.02 and the addition of Krueger flaps reduced the axial-force coefficients  $C_A$  significantly at the higher angles of attack. This high-angle-of-attack axial-force reduction probably resulted from the fact that the Krueger flaps added sufficient camber to alleviate leading-edge separation, and, as a result, a portion of the leading-edge thrust was recovered. These large increases in leading-edge thrust are also evident in the drag and lift-to-drag results of figure 6(b). For instance, with the Krueger flaps deflected  $30^\circ$ , the drag level at a lift coefficient of 0.90 was reduced from 0.259 to 0.185, whereas the lift-to-drag ratio was increased from about 3.6 to 4.8. This type of behavior, as discussed in reference 6, usually suggests that the onset of buffet would be delayed to higher values of  $C_L$ .



The results in figure 6(c) show that adding the Krueger flaps increased the nose-down pitching moment near zero lift, and, although adding the Krueger flaps eliminated the "pitchup" that occurred at high lift, it reduced the level of static margin ( $\partial C_m / \partial C_L$ ) from 0.04 to 0.02. Adding either an inboard Krueger flap or plain flap (see figs. 8(c) and 10(c)) in combination with midboard and outboard Krueger flaps increased the Mach 0.60 high-lift stability level, but it caused an undesirable pitchup condition just below the angle of attack for stall. This pitchup was alleviated somewhat by using an outboard slat arrangement in combination with midboard Krueger flaps (fig. 12(c)) and was greatly improved by using a combination of outboard slat, midboard Krueger, and inboard plain flap (fig. 14(c)).

At  $M = 0.90$ , the results presented in figure 7(a) indicate that, as in the  $M = 0.60$  case, adding the midboard and outboard Krueger combination produced a favorable lift increment and large reductions in the axial-force coefficients at the higher angles of attack. The high lift, drag, and lift-to-drag ratios are noticeably improved by the addition of the Kruegers. (See fig. 7(b).) Again, there was a reduction in the longitudinal-stability level at high angles of attack. (See fig. 7(c).) A comparison of the pitching-moment results of figure 13(c) with those of figure 14(c) shows that, as in the  $M = 0.60$  case, deflecting the inboard plain flap (droop) in combination with the outboard slat and midboard Krueger arrangement reduced the "noseup" tendency at the higher lifts.

The results obtained at Mach numbers of 0.60 and 0.90 during the brief horizontal-control-effectiveness survey are shown in figures 16 and 17. These results indicate that the horizontal tail remained effective throughout the angle-of-attack range of the study for the basic configuration with outboard and midboard Krueger flaps. Detailed control studies were not made for the other leading-edge flap and slat configurations; however, some preliminary results obtained on the model of the present investigation indicated that within the present range of variables the type of leading-edge device would have very little effect on the horizontal-control effectiveness.

A summarized comparison of several longitudinal parameters which indicate the effects of a typical Krueger flap addition is presented in figure 18. The comparisons were made at higher angles of attack to indicate the flap effect in a maneuver situation. These summary results again show the beneficial effects on the drag and lift characteristics at the higher angles of attack. These improvements would enhance the maximum instantaneous and sustained load-factor capabilities of the aircraft. It is recognized that these results do not represent "trimmed" characteristics; however, a review of the  $C_m / C_L$  plot in figure 18 and of the pitch characteristics included in figures 6(c) and 7(c) indicates that, due to the reduction in stability level produced by the flap addition, there would be no adverse flap trim increments at these higher lift coefficients.

## Lateral-Directional Characteristics

The variations of static lateral-directional force and moment coefficients with angle of sideslip are shown for the basic configuration and for a representative Krueger configuration in figures 19 and 20, respectively. The variations were generally linear over the low-to-moderate sideslip range. However, the results in figure 19(b) show a marked non-linearity in the rolling-moment variation at an angle of attack of  $12^\circ$ . This behavior is not fully understood, but previous wind-tunnel studies on this configuration have indicated similar trends and it is believed that this effect could be associated with flow breakdown at the Reynolds number of the present study about the sharp, discontinuous leading edge of the wing. It will be noted from figure 20(b) that adding the outboard and midboard Krueger flaps reduced the nonlinearity at  $\alpha = 12^\circ$ .

A summary of the lateral-directional stability derivatives of the basic and selected Krueger configurations is presented in figure 21. At a Mach number of 0.60 (fig. 21(a)), the addition of the Krueger flaps increased the positive effective dihedral  $-C_{l_\beta}$  and directional-stability parameter  $C_{n_\beta}$  at the high angles of attack at both  $0^\circ$  and  $5^\circ$  sideslip. These combined improvements are reflected in a significant increase in the  $C_{n_\beta}$  dynamic derivative at angles of attack above  $14^\circ$ . At a Mach number of 0.90 the differences in the sideslip characteristics between the basic and Krueger flap configurations were not as pronounced as in the Mach 0.60 case.

## CONCLUDING REMARKS

An investigation has been conducted in the Langley high-speed 7- by 10-foot tunnel to determine the static aerodynamic characteristics of a 5-percent-scale twin-jet swept-wing fighter configuration with the addition of various combinations of leading-edge Krueger flaps, inboard plain flaps, and outboard slats. The incorporation of Krueger flaps increases the maximum usable lift coefficients and reduces the drag at high lift coefficients. These improvements would enhance the maximum instantaneous and sustained load-factor capabilities of the airplane. The results also indicate that, assuming a constant center-of-gravity location, the addition of Krueger flaps increases the nose-down pitching moment near zero lift and decreases the level of static longitudinal stability. In addition, the results suggest that the high-angle-of-attack lateral-directional handling qualities would be improved with the use of leading-edge Krueger flaps.

Langley Research Center,

National Aeronautics and Space Administration,  
Hampton, Va., July 23, 1971.

## REFERENCES

1. Ray, Edward J.: Techniques for Determining Buffet Onset. NASA TM X-2103, 1970.
2. Hollingsworth, E. G.; and Cohen, M.: Comparison of Wind Tunnel and Flight Test Techniques for Determining Transonic Buffet Characteristics on the McDonnell Douglas F-4 Airplane. AIAA Paper No. 70-584, May 1970.
3. Sullivan, D. A.; Curtis, E. R.; Raley, F. C.; Gentry, J. R.; McElroy, C. E.; Rutan, E. L.; and Crane, R. C.: Military Evaluation of the F-4 Wing Leading Edge Slats. NATC Tech. Rep. FT-119R-69, U.S. Navy, Oct. 15, 1969.
4. Gillis, Clarence L.; Polhamus, Edward C.; and Gray, Joseph L., Jr.: Charts for Determining Jet-Boundary Corrections for Complete Models in 7- by 10-Foot Closed Rectangular Wing Tunnels. NACA WR L-123, 1945.
5. Herriot, John G.: Blockage Corrections for Three-Dimensional-Flow Closed-Throat Wind Tunnels, With Consideration of the Effect of Compressibility. NACA Rep. 995, 1950. (Supersedes NACA RM A7B28.)
6. Ray, Edward J.; and Taylor, Robert T.: Buffet and Static Aerodynamic Characteristics of a Systematic Series of Wings Determined From a Subsonic Wind-Tunnel Study. NASA TN D-5805, 1970.

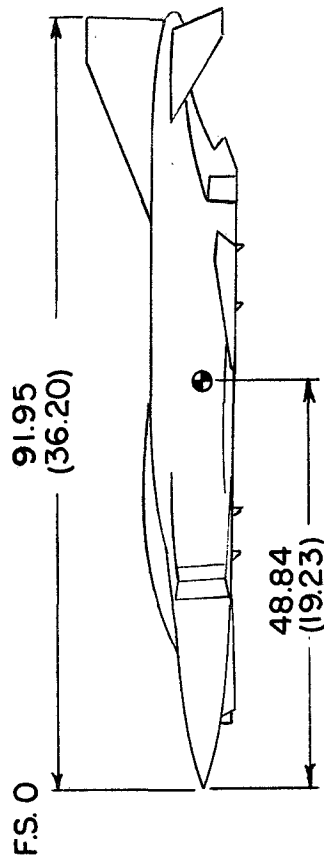
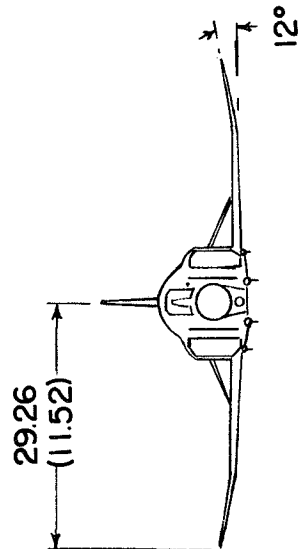
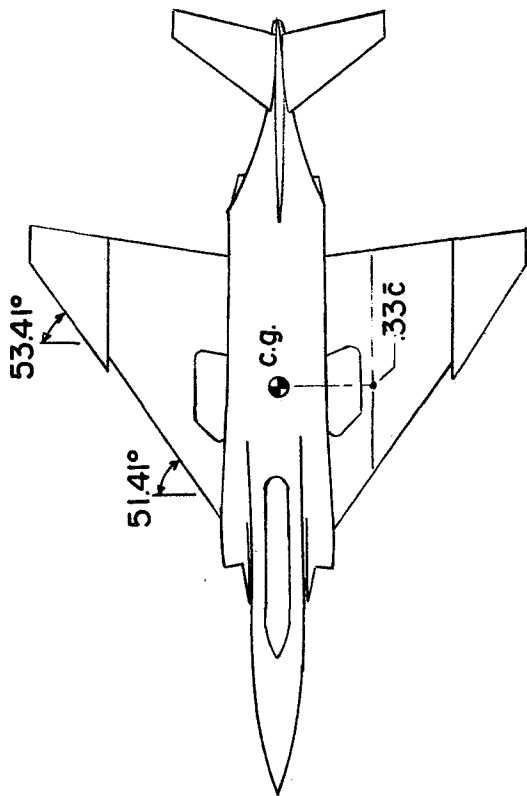
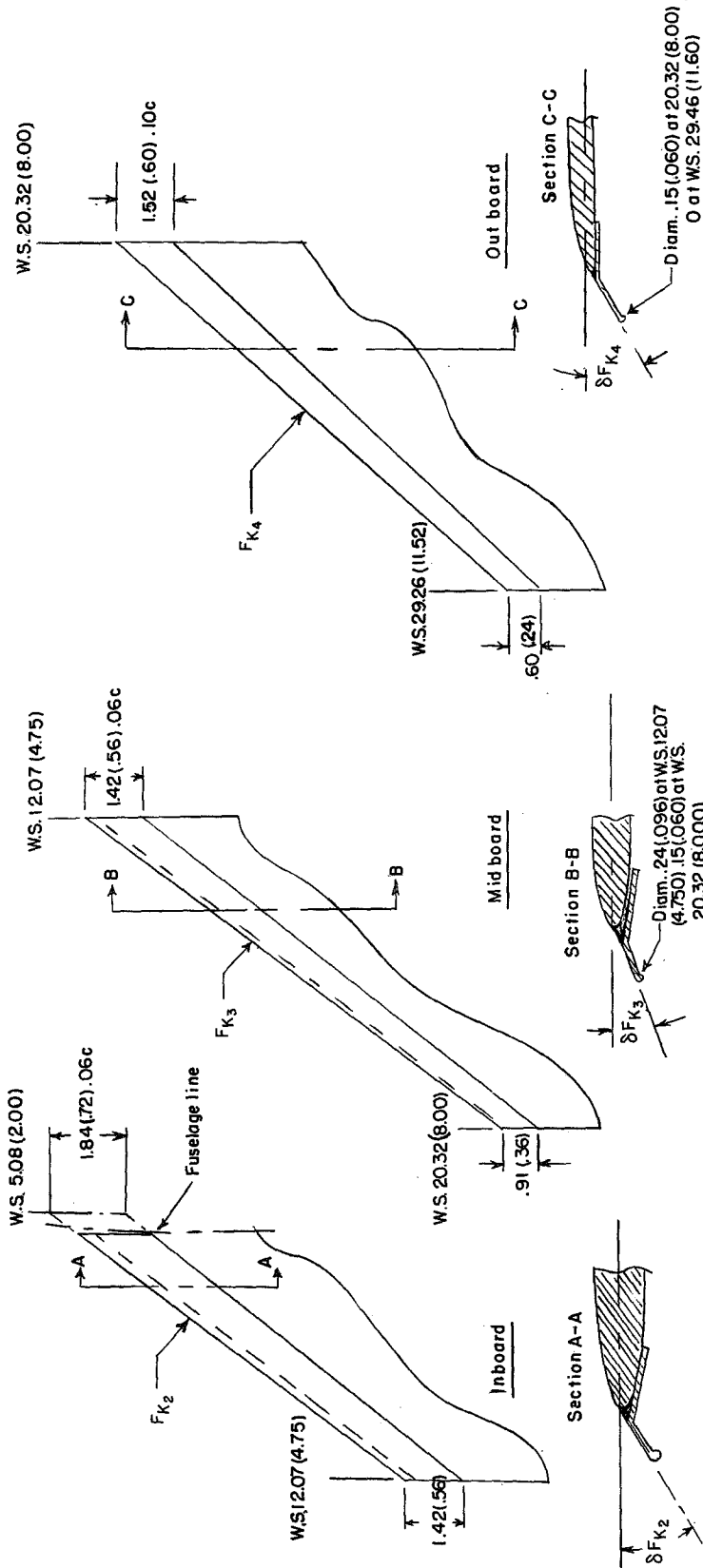
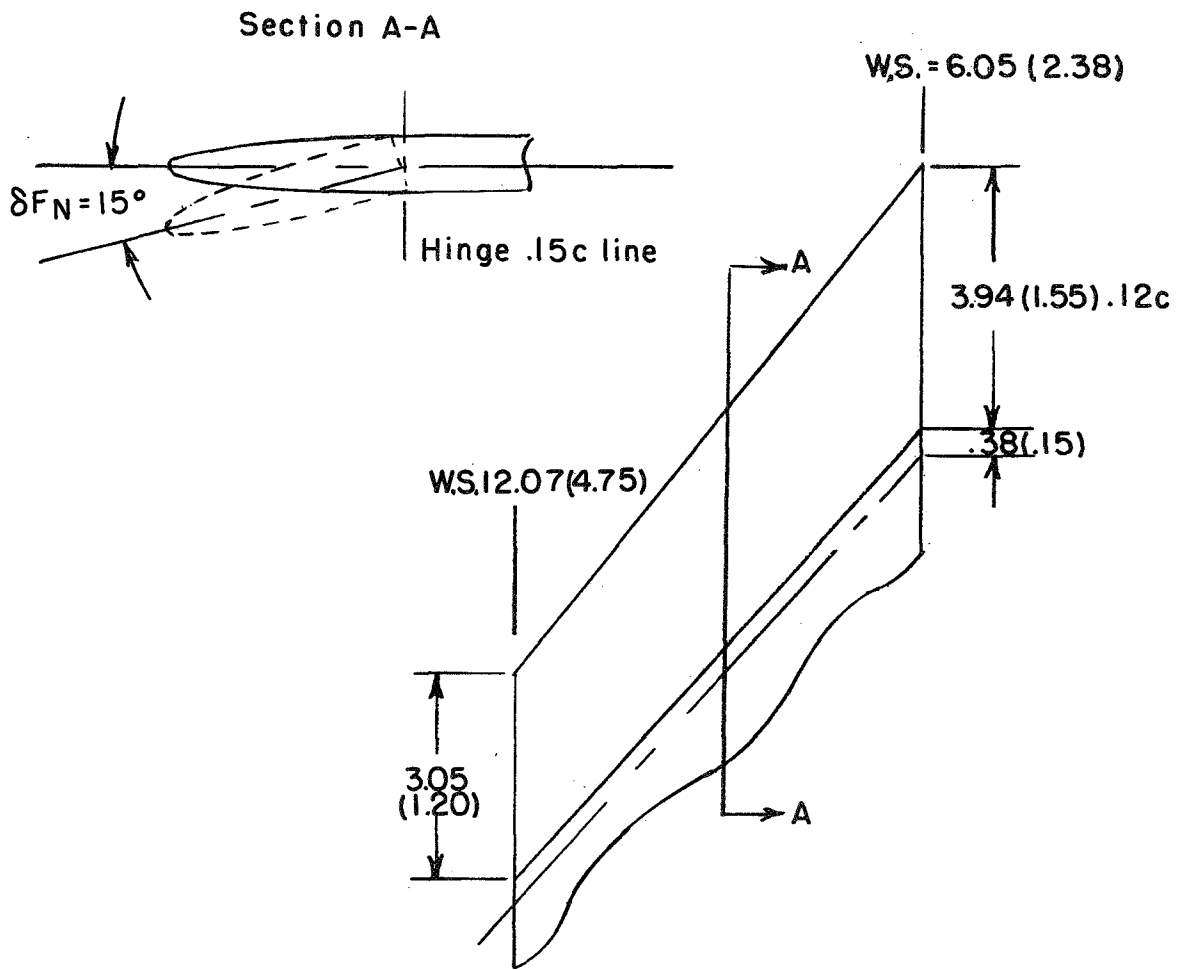


Figure 1.- Three-view sketch of basic model. All linear dimensions are given in centimeters (inches).



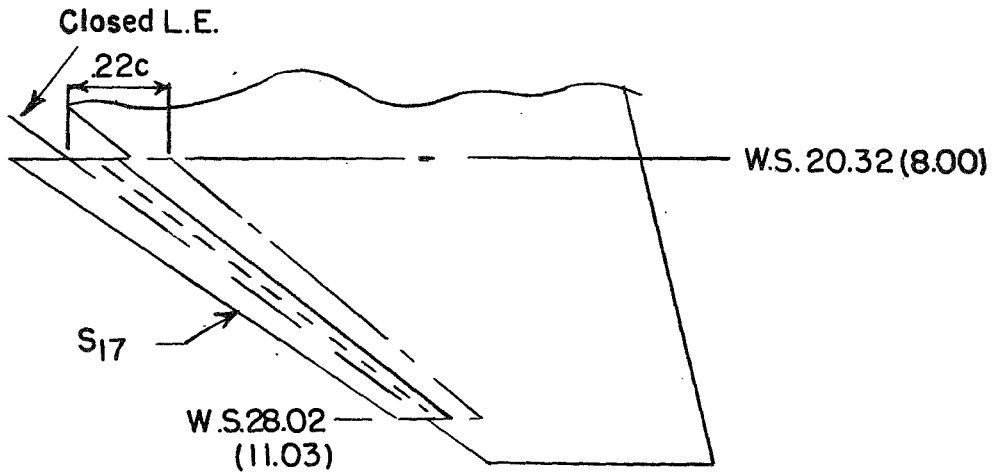
(a) Krueger flaps.

Figure 2.- Details of wing leading-edge devices. All linear dimensions are given in centimeters (inches).

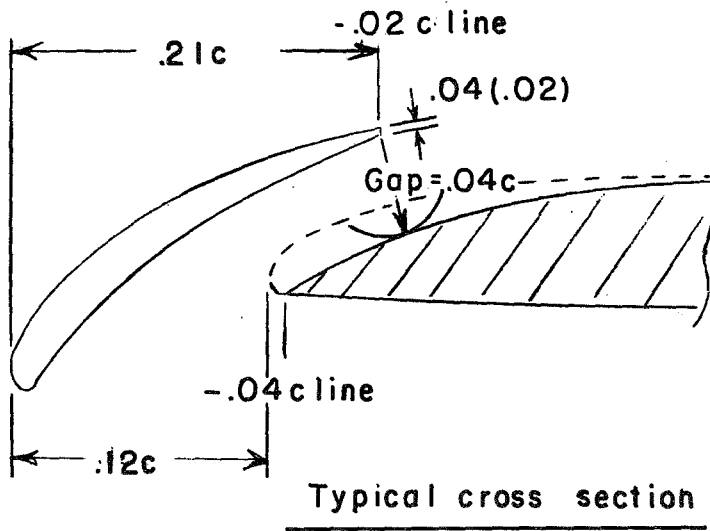


(b) Inboard leading-edge flap.

Figure 2.- Continued.



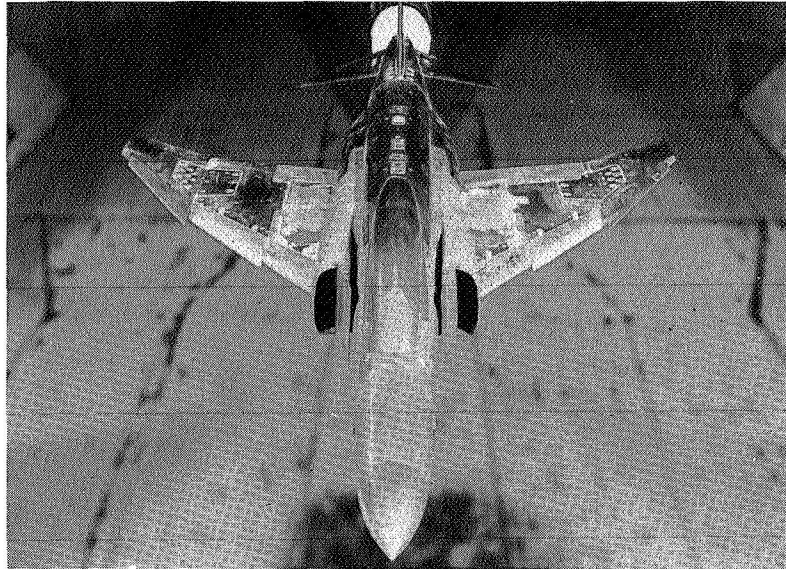
Planform view of outer panel



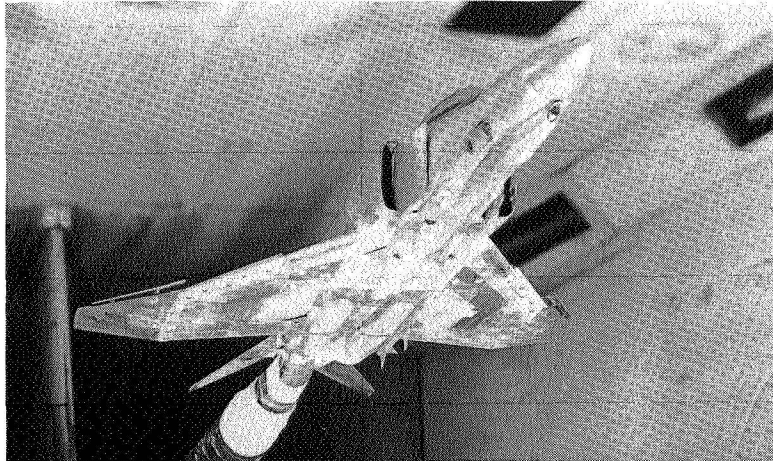
Typical cross section

(c) Outboard leading-edge slat.

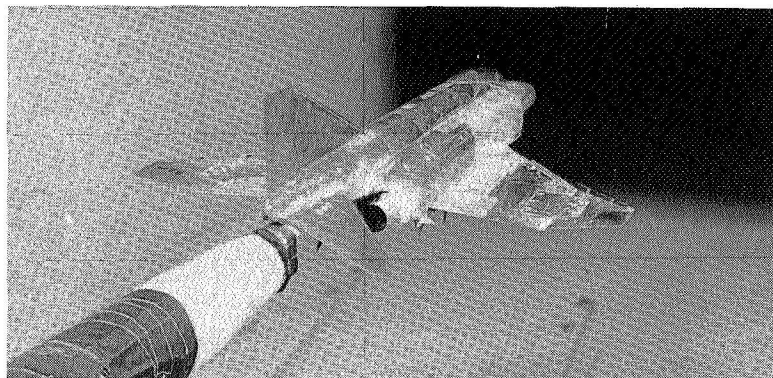
Figure 2.- Concluded.



(a) Top front view.



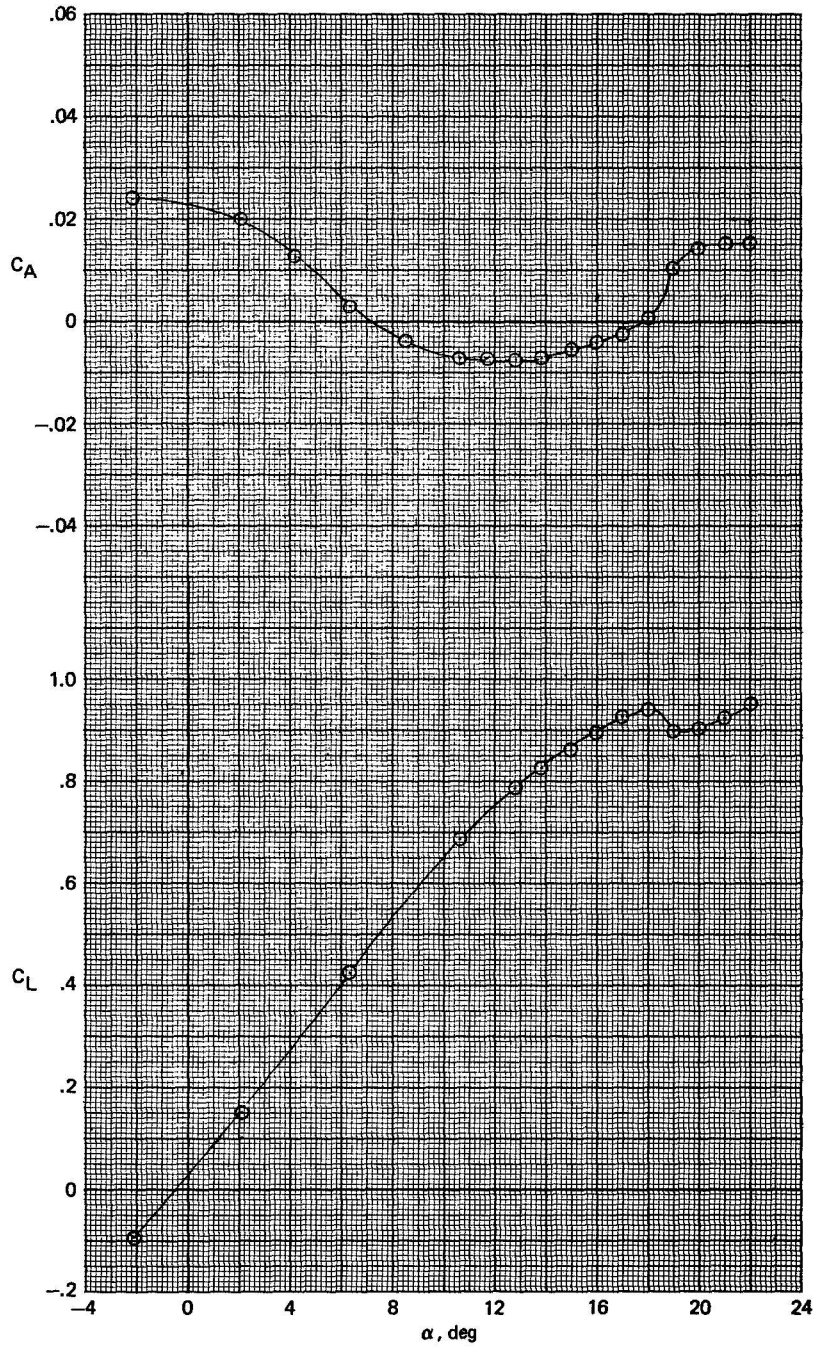
(b) Three-quarter front view.



(c) Three-quarter rear view.

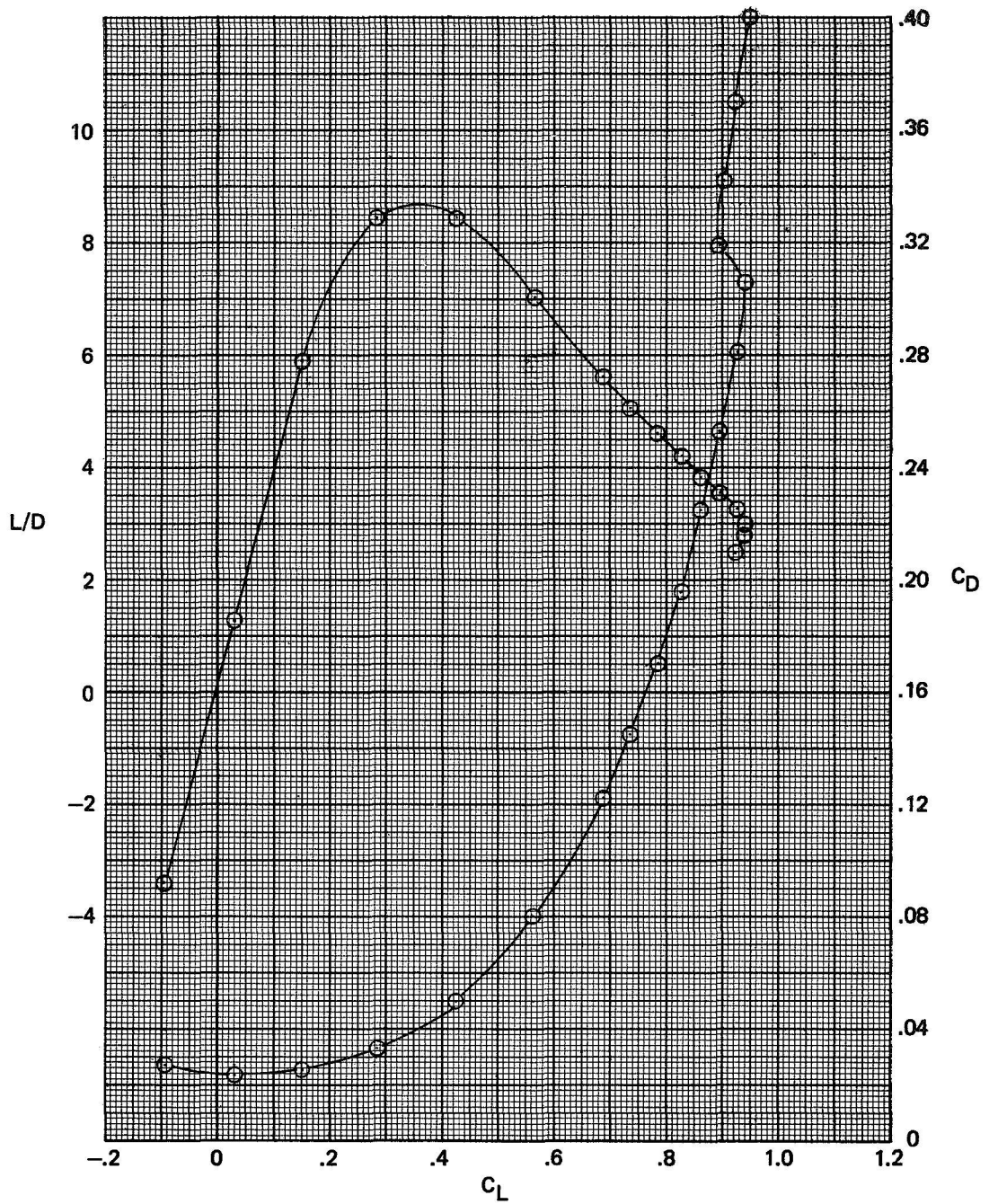
Figure 3.- Photographs of the 5-percent-scale twin-jet swept-wing fighter model installed in the Langley high-speed 7- by 10-foot tunnel. L-71-699





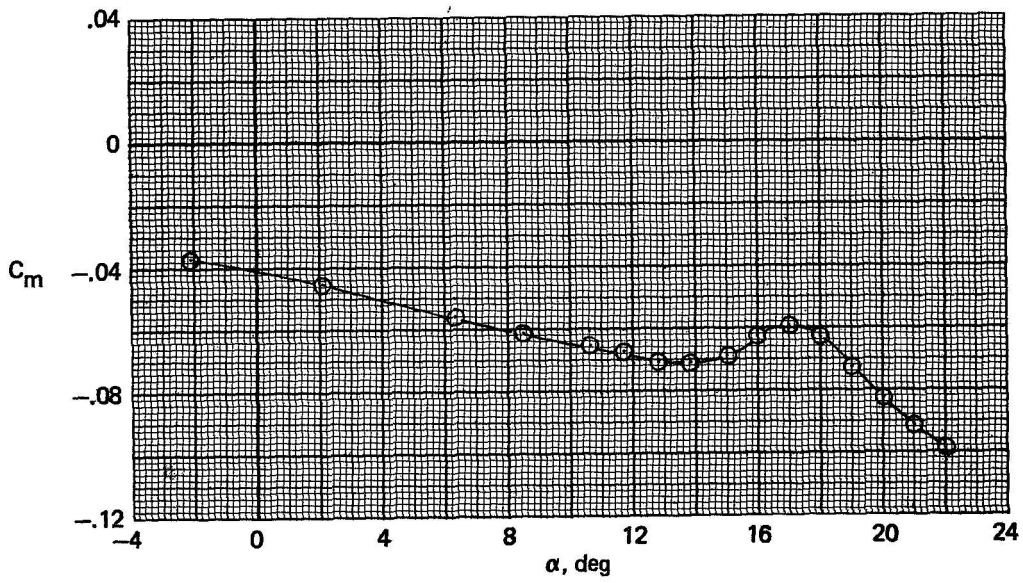
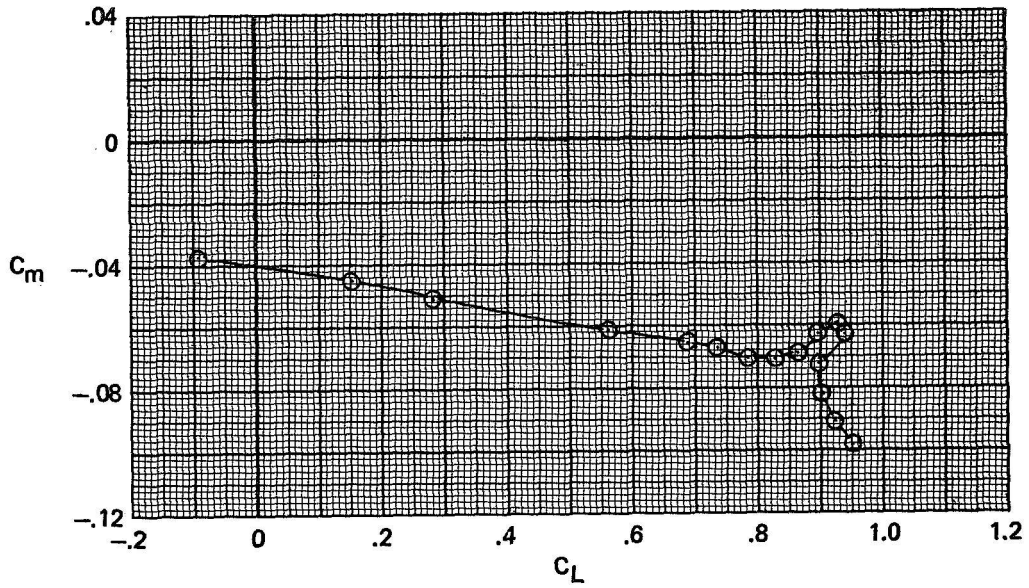
(a)  $C_A$  and  $C_L$  plotted against  $\alpha$ .

Figure 4.- Longitudinal characteristics of the basic configuration.  $M = 0.60$ .



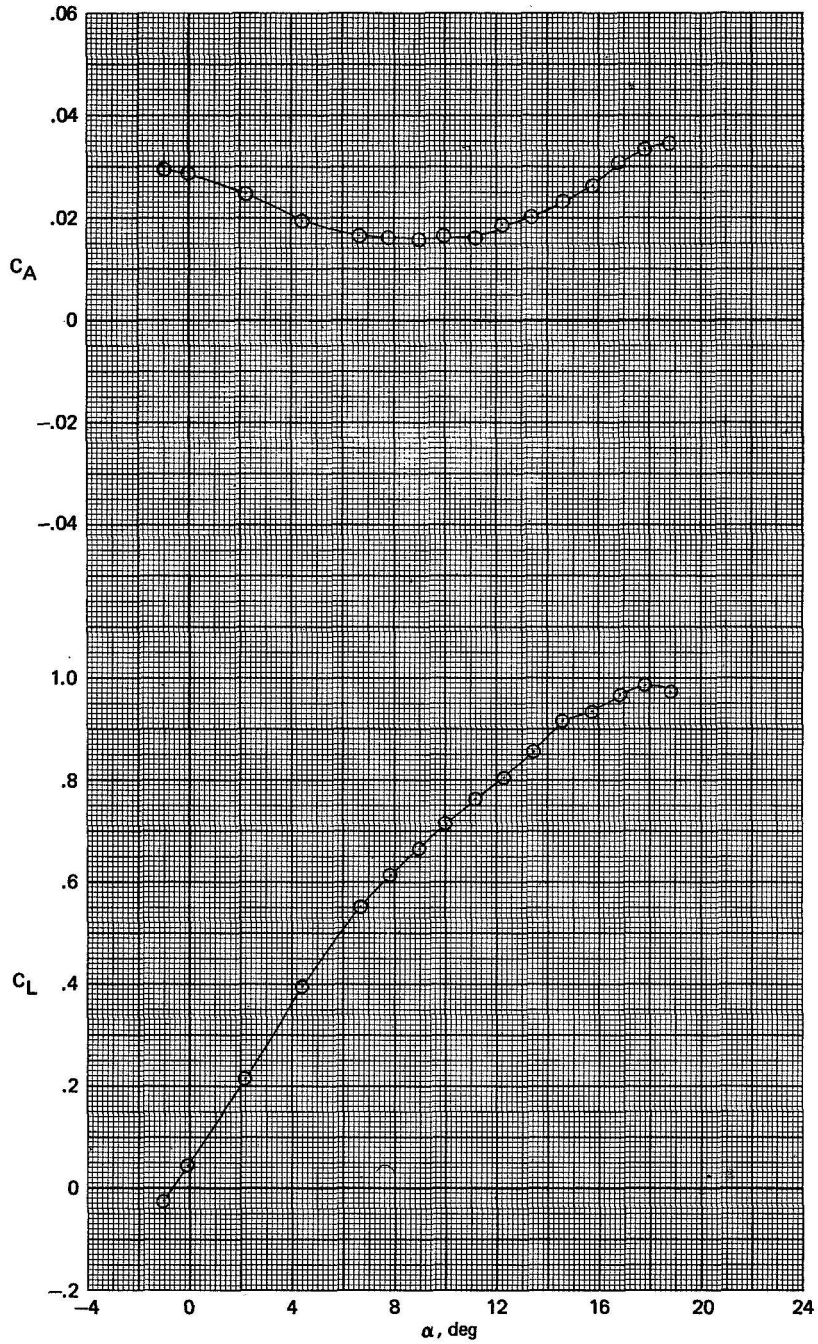
(b)  $L/D$  and  $C_D$  plotted against  $C_L$ .

Figure 4.- Continued.



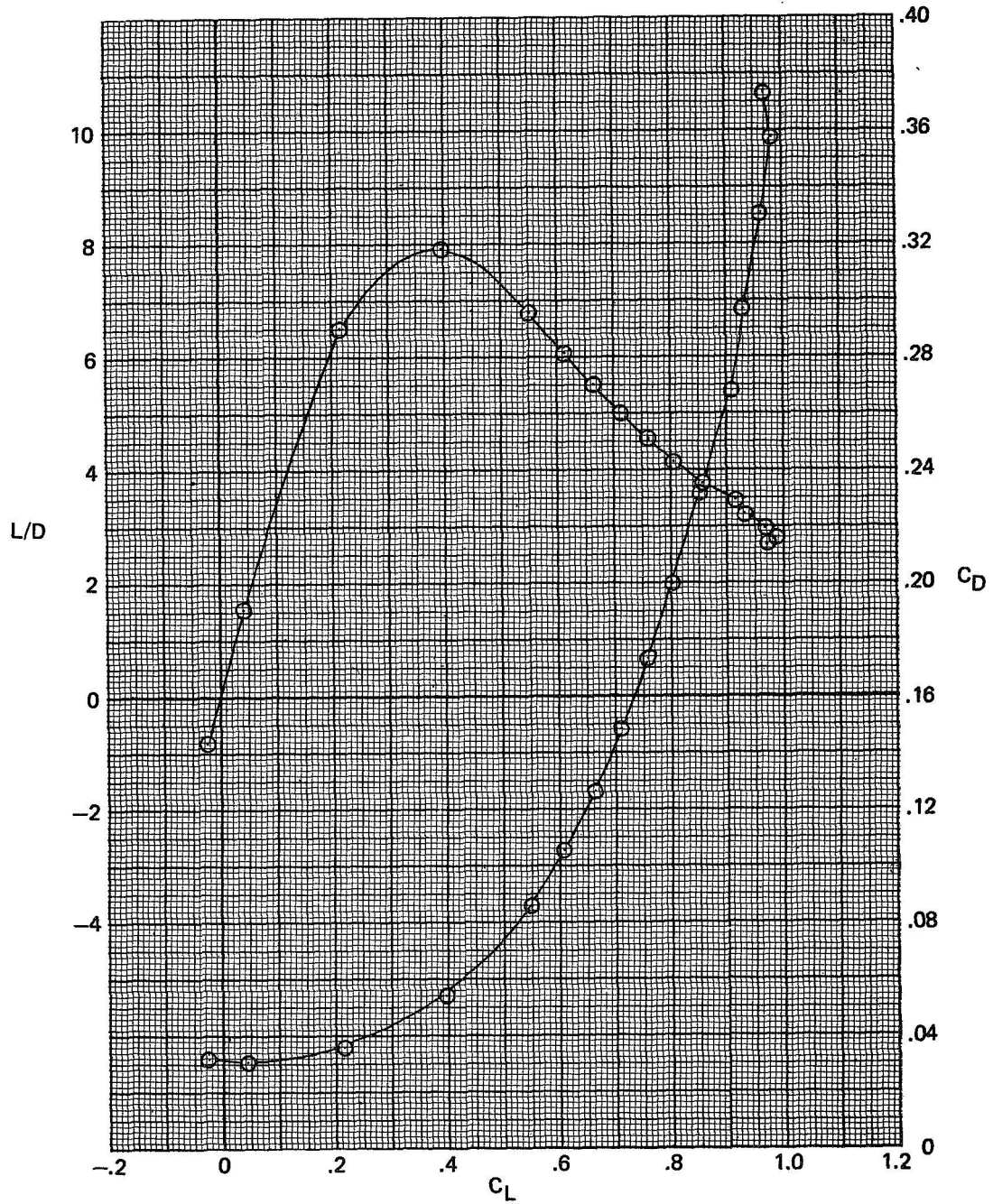
(c)  $C_m$  plotted against  $C_L$  and  $\alpha$ .

Figure 4.- Concluded.



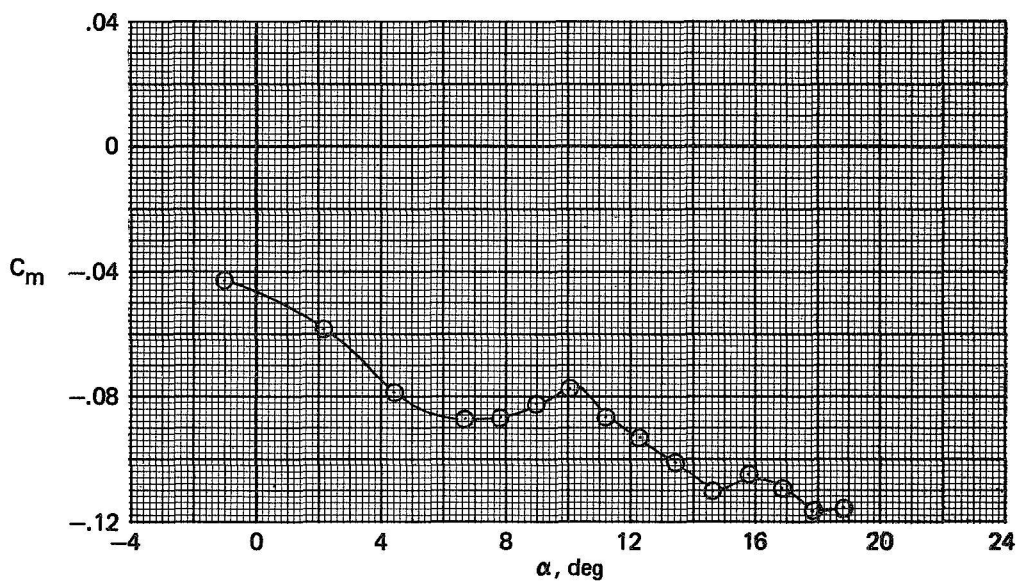
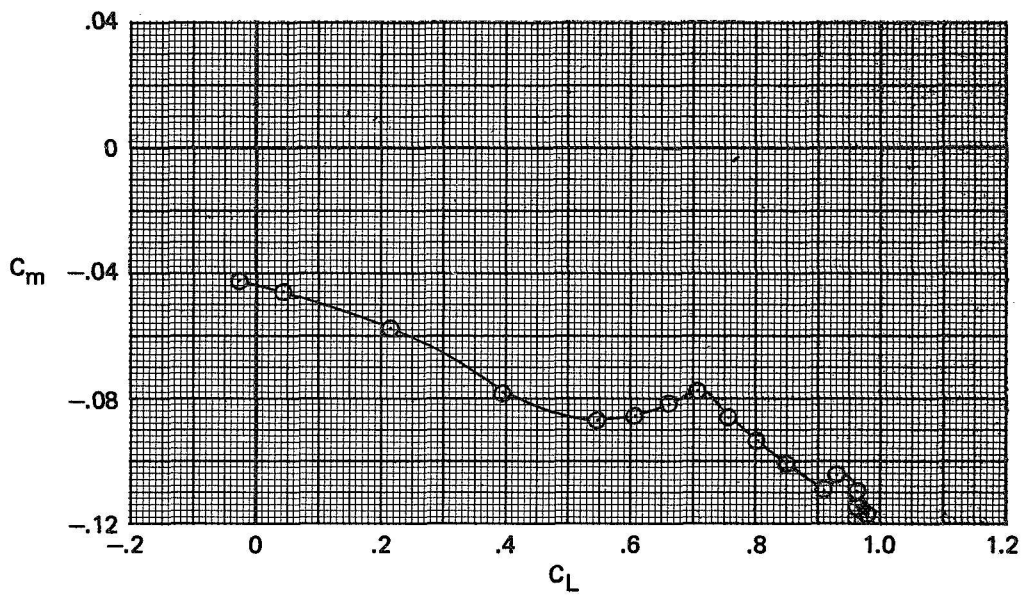
(a)  $C_A$  and  $C_L$  plotted against  $\alpha$ .

Figure 5.- Longitudinal characteristics of the basic configuration.  $M = 0.90$ .



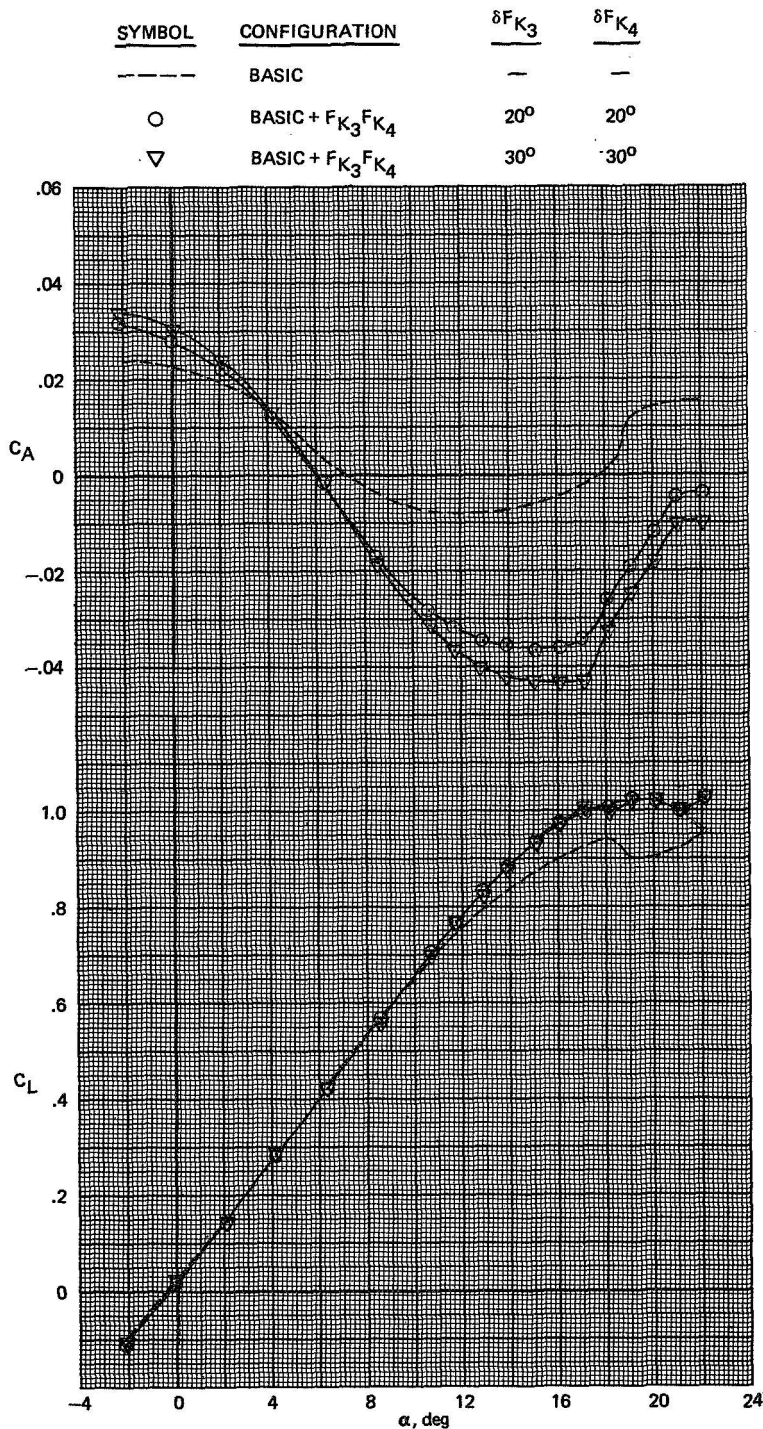
(b)  $L/D$  and  $C_D$  plotted against  $C_L$ .

Figure 5.- Continued.



(c)  $C_m$  plotted against  $C_L$  and  $\alpha$ .

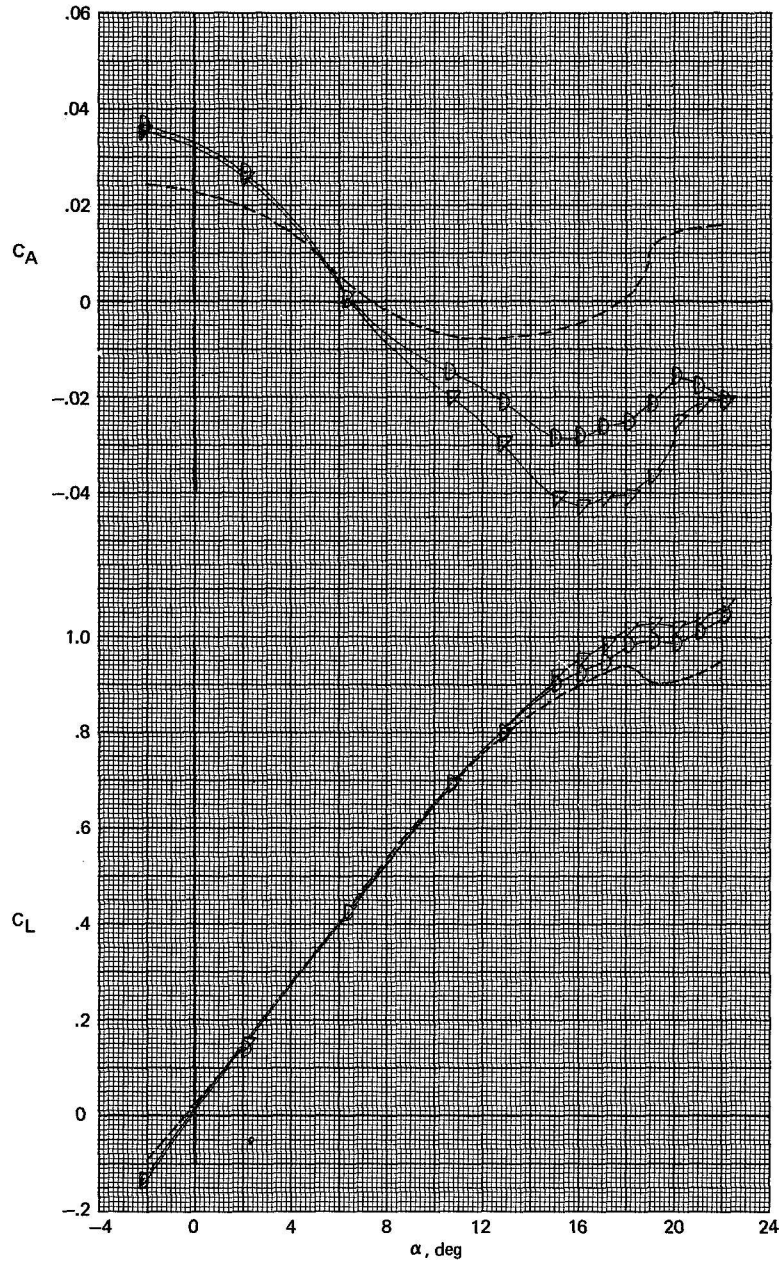
Figure 5.- Concluded.



(a)  $C_A$  and  $C_L$  plotted against  $\alpha$ .

Figure 6.- Effect of deflecting the  $F_{K_3}F_{K_4}$  Krueger flaps on the basic configuration incorporating the  $F_{K_3}F_{K_4}$  leading-edge devices.  $M = 0.60$ .

<u>SYMBOL</u>	<u>CONFIGURATION</u>	$\delta F_{K_3}$	$\delta F_{K_4}$
-----	BASIC	—	—
▽	BASIC + $F_{K_3} F_{K_4}$	50°	50°
D	BASIC + $F_{K_3} F_{K_4}$	70°	70°

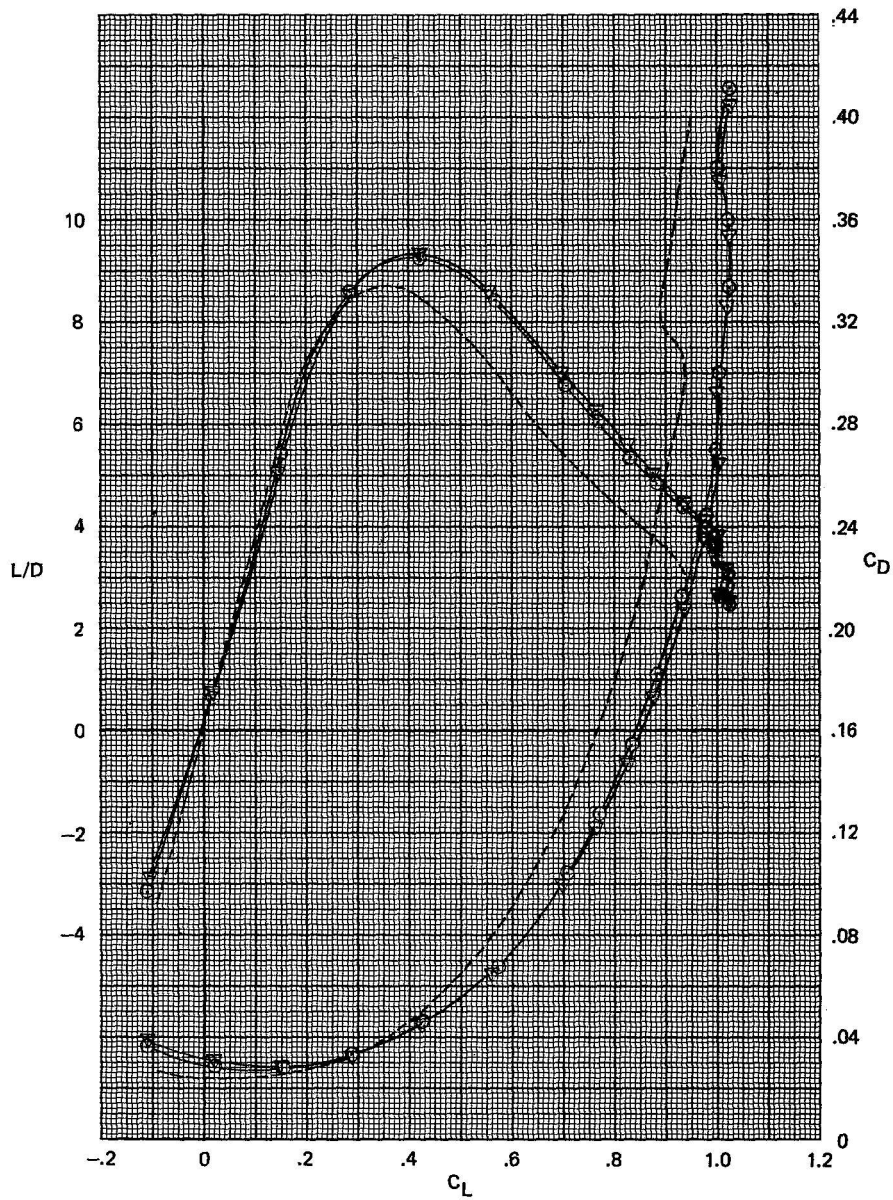


(a) Concluded.

Figure 6.- Continued.



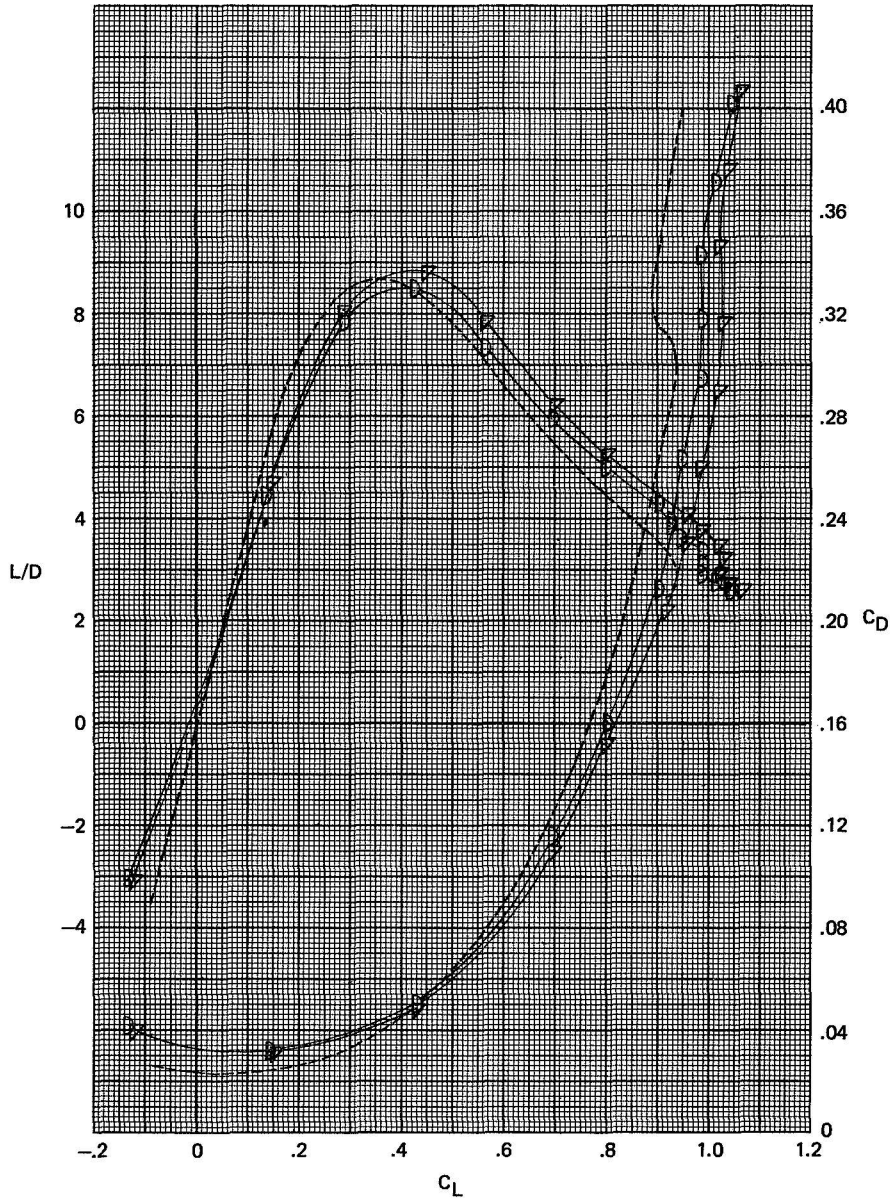
<u>SYMBOL</u>	<u>CONFIGURATION</u>	$\frac{\delta F_{K_3}}{\delta F_{K_4}}$	$\frac{\delta F_{K_4}}{\delta F_{K_3}}$
---	BASIC	—	—
○	BASIC + $F_{K_3} F_{K_4}$	20°	20°
▽	BASIC + $F_{K_3} F_{K_4}$	30°	30°



(b)  $L/D$  and  $C_D$  plotted against  $C_L$ .

Figure 6.- Continued.

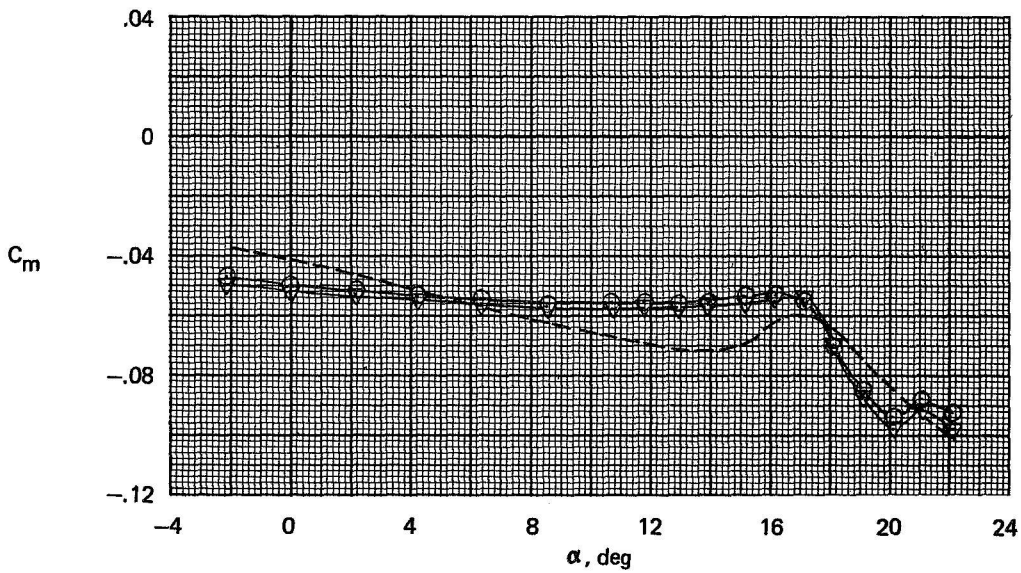
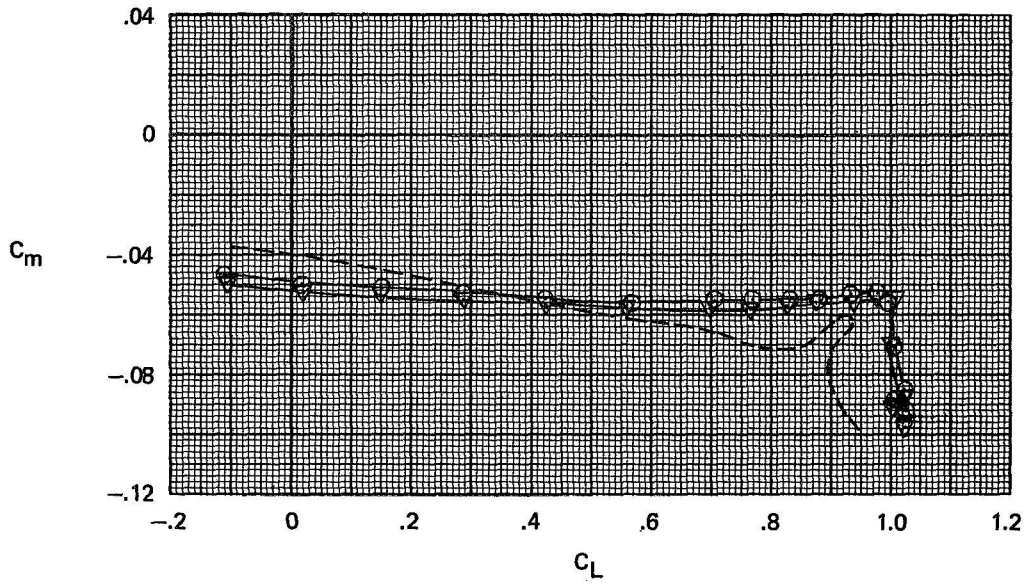
<u>SYMBOL</u>	<u>CONFIGURATION</u>	$\delta F_{K_3}$	$\delta F_{K_4}$
-----	BASIC	—	—
▽	BASIC + $F_{K_3} F_{K_4}$	50°	50°
D	BASIC + $F_{K_3} F_{K_4}$	70°	70°



(b) Concluded.

Figure 6.- Continued.

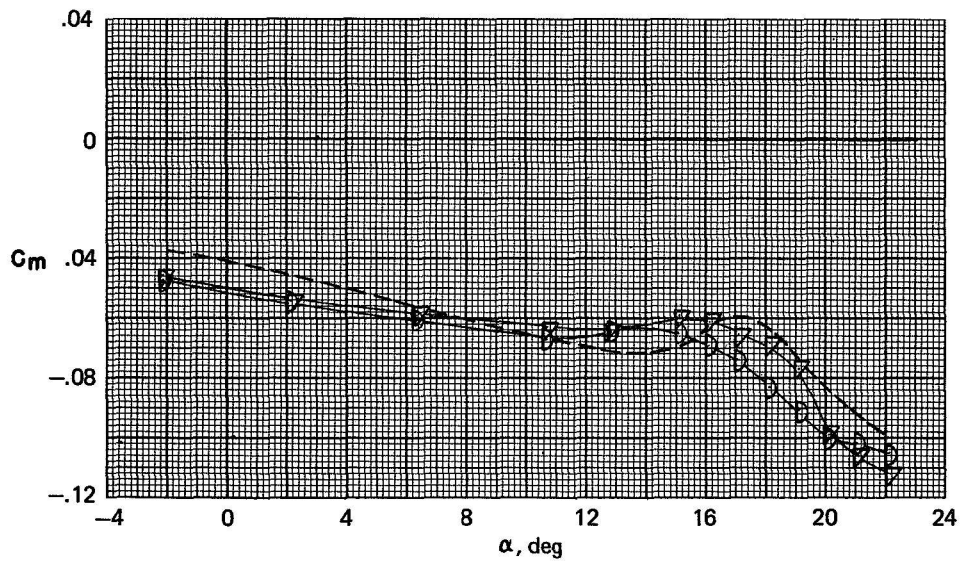
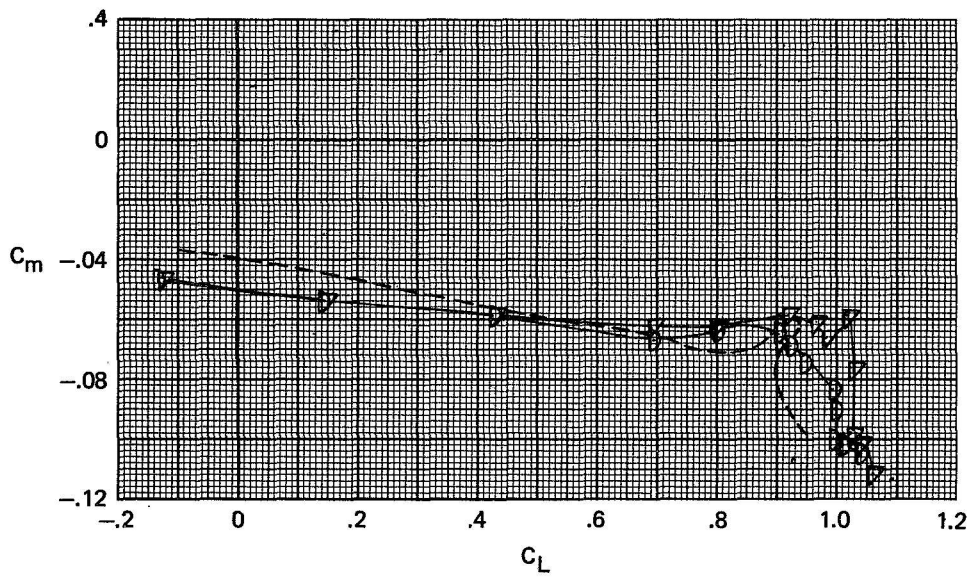
<u>SYMBOL</u>	<u>CONFIGURATION</u>	<u><math>\delta F_{K_3}</math></u>	<u><math>\delta F_{K_4}</math></u>
---	BASIC	—	—
○	BASIC + $F_{K_3} F_{K_4}$	20°	20°
▽	BASIC + $F_{K_3} F_{K_4}$	30°	30°



(c)  $C_m$  plotted against  $C_L$  and  $\alpha$ .

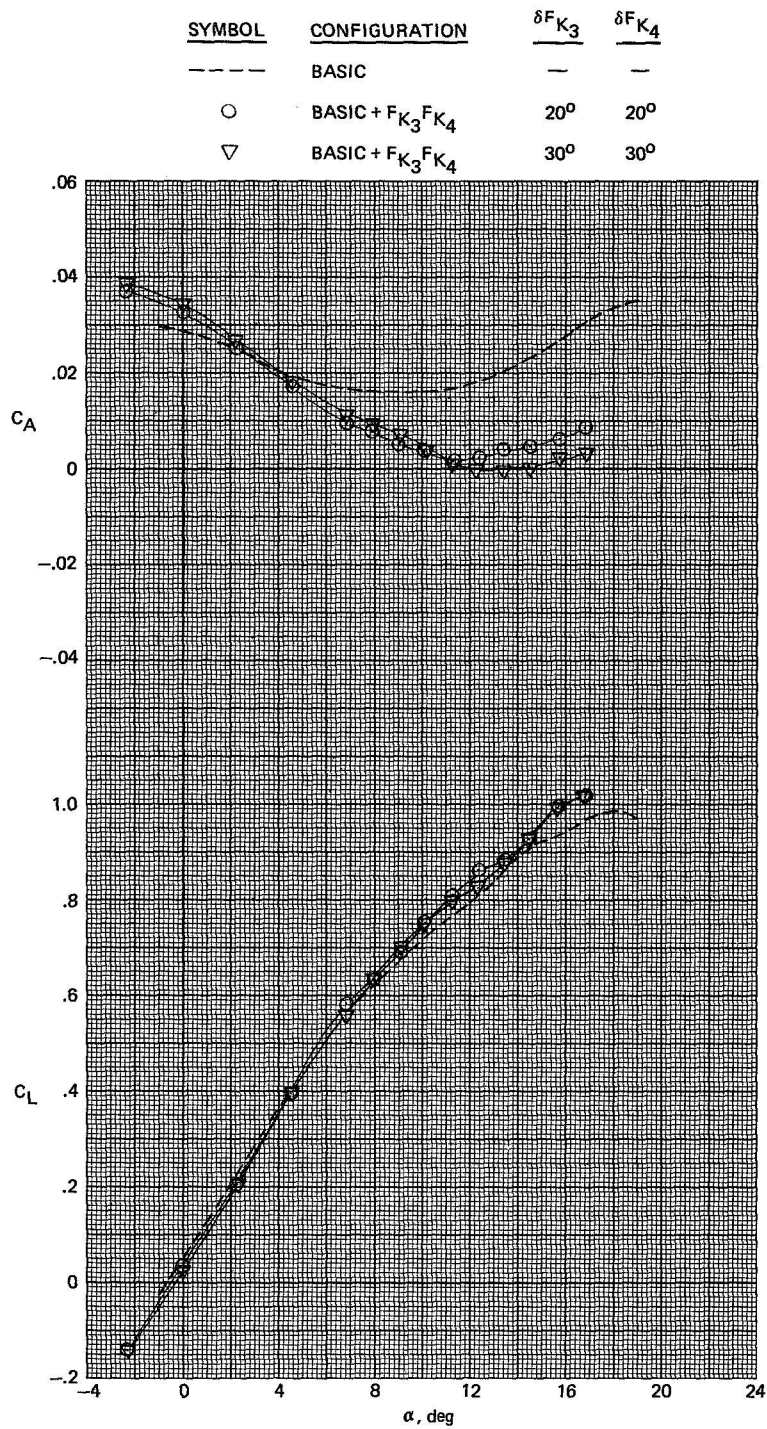
Figure 6.- Continued.

<u>SYMBOL</u>	<u>CONFIGURATION</u>	$\delta F_{K_3}$	$\delta F_{K_4}$
-----	BASIC	—	—
▽	BASIC + $F_{K_3} F_{K_4}$	50°	50°
D	BASIC + $F_{K_3} F_{K_4}$	70°	70°



(c) Concluded.

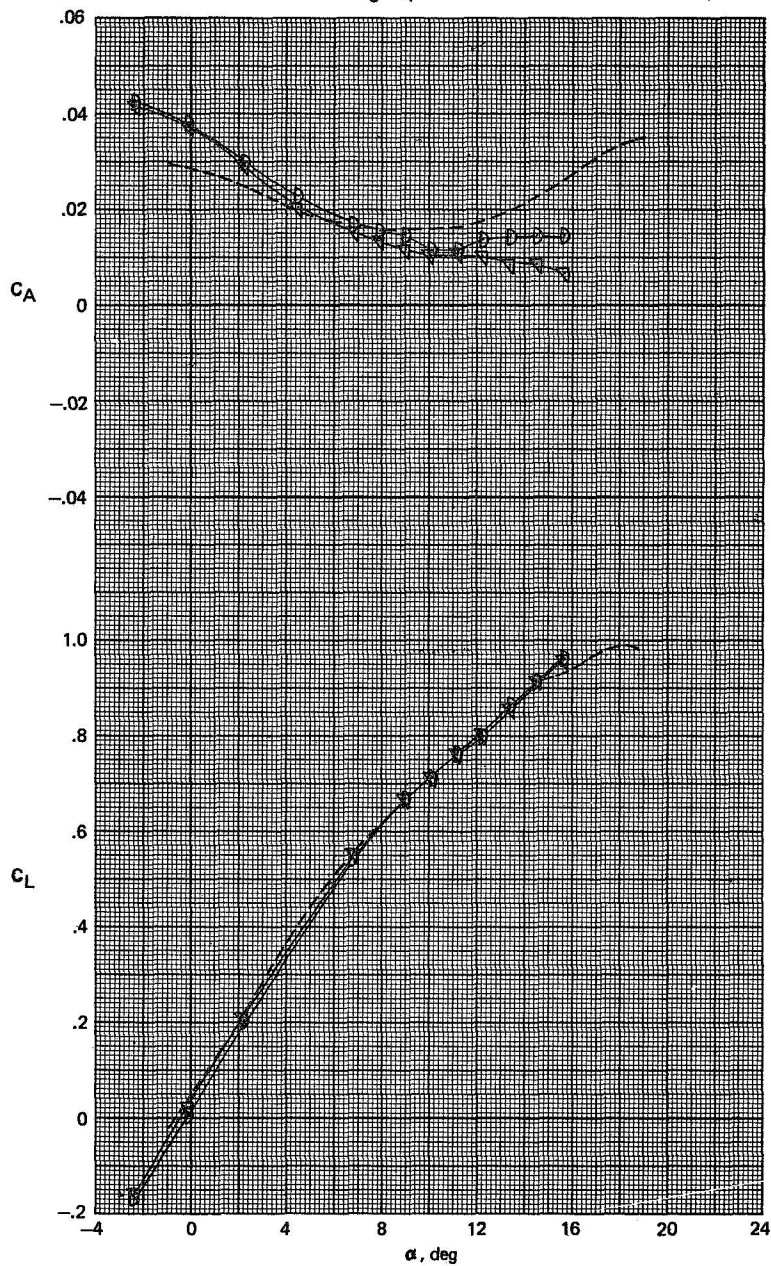
Figure 6.- Concluded.



(a)  $C_A$  and  $C_L$  plotted against  $\alpha$ .

Figure 7.- Effect of deflecting the  $F_{K3}F_{K4}$  Krueger flaps on the basic configuration incorporating the  $F_{K3}F_{K4}$  leading-edge devices.  $M = 0.90$ .

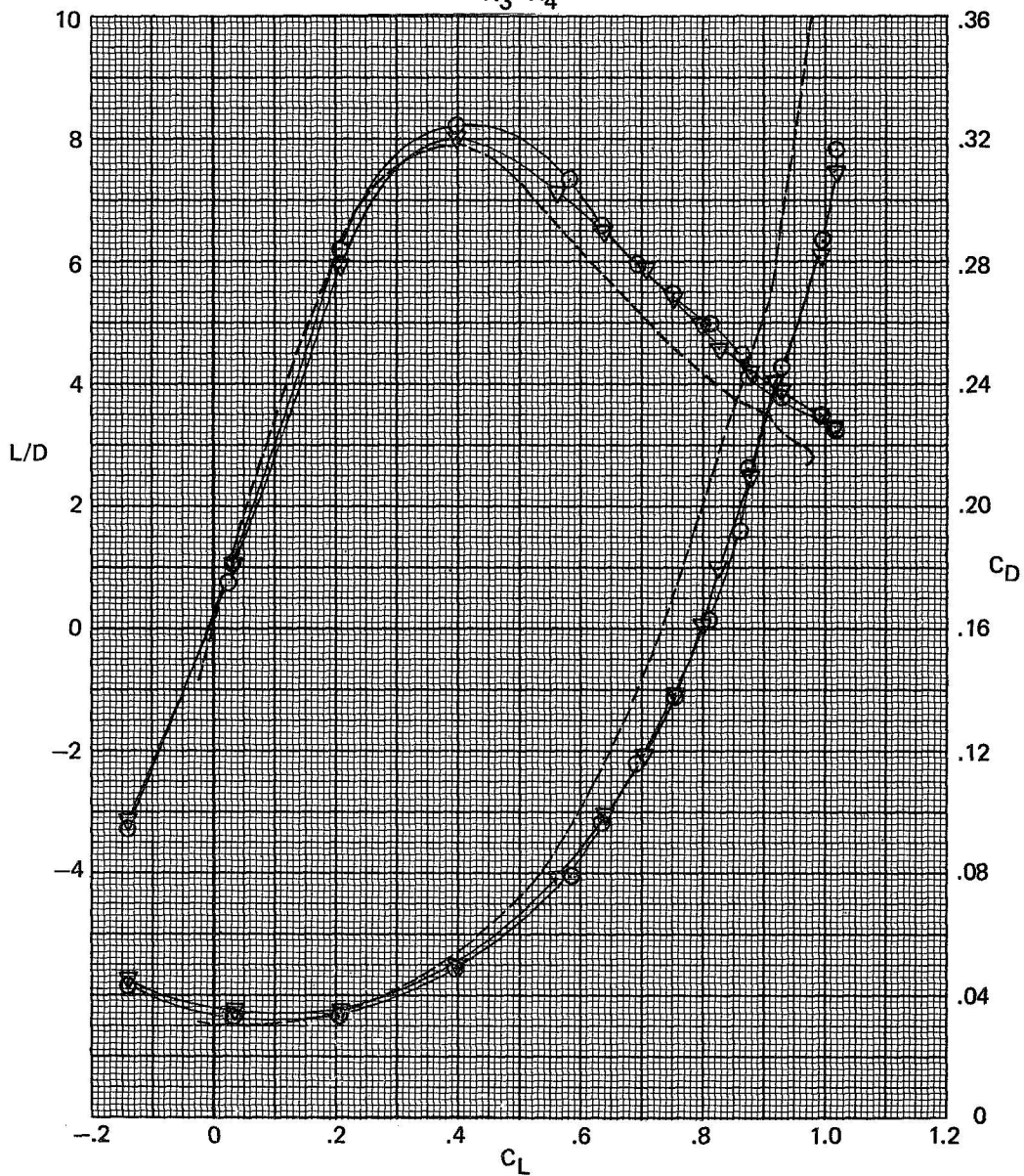
SYMBOL	CONFIGURATION	$\delta F_{K_3}$	$\delta F_{K_4}$
---	BASIC	—	—
$\nabla$	BASIC + $F_{K_3} F_{K_4}$	50°	50°
D	BASIC + $F_{K_3} F_{K_4}$	70°	70°



(a) Concluded.

Figure 7.- Continued.

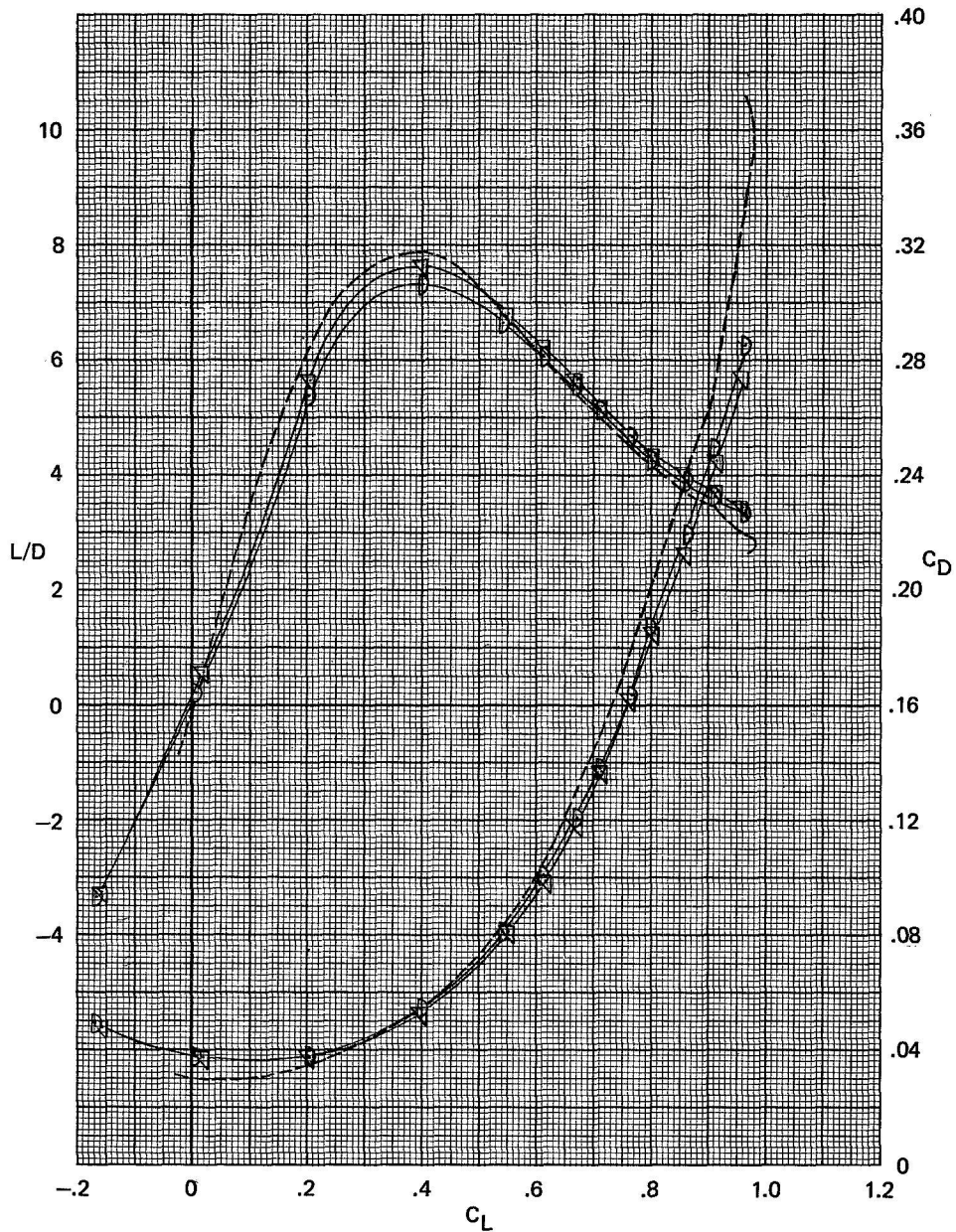
<u>SYMBOL</u>	<u>CONFIGURATION</u>	<u><math>\delta F_{K_3}</math></u>	<u><math>\delta F_{K_4}</math></u>
-----	BASIC	—	—
○	BASIC + $F_{K_3} F_{K_4}$	20°	20°
▽	BASIC + $F_{K_3} F_{K_4}$	30°	30°



(b)  $L/D$  and  $C_D$  plotted against  $C_L$ .

Figure 7.- Continued.

<u>SYMBOL</u>	<u>CONFIGURATION</u>	$\delta F_{K_3}$	$\delta F_{K_4}$
-----	BASIC	—	—
▽	BASIC + $F_{K_3} F_{K_4}$	50°	50°
D	BASIC + $F_{K_3} F_{K_4}$	70°	70°

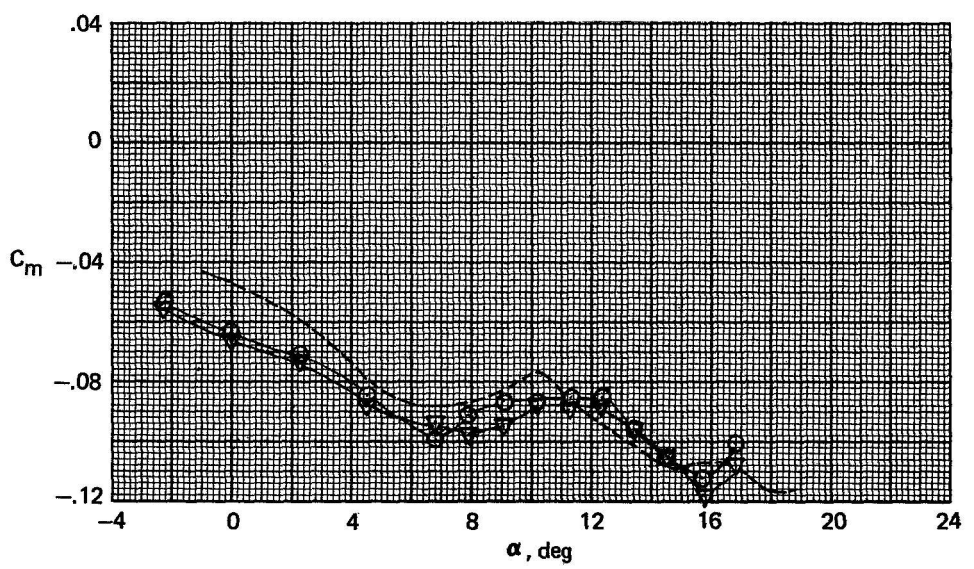
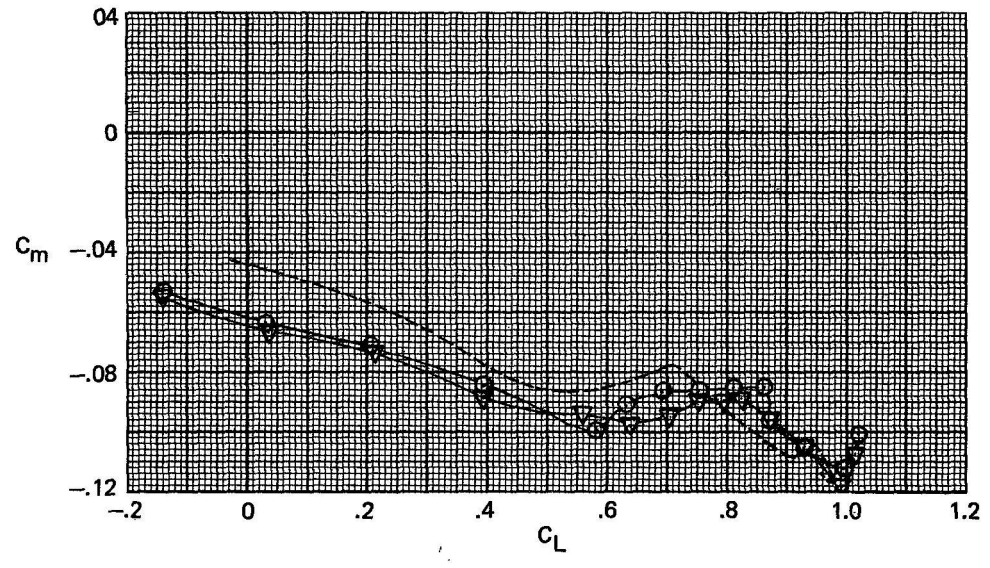


(b) Concluded.

Figure 7.- Continued.



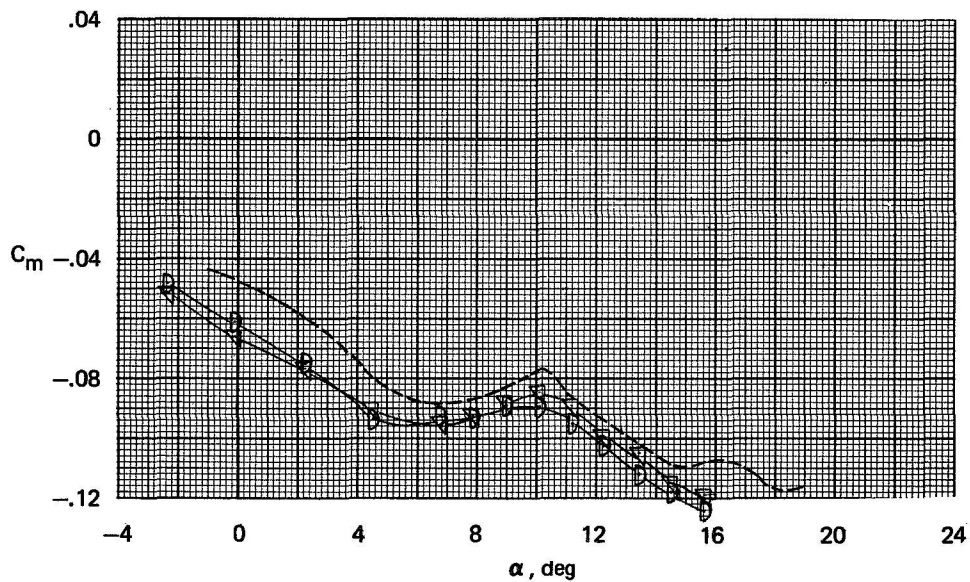
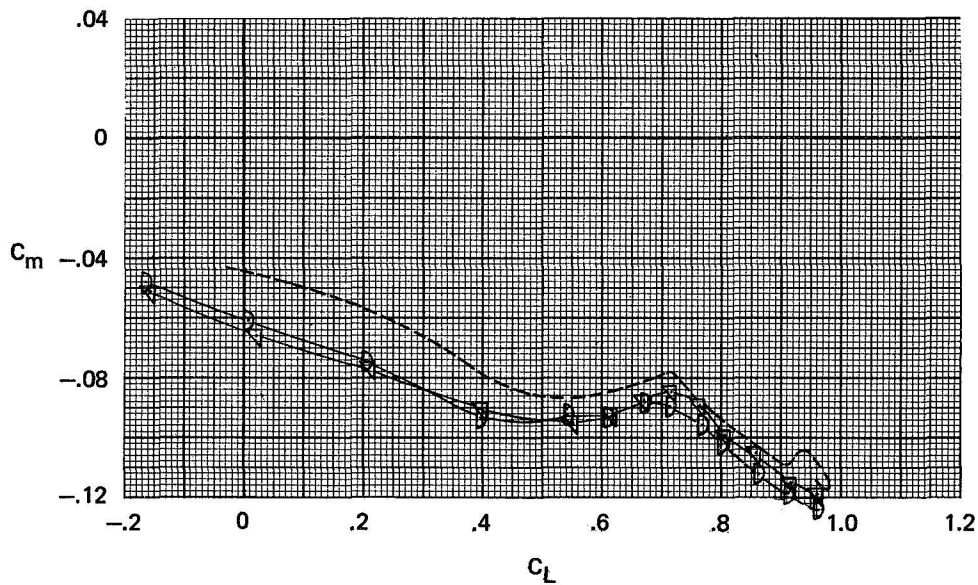
<u>SYMBOL</u>	<u>CONFIGURATION</u>	<u><math>\delta F_{K_3}</math></u>	<u><math>\delta F_{K_4}</math></u>
---	BASIC	---	---
○	BASIC + $F_{K_3} F_{K_4}$	20°	20°
▽	BASIC + $F_{K_3} F_{K_4}$	30°	30°



(c)  $C_m$  plotted against  $C_L$  and  $\alpha$ .

Figure 7.- Continued.

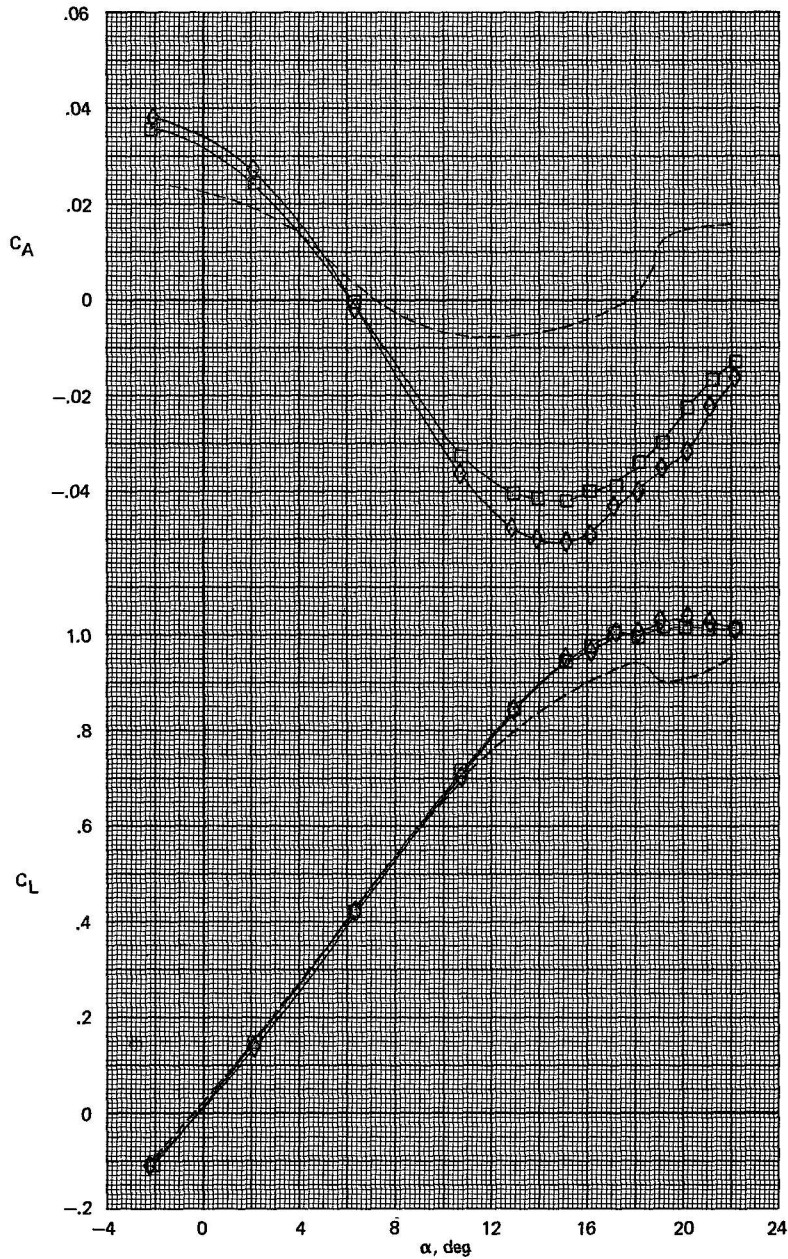
<u>SYMBOL</u>	<u>CONFIGURATION</u>	<u><math>\delta F_{K_3}</math></u>	<u><math>\delta F_{K_4}</math></u>
---	BASIC	—	—
▽	BASIC + $F_{K_3} F_{K_4}$	50°	50°
D	BASIC + $F_{K_3} F_{K_4}$	70°	70°



(c) Concluded.

Figure 7.- Concluded.

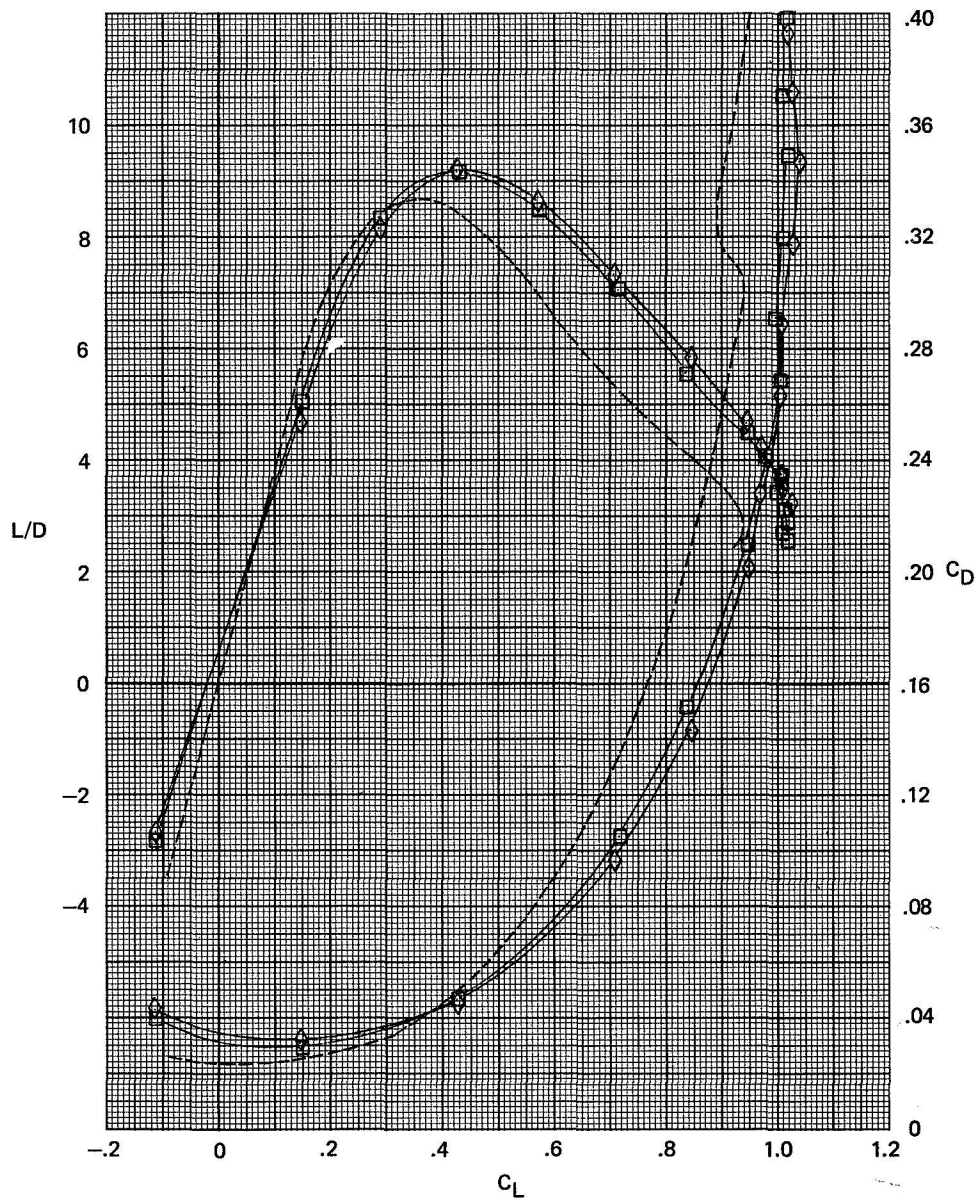
SYMBOL	CONFIGURATION	$\delta F_{K_2}$	$\delta F_{K_3}$	$\delta F_{K_4}$
-----	BASIC	—	—	—
□	BASIC + $F_{K_2} F_{K_3} F_{K_4}$	30°	20°	20°
◇	BASIC + $F_{K_2} F_{K_3} F_{K_4}$	30°	30°	30°



(a)  $C_A$  and  $C_L$  plotted against  $\alpha$ .

Figure 8.- Effect of deflecting the  $F_{K_3} F_{K_4}$  Krueger flaps on the basic configuration incorporating the  $F_{K_2} F_{K_3} F_{K_4}$  leading-edge devices.  $M = 0.60$ .

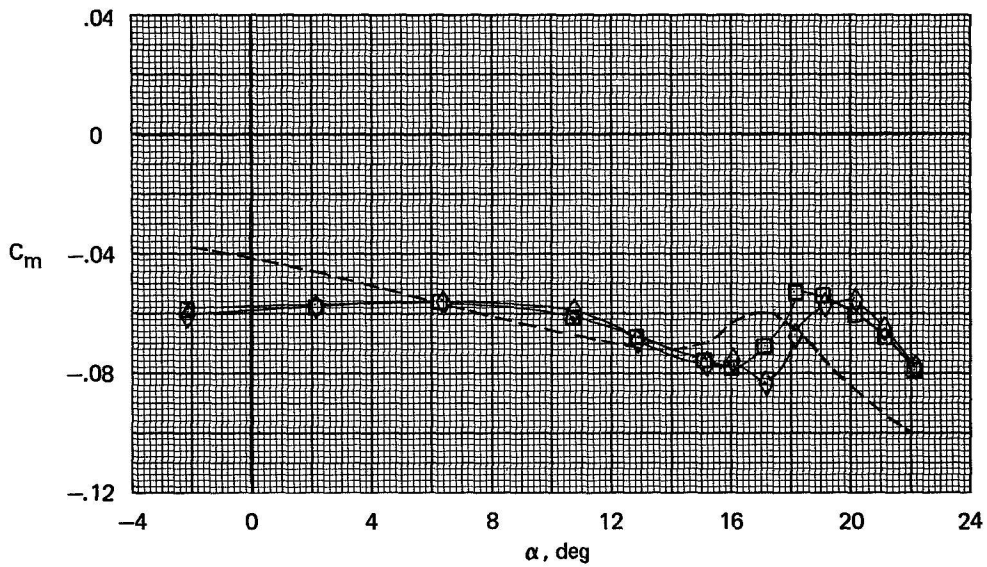
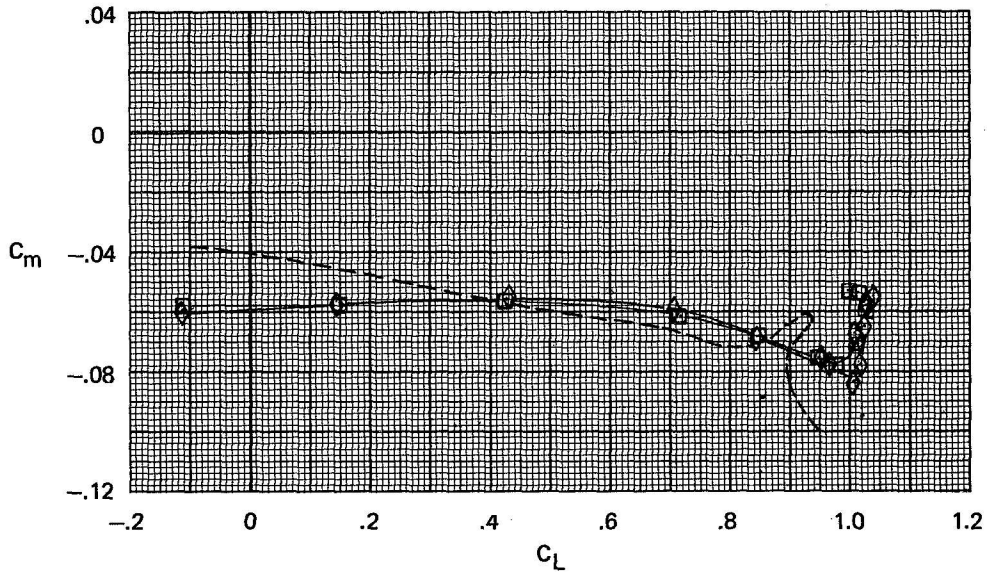
<u>SYMBOL</u>	<u>CONFIGURATION</u>	$\delta F_{K_2}$	$\delta F_{K_3}$	$\delta F_{K_4}$
-----	BASIC	—	—	—
□	BASIC + $F_{K_2} F_{K_3} F_{K_4}$	30°	20°	20°
◇	BASIC + $F_{K_2} F_{K_3} F_{K_4}$	30°	30°	30°



(b) L/D and C<sub>D</sub> plotted against C<sub>L</sub>.

Figure 8.- Continued.

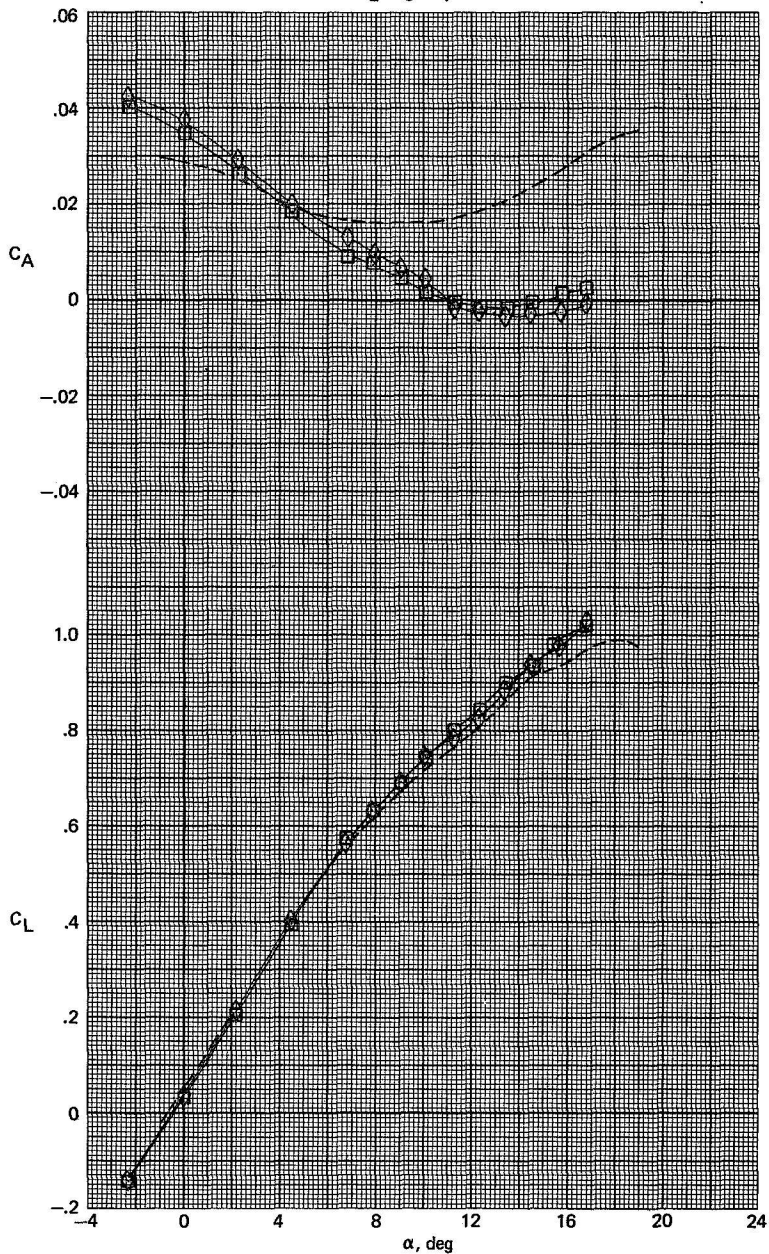
<u>SYMBOL</u>	<u>CONFIGURATION</u>	<u><math>\delta F_{K_2}</math></u>	<u><math>\delta F_{K_3}</math></u>	<u><math>\delta F_{K_4}</math></u>
---	BASIC	—	—	—
□	BASIC + $F_{K_2} F_{K_3} F_{K_4}$	30°	20°	20°
◇	BASIC + $F_{K_2} F_{K_3} F_{K_4}$	30°	30°	30°



(c)  $C_m$  plotted against  $C_L$  and  $\alpha$ .

Figure 8.- Concluded.

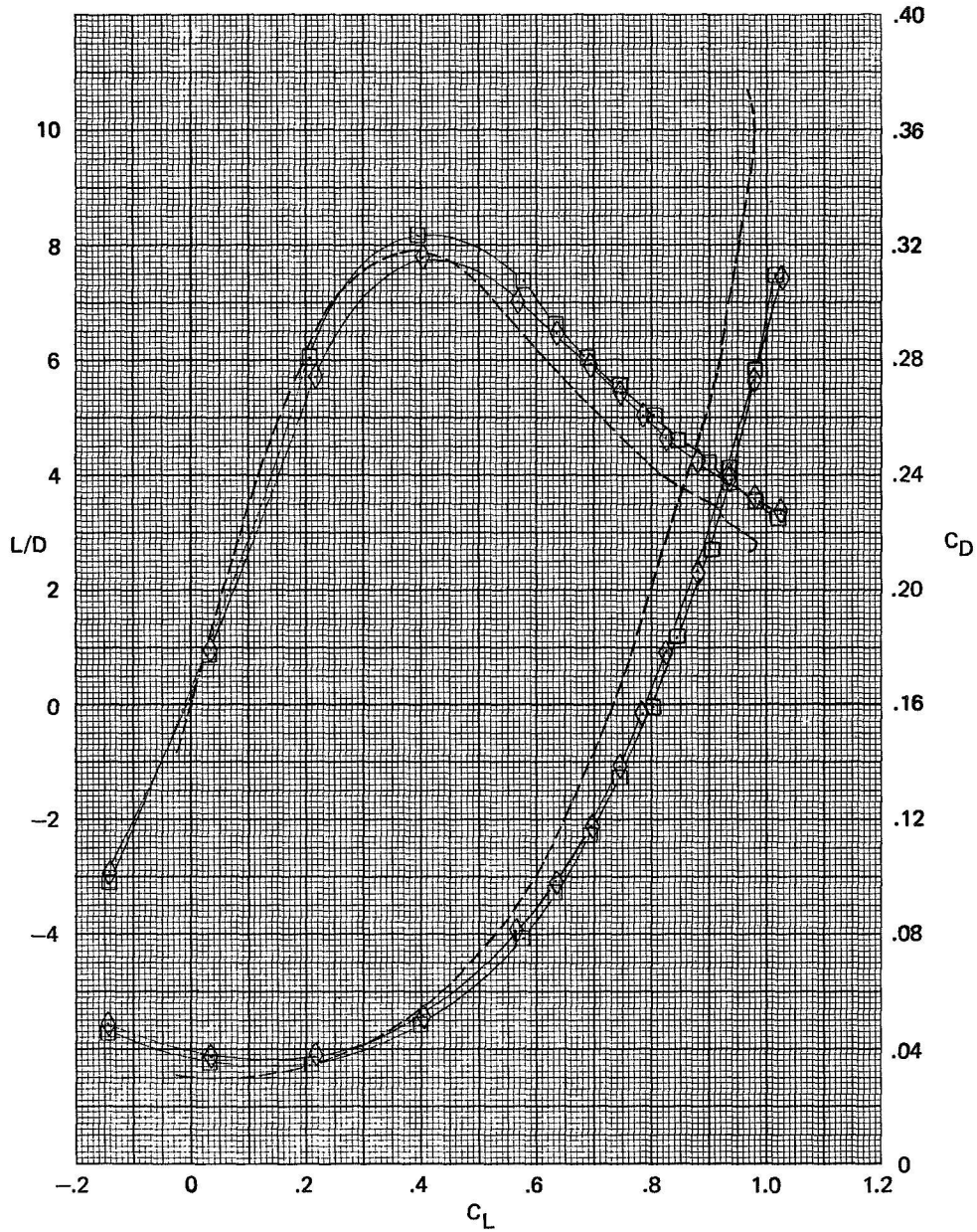
SYMBOL	CONFIGURATON	$\delta F_{K_2}$	$\delta F_{K_3}$	$\delta F_{K_4}$
---	BASIC	—	—	—
□	BASIC + $F_{K_2}F_{K_3}F_{K_4}$	30°	20°	20°
◇	BASIC + $F_{K_2}F_{K_3}F_{K_4}$	30°	30°	30°



(a)  $C_A$  and  $C_L$  plotted against  $\alpha$ .

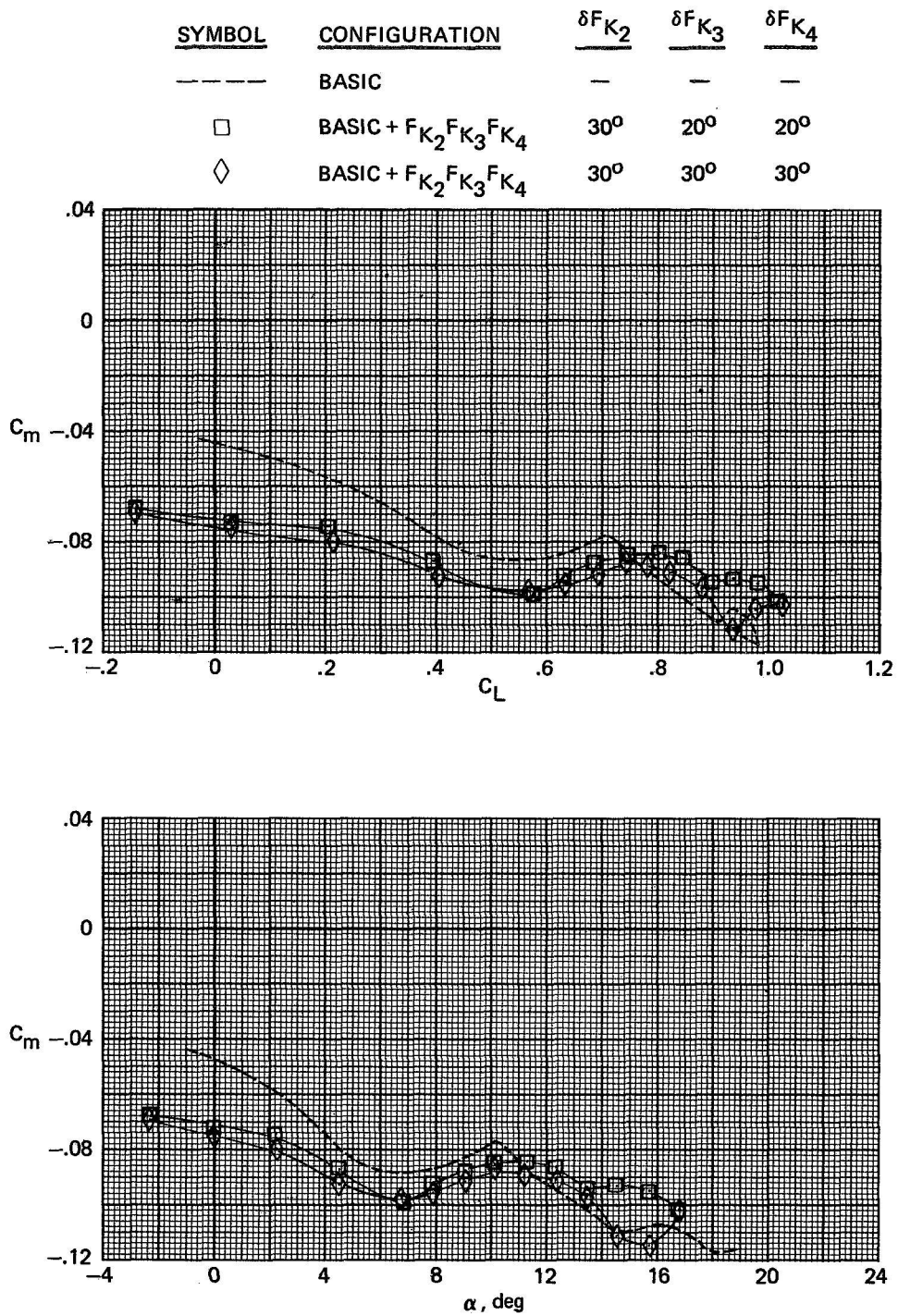
Figure 9.- Effect of deflecting the  $F_{K_3}F_{K_4}$  Krueger flaps on the basic configuration incorporating the  $F_{K_2}F_{K_3}F_{K_4}$  leading-edge devices.  $M = 0.90$ .

<u>SYMBOL</u>	<u>CONFIGURATION</u>	$\delta F_{K_2}$	$\delta F_{K_3}$	$\delta F_{K_4}$
---	BASIC	—	—	—
□	BASIC + $F_{K_2} F_{K_3} F_{K_4}$	30°	20°	20°
◇	BASIC + $F_{K_2} F_{K_3} F_{K_4}$	30°	30°	30°



(b)  $L/D$  and  $C_D$  plotted against  $C_L$ .

Figure 9.- Continued.

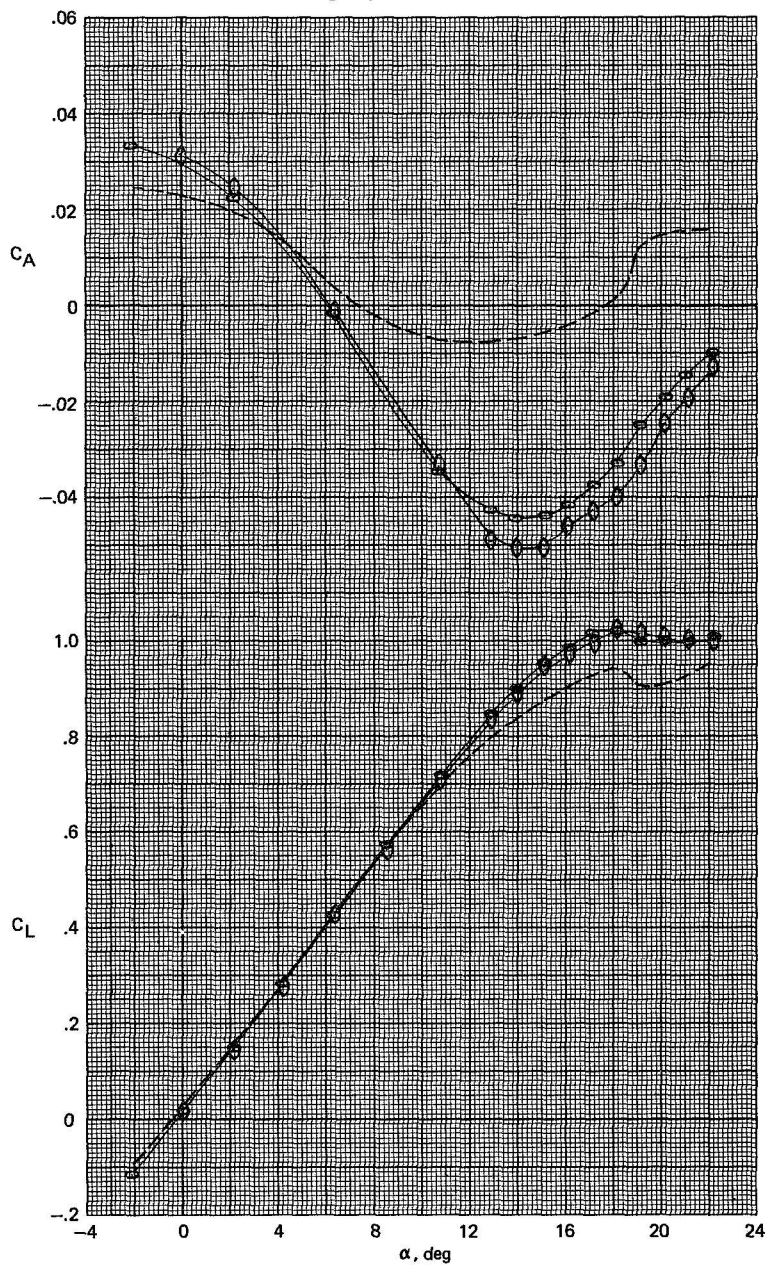


(c)  $C_m$  plotted against  $C_L$  and  $\alpha$ .

Figure 9.- Concluded.



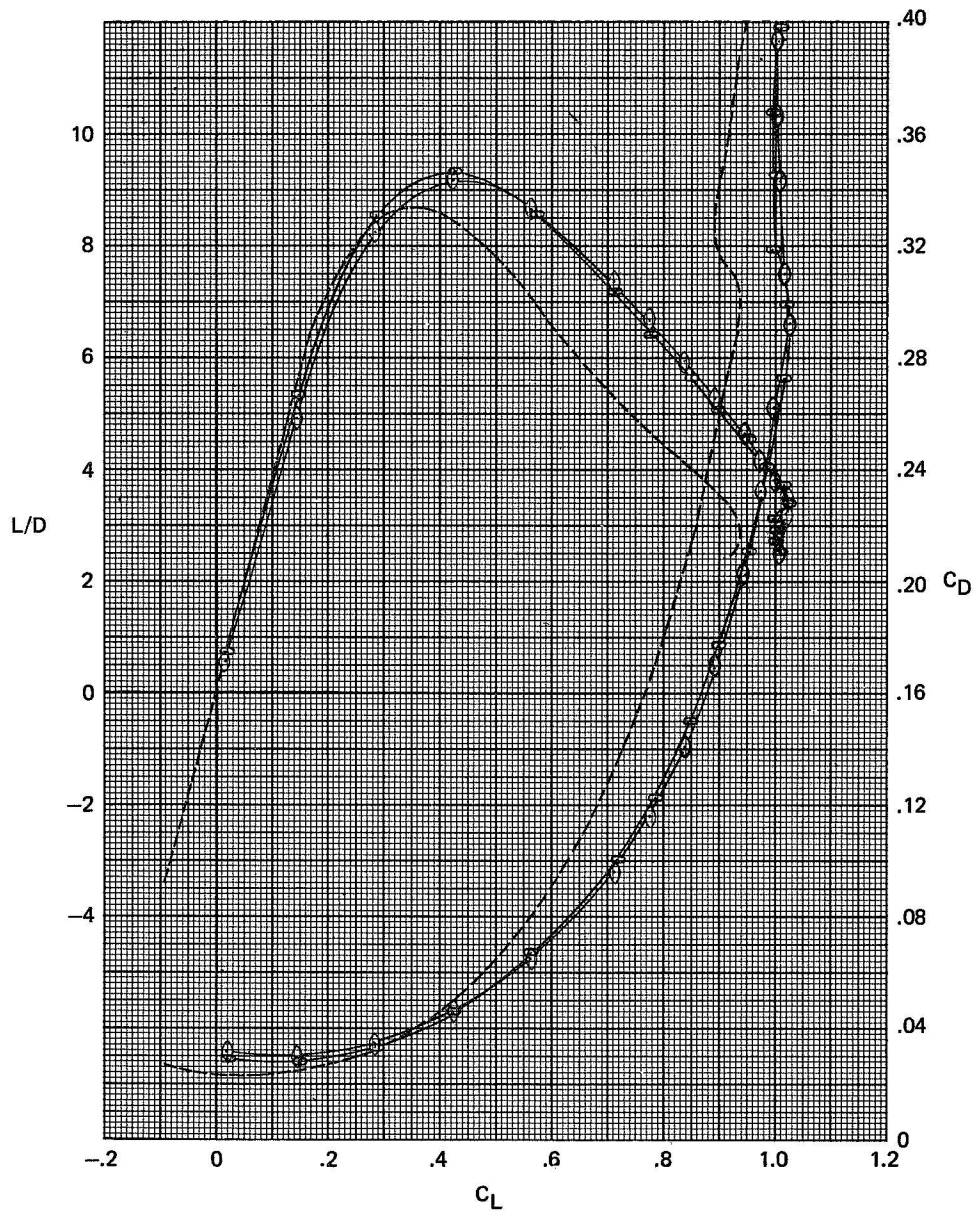
<u>SYMBOL</u>	<u>CONFIGURATION</u>	$\delta F_{K_3}$	$\delta F_{K_4}$	$\delta F_N$
-----	BASIC	—	—	—
○	BASIC + $F_{K_3} F_{K_4} F_N$	20°	20°	15°
○	BASIC + $F_{K_3} F_{K_4} F_N$	30°	15°	



(a)  $C_A$  and  $C_L$  plotted against  $\alpha$ .

Figure 10.- Effect of deflecting the  $F_{K_3} F_{K_4}$  Krueger flaps on the basic configuration incorporating the  $F_{K_3} F_{K_4} F_N$  leading-edge devices.  $M = 0.60$ .

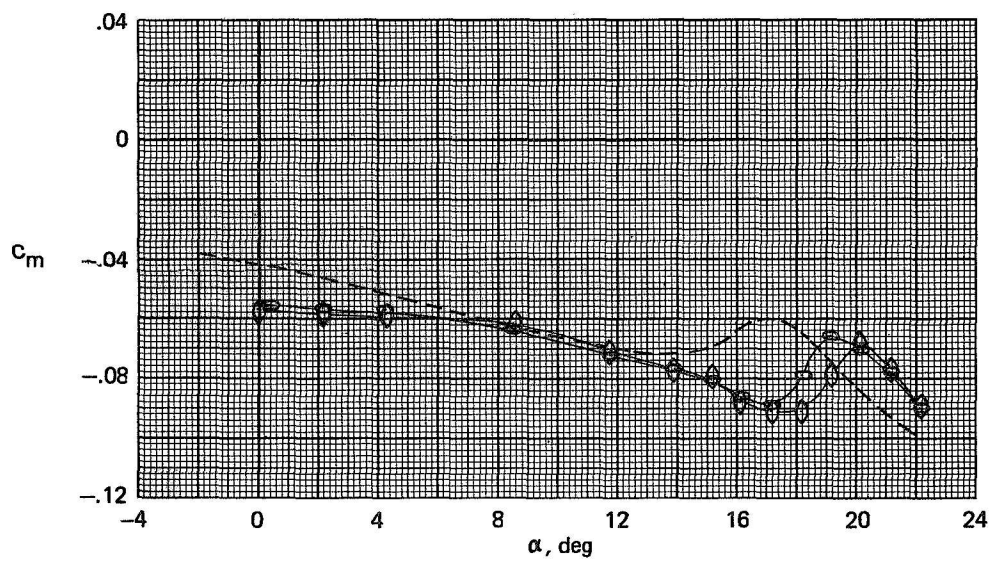
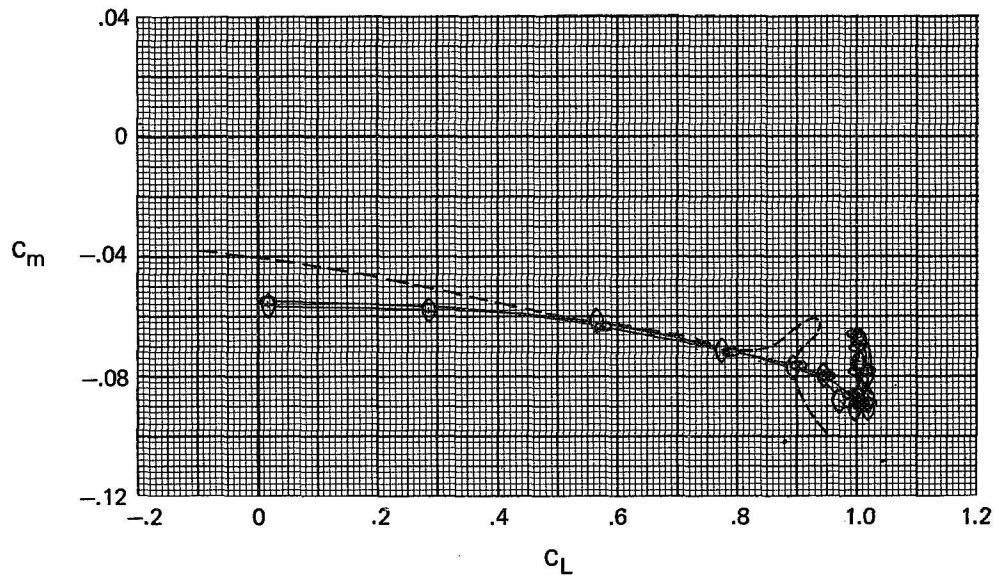
<u>SYMBOL</u>	<u>CONFIGURATION</u>	<u><math>\delta F_{K3}</math></u>	<u><math>\delta F_{K4}</math></u>	<u><math>\delta F_N</math></u>
-----	BASIC	—	—	—
○	BASIC + $F_{K3} F_{K4} F_N$	20°	20°	15°
◇	BASIC + $F_{K3} F_{K4} F_N$	30°	30°	15°



(b)  $L/D$  and  $C_D$  plotted against  $C_L$ .

Figure 10.- Continued.

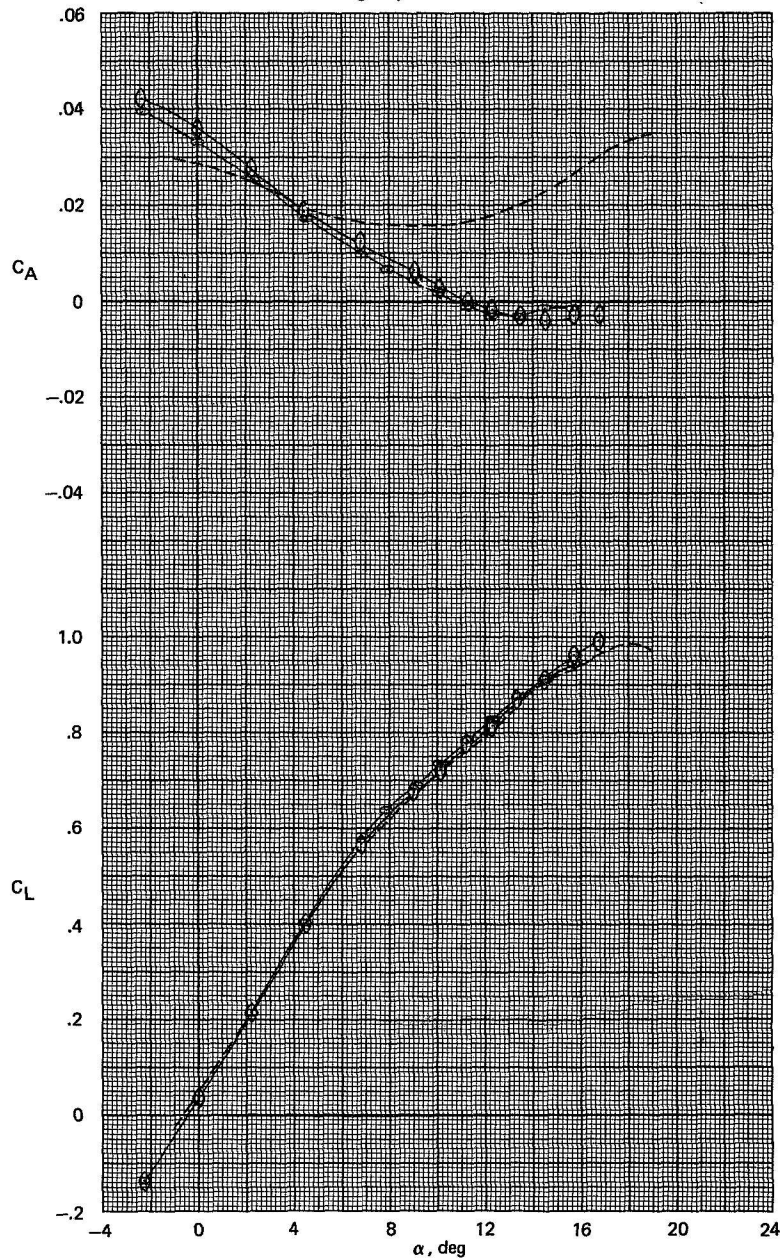
<u>SYMBOL</u>	<u>CONFIGURATION</u>	$\delta F_{K_3}$	$\delta F_{K_4}$	$\delta F_N$
---	BASIC	-	-	-
○	BASIC + $F_{K_3} F_{K_4} F_N$	20°	20°	15°
◇	BASIC + $F_{K_3} F_{K_4} F_N$	30°	30°	15°



(c)  $C_m$  plotted against  $C_L$  and  $\alpha$ .

Figure 10.- Concluded.

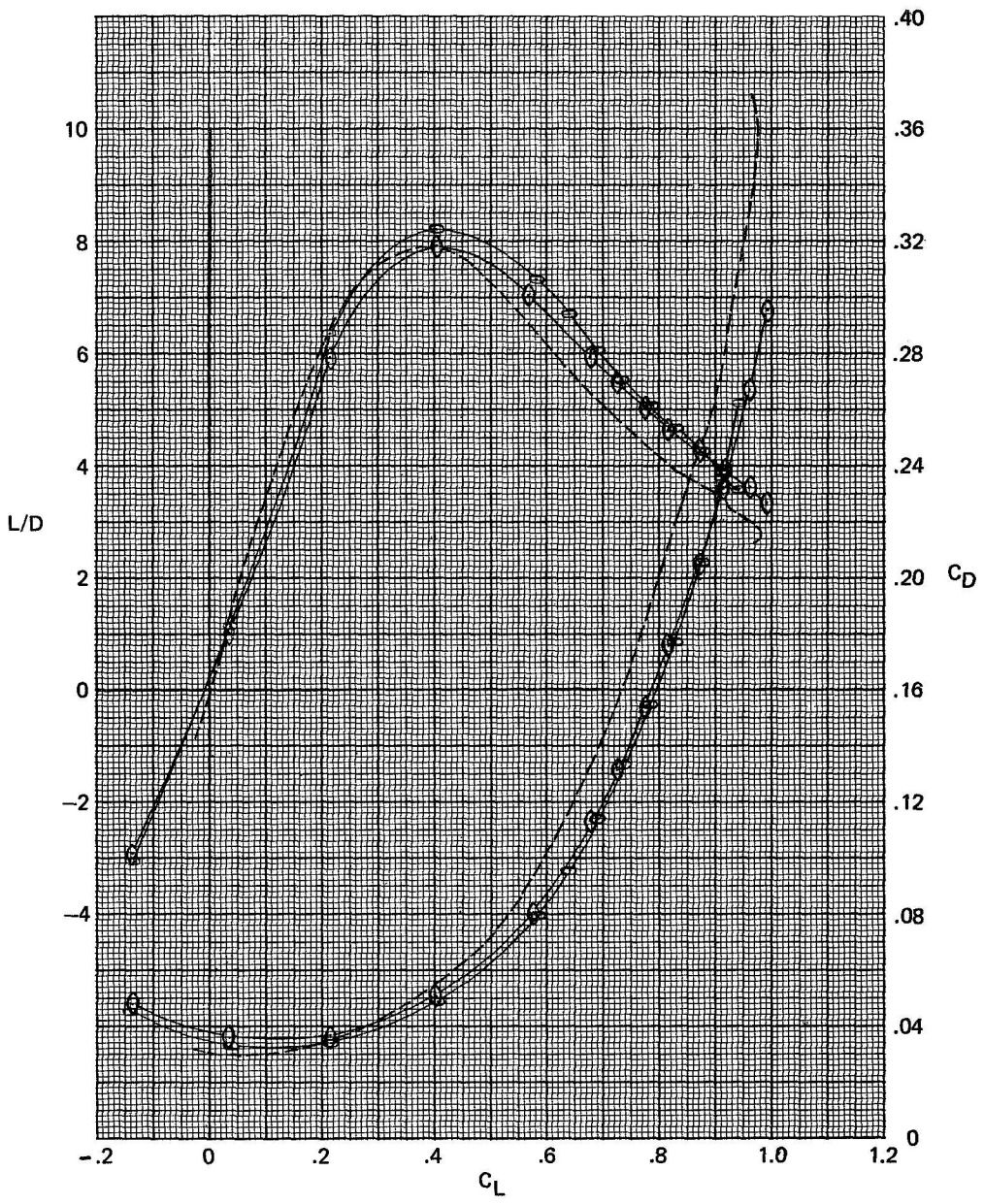
<u>SYMBOL</u>	<u>CONFIGURATION</u>	$\delta F_{K_3}$	$\delta F_{K_4}$	$\delta F_N$
---	BASIC	—	—	—
○	BASIC + $F_{K_3} F_{K_4} F_N$	20°	20°	15°
◇	BASIC + $F_{K_3} F_{K_4} F_N$	30°	30°	15°



(a)  $C_A$  and  $C_L$  plotted against  $\alpha$ .

Figure 11.- Effect of deflecting the  $F_{K_3} F_{K_4}$  Krueger flaps on the basic configuration incorporating the  $F_{K_3} F_{K_4} F_N$  leading-edge devices.  $M = 0.90$ .

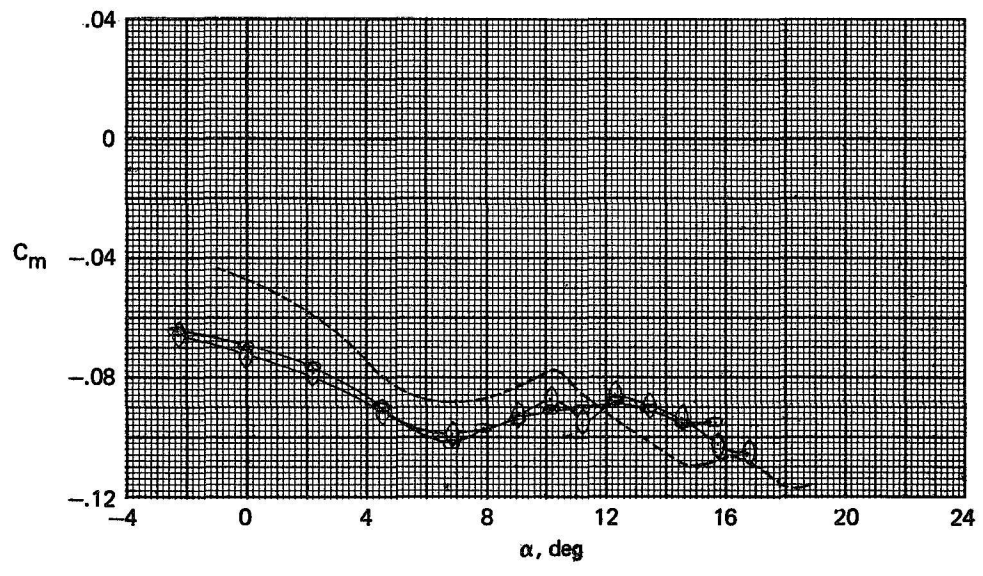
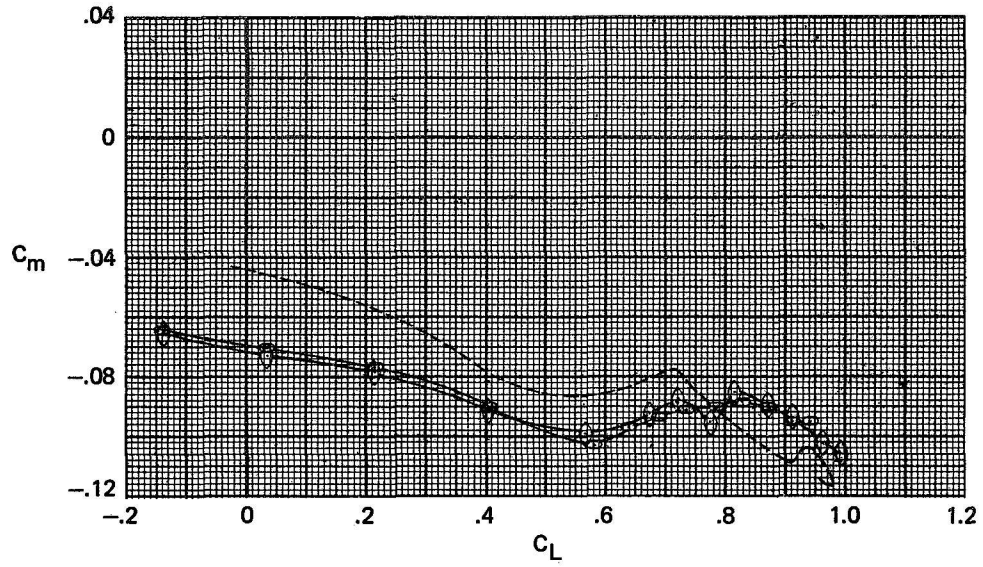
<u>SYMBOL</u>	<u>CONFIGURATION</u>	<u><math>\delta F_{K_3}</math></u>	<u><math>\delta F_{K_4}</math></u>	<u><math>\delta F_N</math></u>
-----	BASIC	—	—	—
○	BASIC + $F_{K_3} F_{K_4} F_N$	20°	20°	15°
◊	BASIC + $F_{K_3} F_{K_4} F_N$	30°	30°	15°



(b) L/D and C<sub>D</sub> plotted against C<sub>L</sub>.

Figure 11.- Continued.

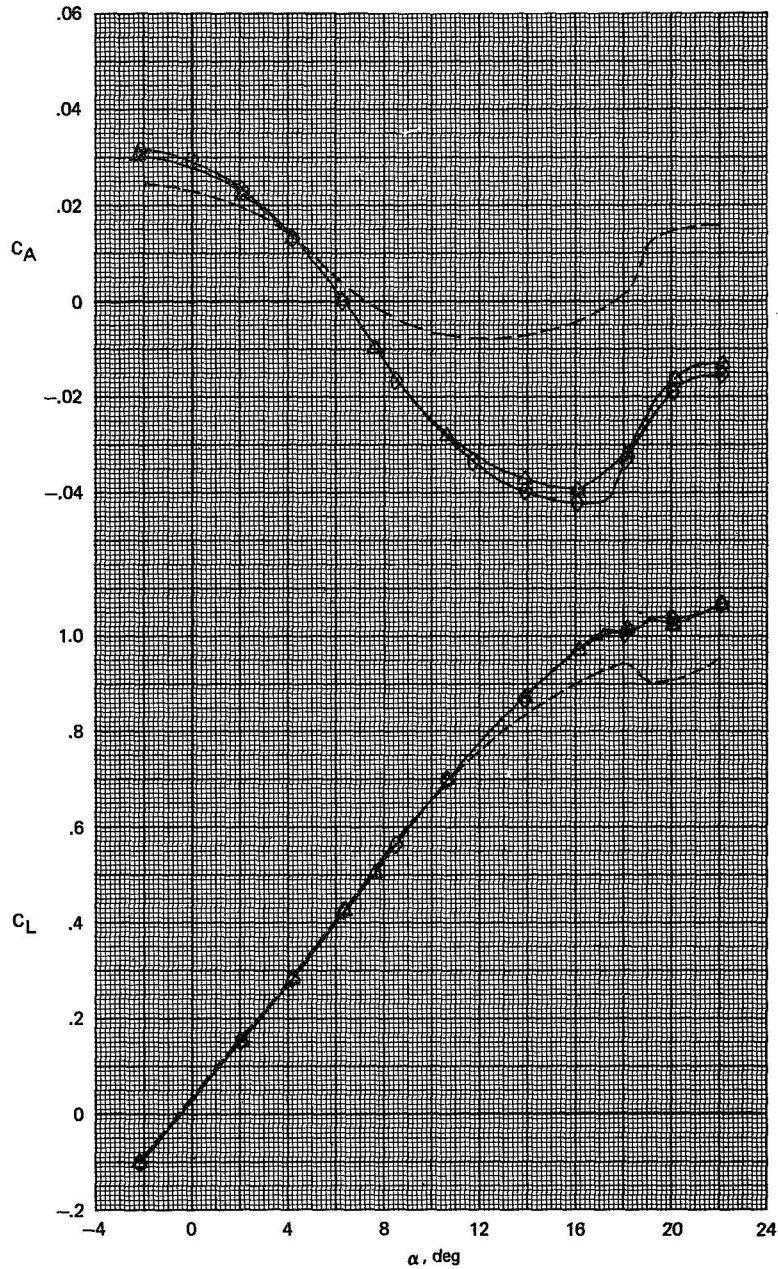
<u>SYMBOL</u>	<u>CONFIGURATION</u>	<u><math>\delta F_{K_3}</math></u>	<u><math>\delta F_{K_4}</math></u>	<u><math>\delta F_N</math></u>
-----	BASIC	—	—	—
○	BASIC + $F_{K_3} F_{K_4} F_N$	20°	20°	15°
◇	BASIC + $F_{K_3} F_{K_4} F_N$	30°	30°	15°



(c)  $C_m$  plotted against  $C_L$  and  $\alpha$ .

Figure 11.- Concluded.

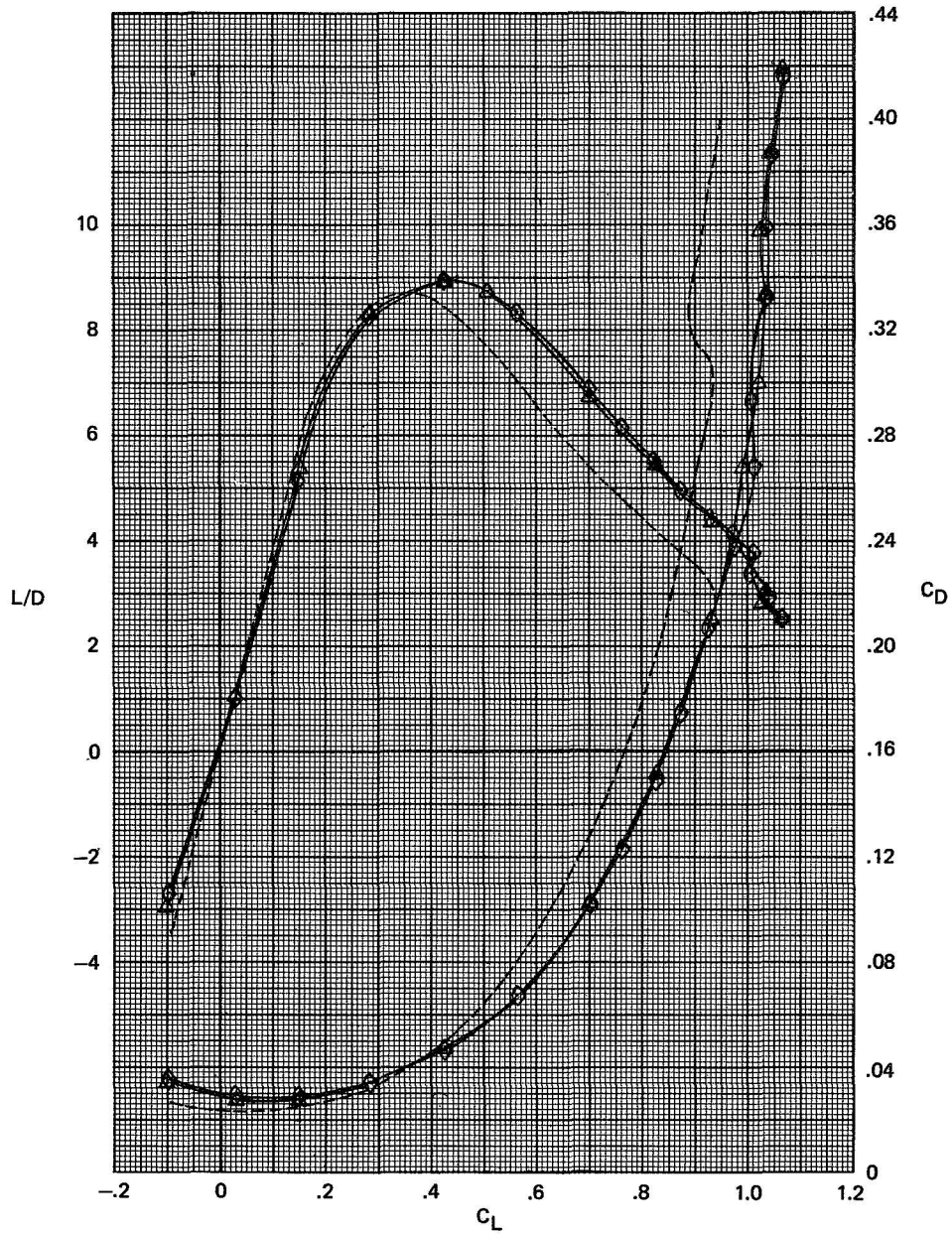
SYMBOL	CONFIGURATION	$\delta F_{K_3}$
-----	BASIC	—
$\triangle$	BASIC + $S_{17}F_{K_3}$	$20^\circ$
$\diamond$	BASIC + $S_{17}F_{K_3}$	$30^\circ$



(a)  $C_A$  and  $C_L$  plotted against  $\alpha$ .

Figure 12.- Effect of deflecting the  $F_{K_3}$  Krueger flaps on the basic configuration incorporating the  $S_{17}F_{K_3}$  leading-edge devices.  $M = 0.60$ .

<u>SYMBOL</u>	<u>CONFIGURATION</u>	$\delta F_{K_3}$
-----	BASIC	—
△	BASIC + S <sub>17</sub> F <sub>K<sub>3</sub></sub>	20°
◇	BASIC + S <sub>17</sub> F <sub>K<sub>3</sub></sub>	30°

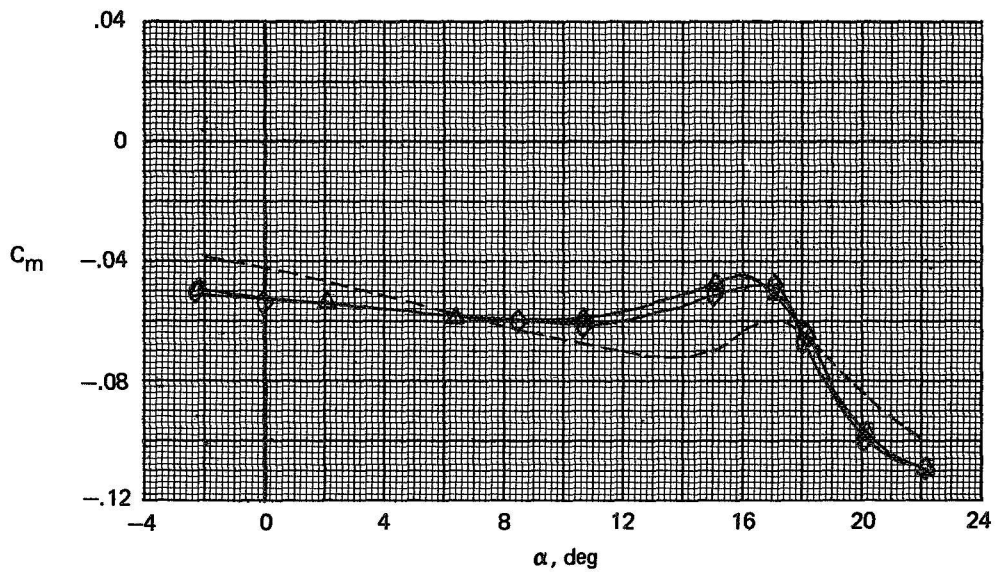
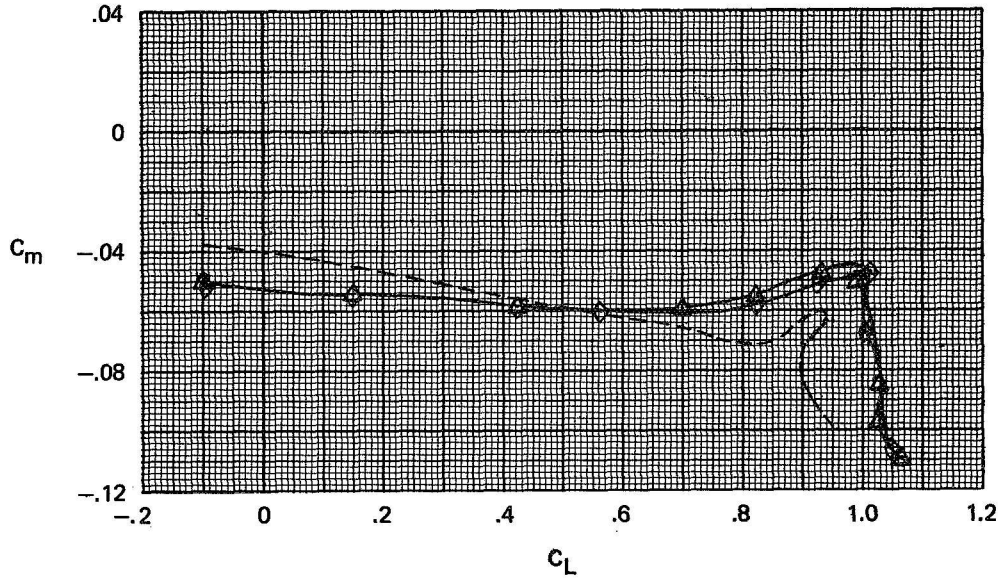


(b)  $L/D$  and  $C_D$  plotted against  $C_L$ .

Figure 12.- Continued.

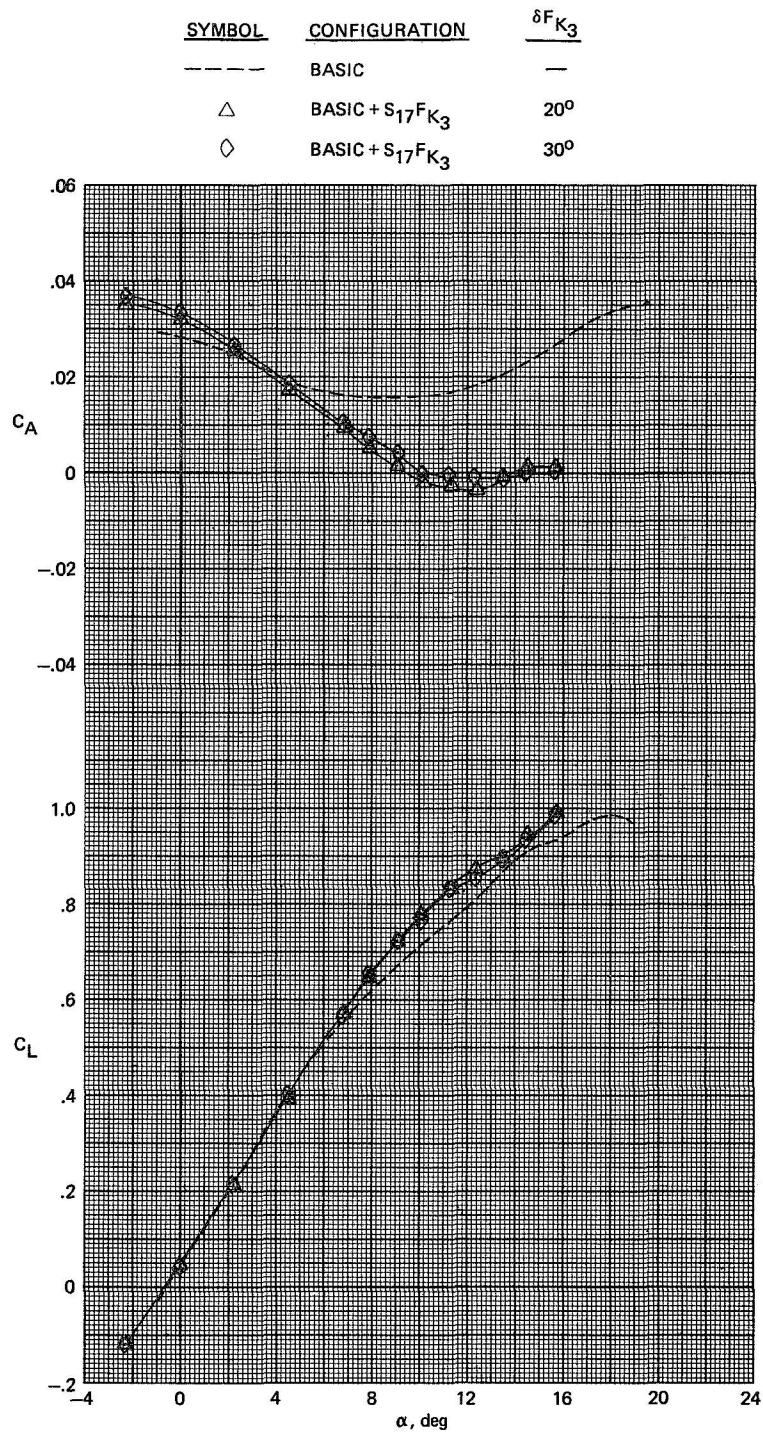


<u>SYMBOL</u>	<u>CONFIGURATION</u>	$\delta F_{K_3}$
-----	BASIC	-
$\triangle$	BASIC + $S_{17}F_{K_3}$	$20^\circ$
$\diamond$	BASIC + $S_{17}F_{K_3}$	$30^\circ$



(c)  $C_m$  plotted against  $C_L$  and  $\alpha$ .

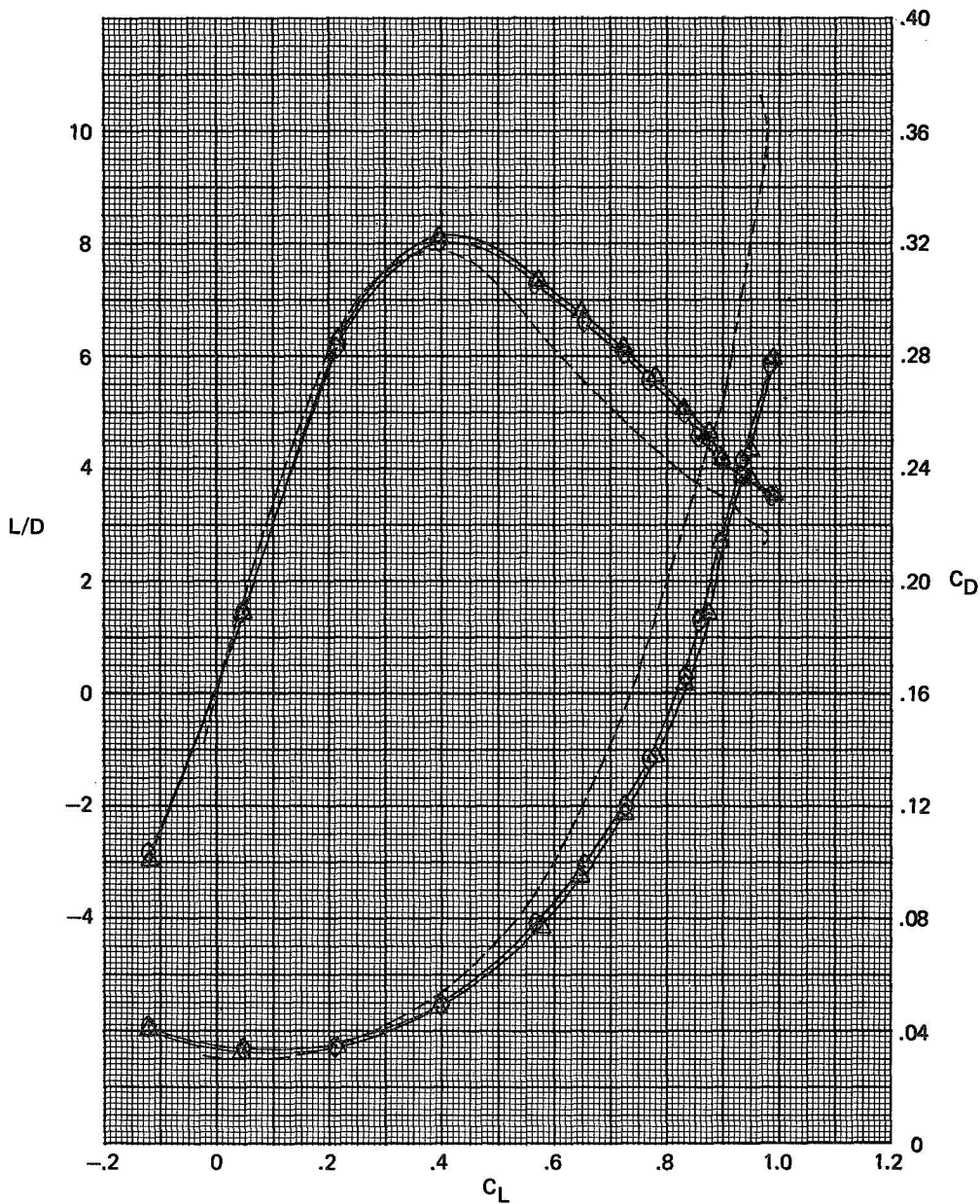
Figure 12.- Concluded.



(a)  $C_A$  and  $C_L$  plotted against  $\alpha$ .

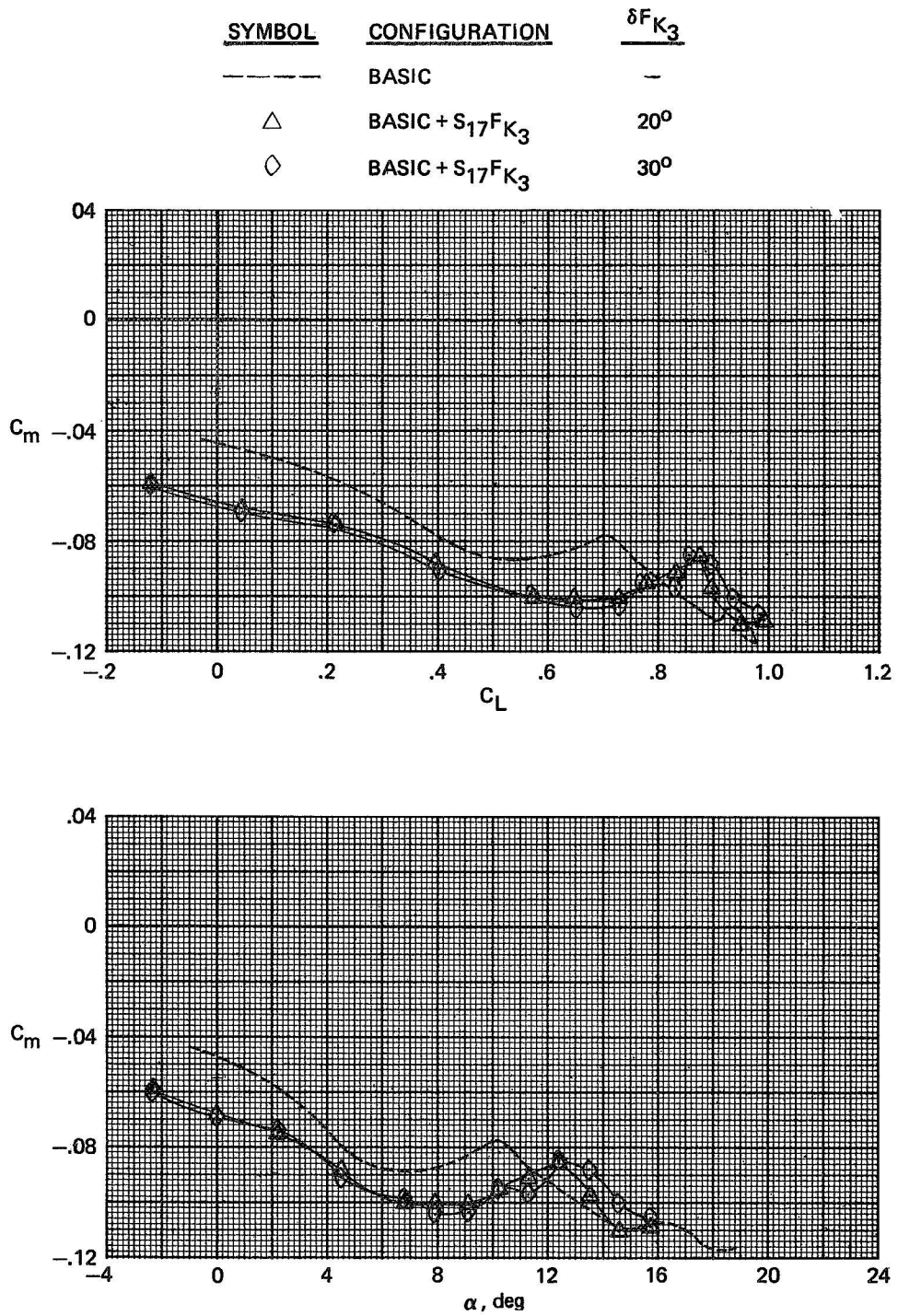
Figure 13.- Effect of deflecting the  $F_{K3}$  Krueger flaps on the basic configuration incorporating the  $S_{17}F_{K3}$  leading-edge devices.  $M = 0.90$ .

<u>SYMBOL</u>	<u>CONFIGURATION</u>	$\delta F_{K_3}$
---	BASIC	—
$\Delta$	BASIC + $S_{17}F_{K_3}$	$20^\circ$
$\diamond$	BASIC + $S_{17}F_{K_3}$	$30^\circ$



(b) L/D and  $C_D$  plotted against  $C_L$ .

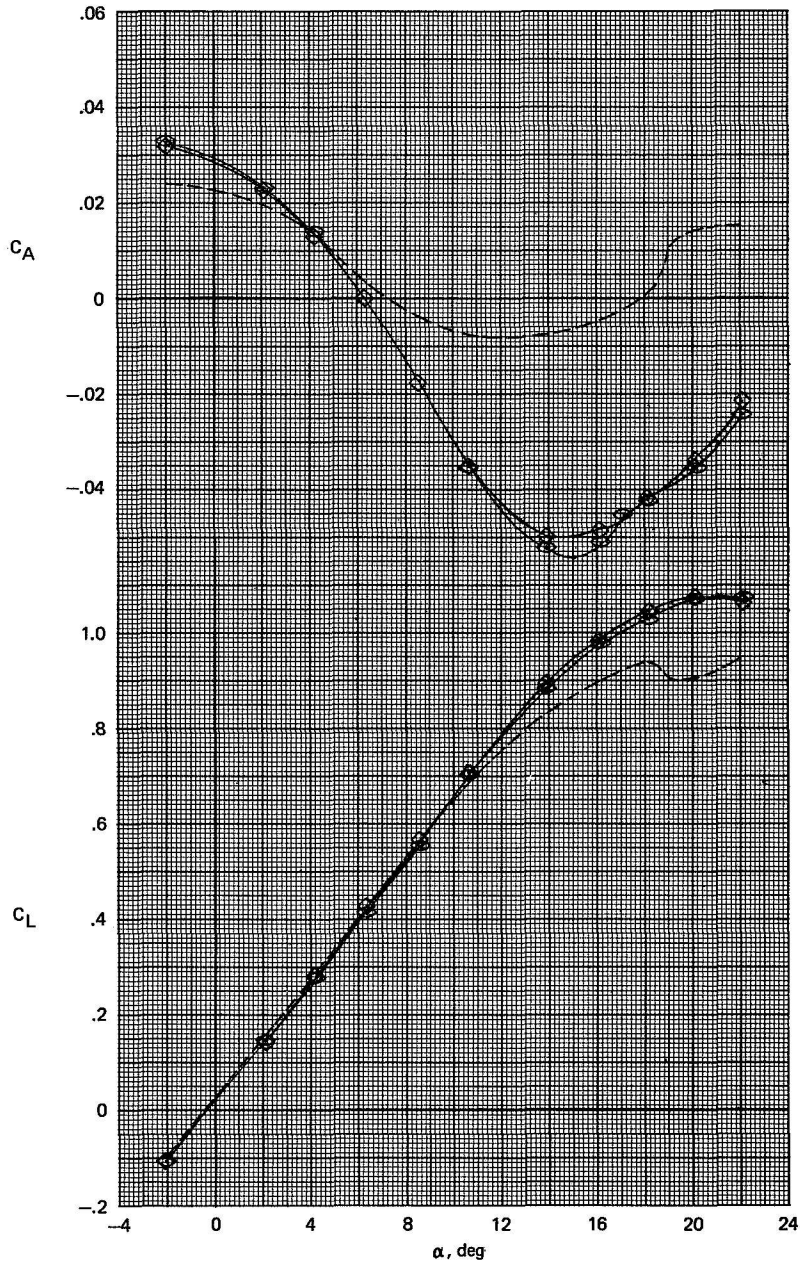
Figure 13.- Continued.



(c)  $C_m$  plotted against  $C_L$  and  $\alpha$ .

Figure 13.- Concluded.

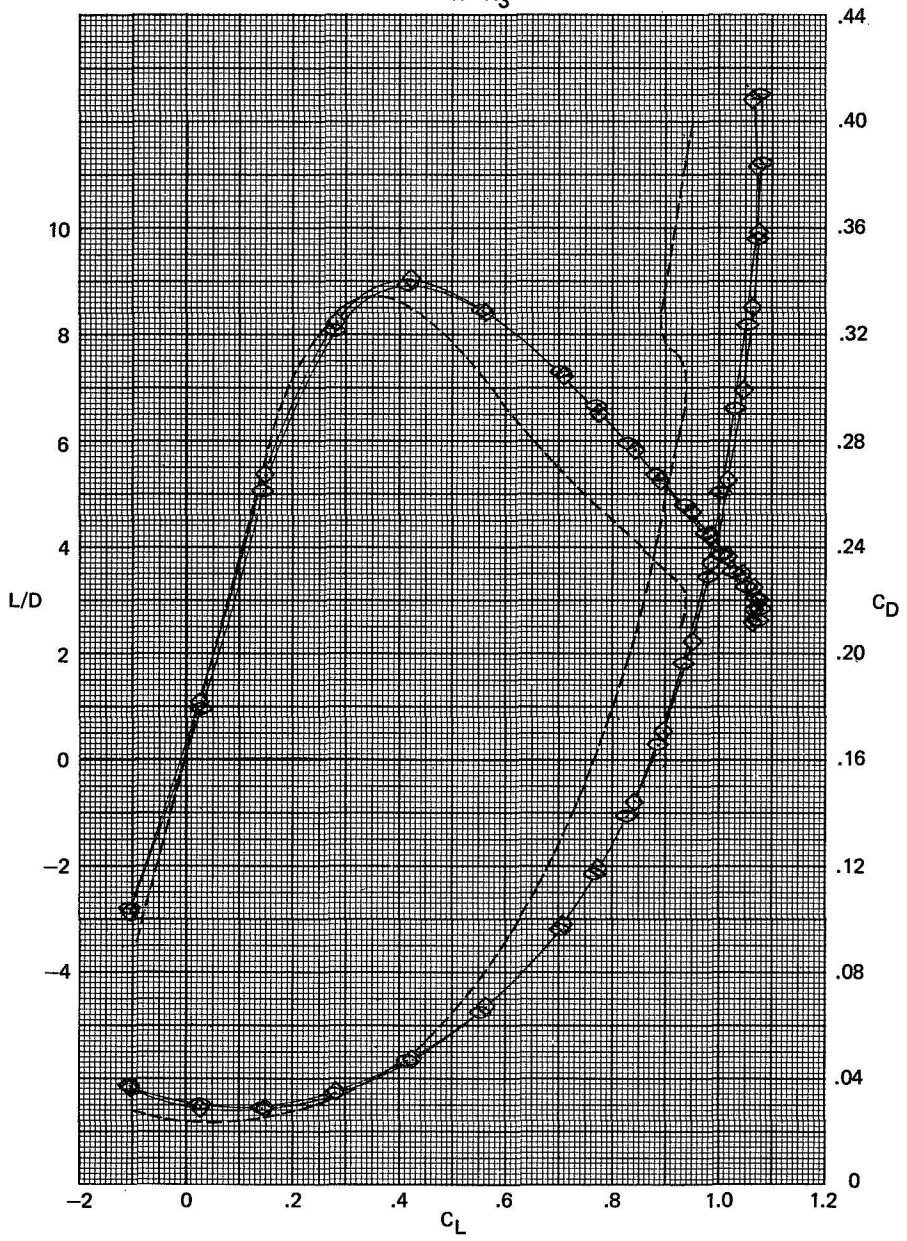
<u>SYMBOL</u>	<u>CONFIGURATION</u>	$\delta F_{K_3}$	$\delta F_N$
-----	BASIC	—	—
◇	BASIC + S <sub>17</sub> F <sub>K<sub>3</sub></sub> F <sub>N</sub>	20°	15°
○	BASIC + S <sub>17</sub> F <sub>K<sub>3</sub></sub> F <sub>N</sub>	30°	15°



(a)  $C_A$  and  $C_L$  plotted against  $\alpha$ .

Figure 14.- Effect of deflecting the  $F_{K_3}$  Krueger flaps on the basic configuration incorporating the  $S_{17}F_{K_3}F_N$  leading-edge devices.  $M = 0.60$ .

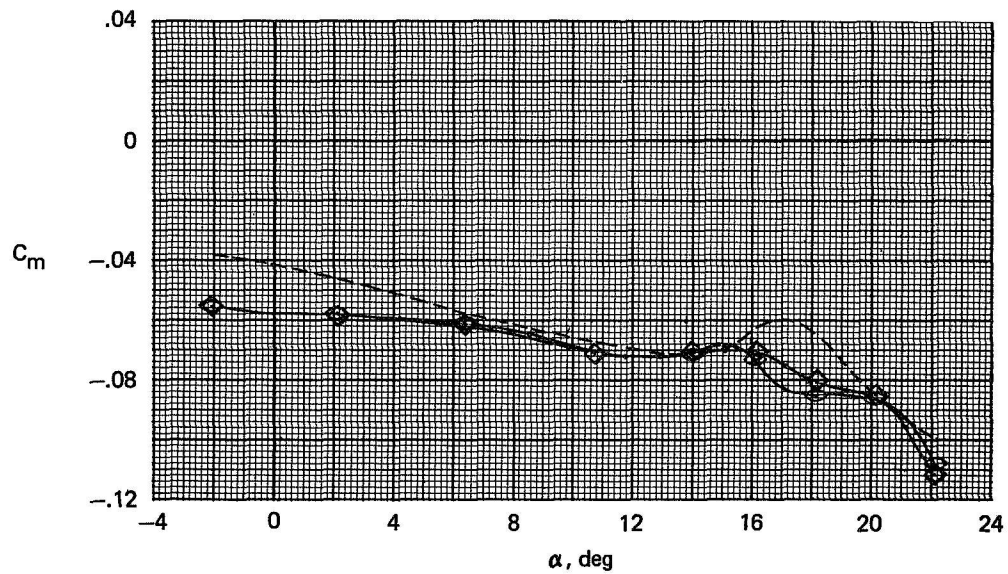
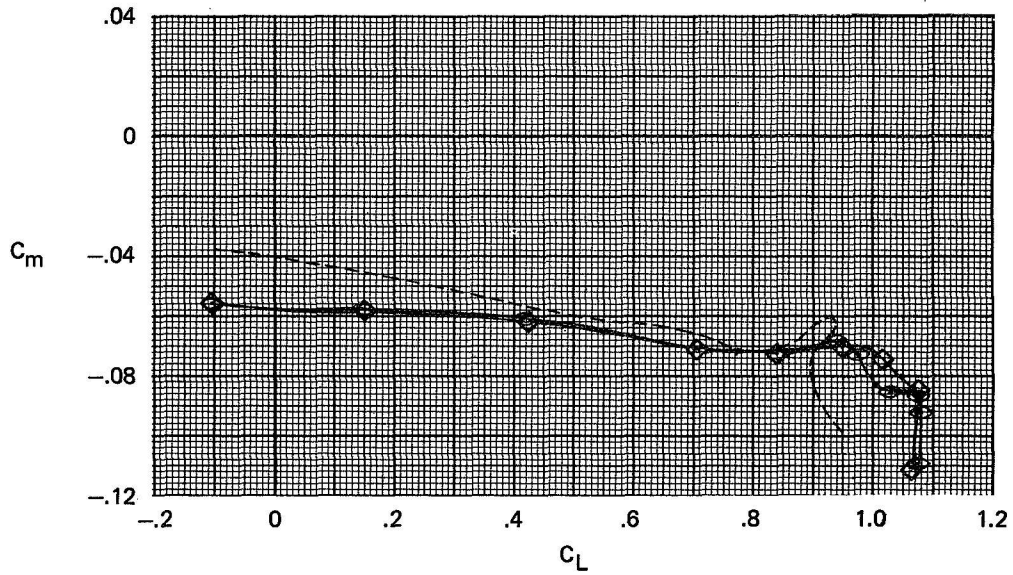
<u>SYMBOL</u>	<u>CONFIGURATION</u>	$\delta F_{K_3}$	$\delta F_N$
---	BASIC	—	—
◇	BASIC + S <sub>17</sub> F <sub>K<sub>3</sub></sub> F <sub>N</sub>	20°	15°
◊	BASIC + S <sub>17</sub> F <sub>K<sub>3</sub></sub> F <sub>N</sub>	30°	15°



(b)  $L/D$  and  $C_D$  plotted against  $C_L$ .

Figure 14.- Continued.

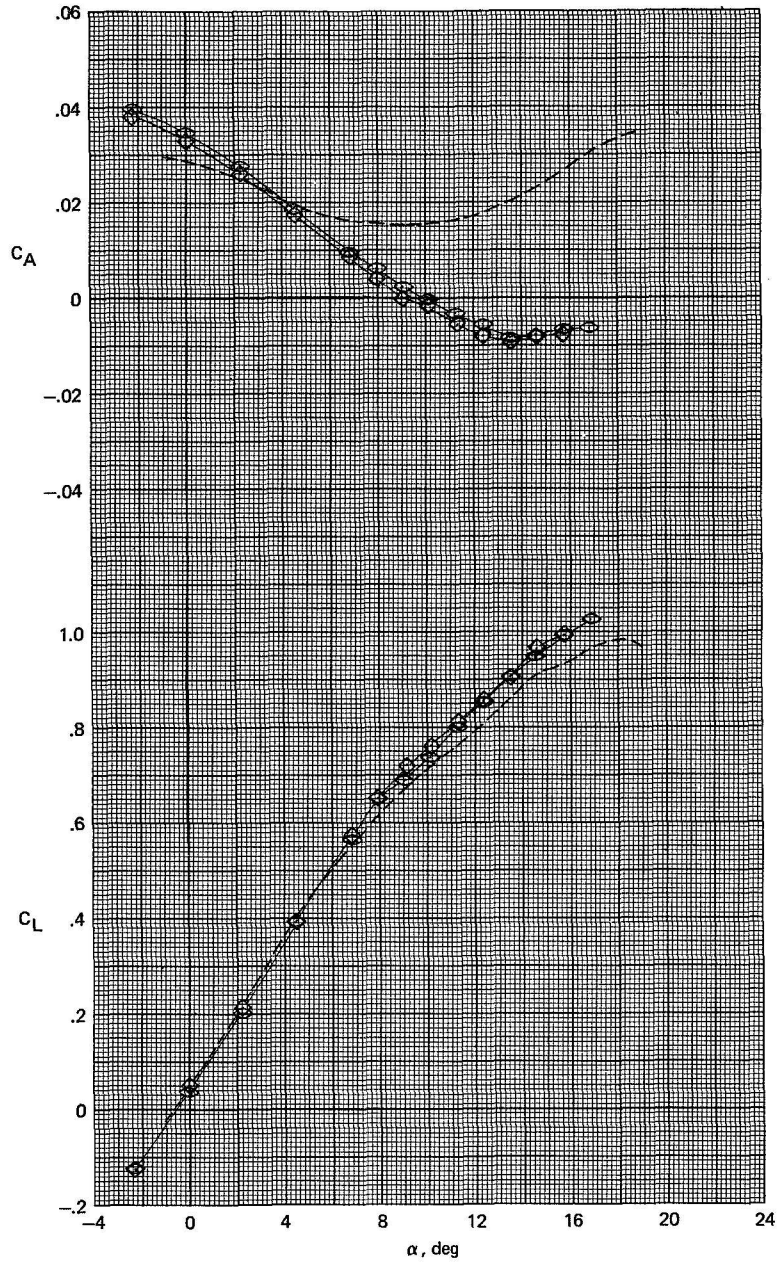
<u>SYMBOL</u>	<u>CONFIGURATION</u>	<u><math>\delta F_{K_3}</math></u>	<u><math>\delta F_N</math></u>
---	BASIC	-	-
◇	BASIC + $S_{17}F_{K_3}F_N$	20°	15°
◊	BASIC + $S_{17}F_{K_3}F_N$	30°	15°



(c)  $C_m$  plotted against  $C_L$  and  $\alpha$ .

Figure 14.- Concluded.

<u>SYMBOL</u>	<u>CONFIGURATION</u>	$\delta F_{K_3}$	$\delta F_N$
---	BASIC	—	—
◇	BASIC + S <sub>17</sub> F <sub>K<sub>3</sub></sub> F <sub>N</sub>	20°	15°
◊	BASIC + S <sub>17</sub> F <sub>K<sub>3</sub></sub> F <sub>N</sub>	30°	15°

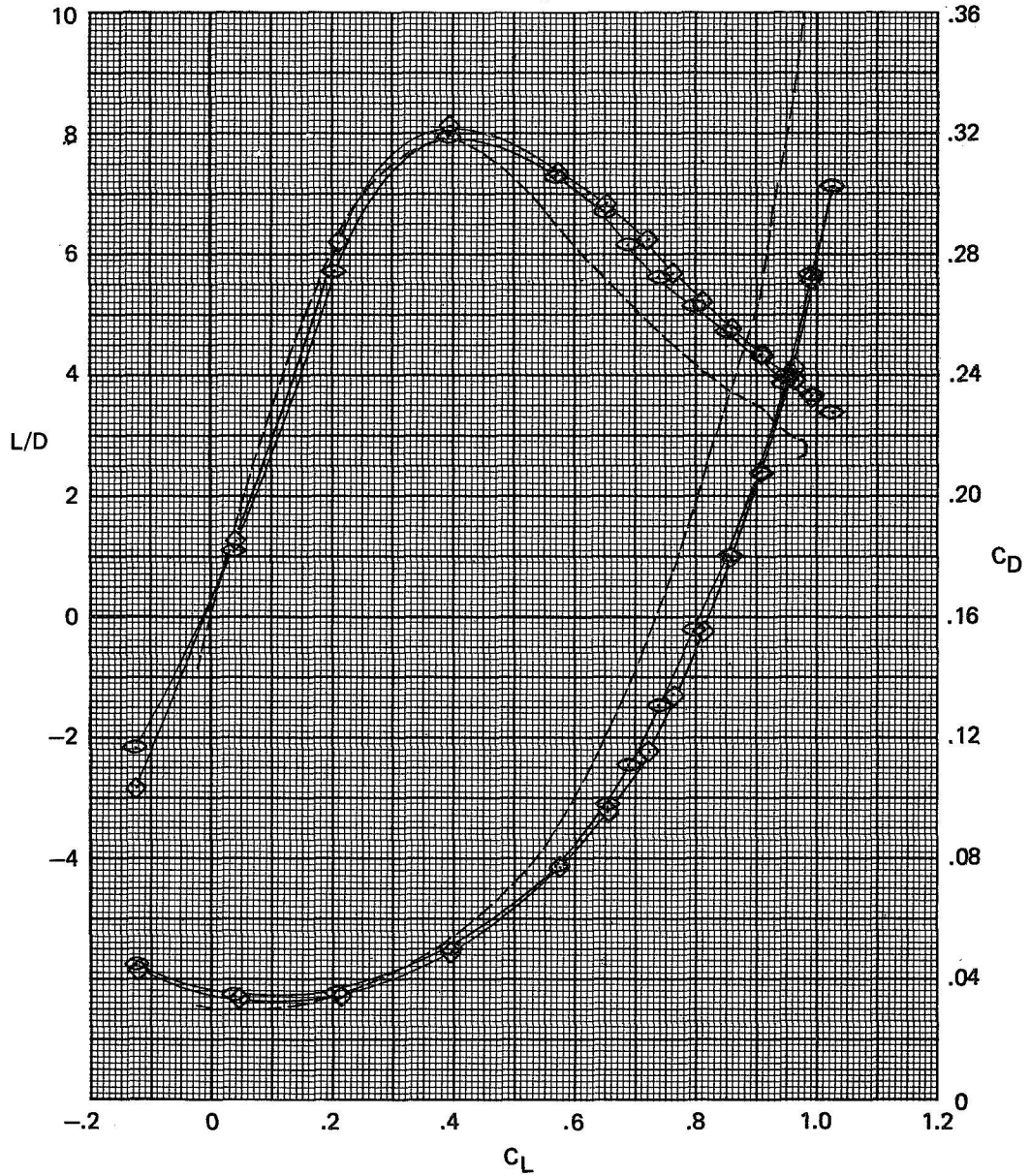


(a)  $C_A$  and  $C_L$  plotted against  $\alpha$ .

Figure 15.- Effect of deflecting the  $F_{K_3}$  Krueger flaps on the basic configuration incorporating the S<sub>17</sub>F<sub>K<sub>3</sub></sub>F<sub>N</sub> leading-edge devices.  $M = 0.90$ .



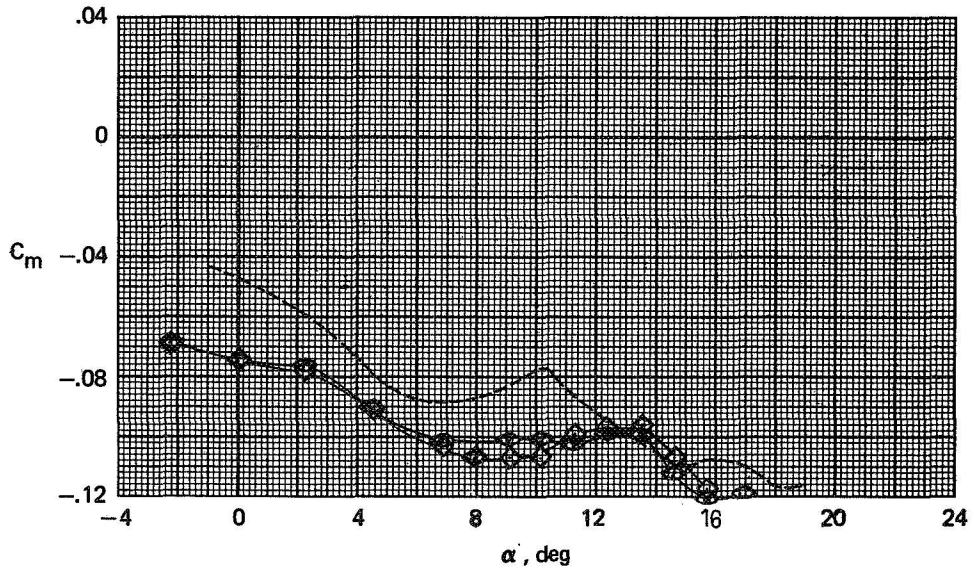
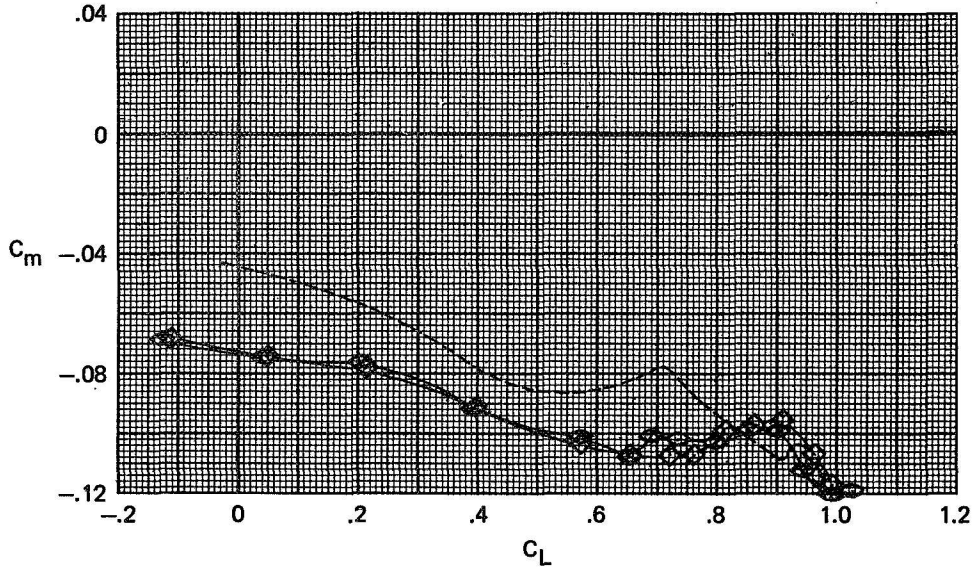
<u>SYMBOL</u>	<u>CONFIGURATION</u>	$\delta F_{K_3}$	$\delta F_N$
-----	BASIC	—	—
◇	BASIC + $S_{17}F_{K_3}F_N$	20°	15°
○	BASIC + $S_{17}F_{K_3}F_N$	30°	15°



(b) L/D and  $C_D$  plotted against  $C_L$ .

Figure 15.- Continued.

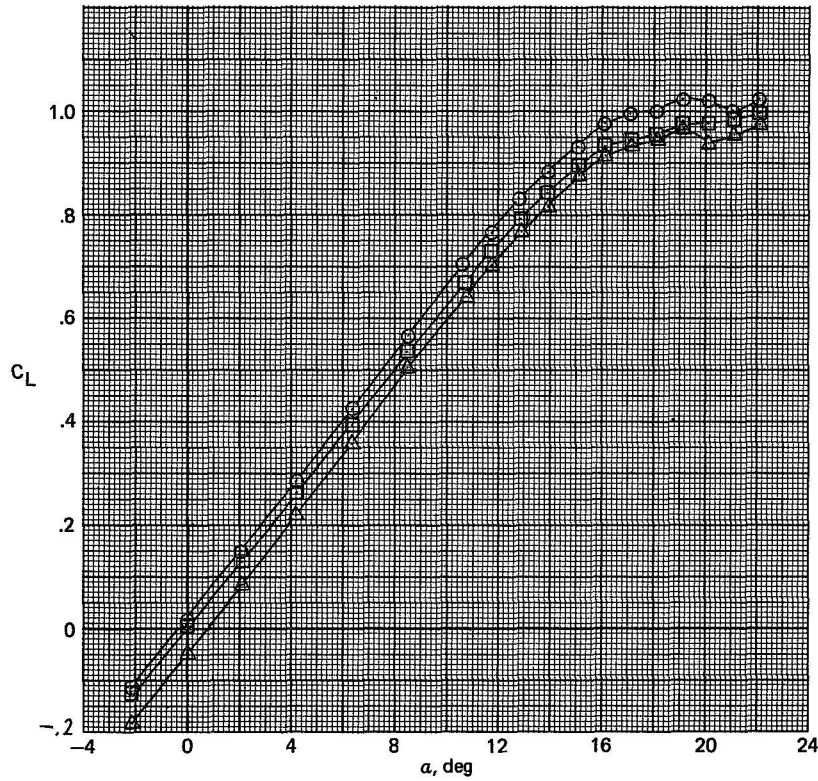
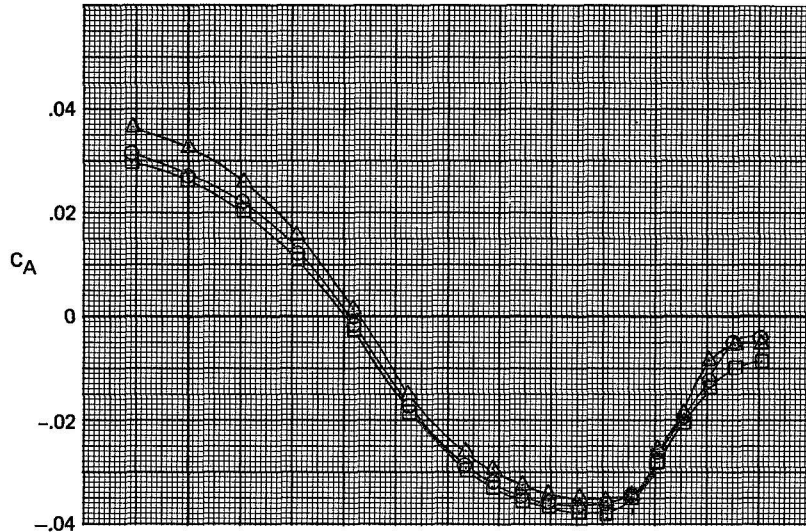
SYMBOL	CONFIGURATION	$\delta F_{K_3}$	$\delta F_N$
---	BASIC	—	—
◇	BASIC + S <sub>17</sub> F <sub>K<sub>3</sub></sub> F <sub>N</sub>	20°	15°
○	BASIC + S <sub>17</sub> F <sub>K<sub>3</sub></sub> F <sub>N</sub>	30°	15°



(c)  $C_m$  plotted against  $C_L$  and  $\alpha$ .

Figure 15.- Concluded.

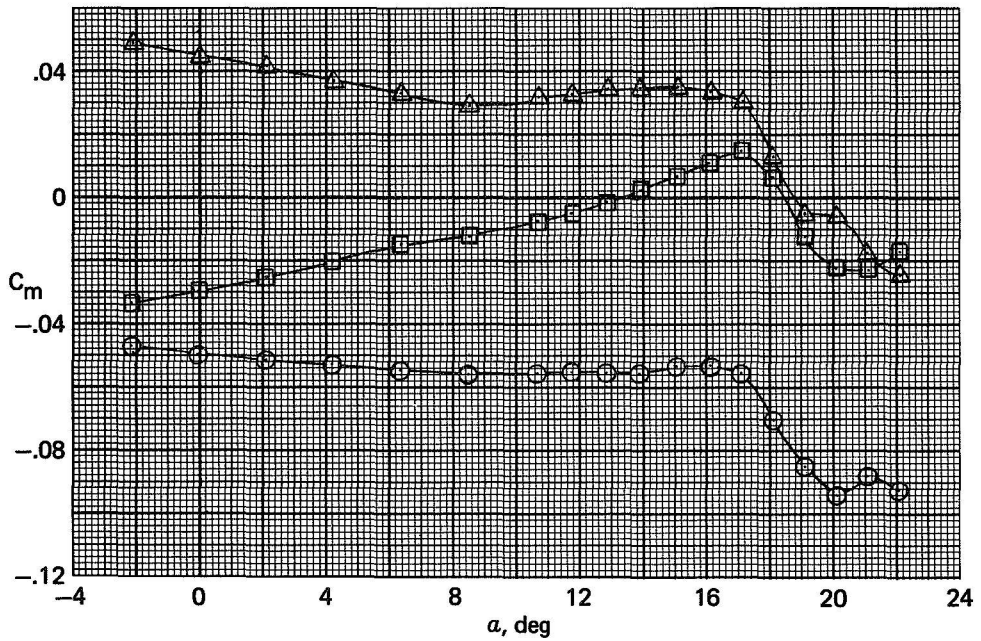
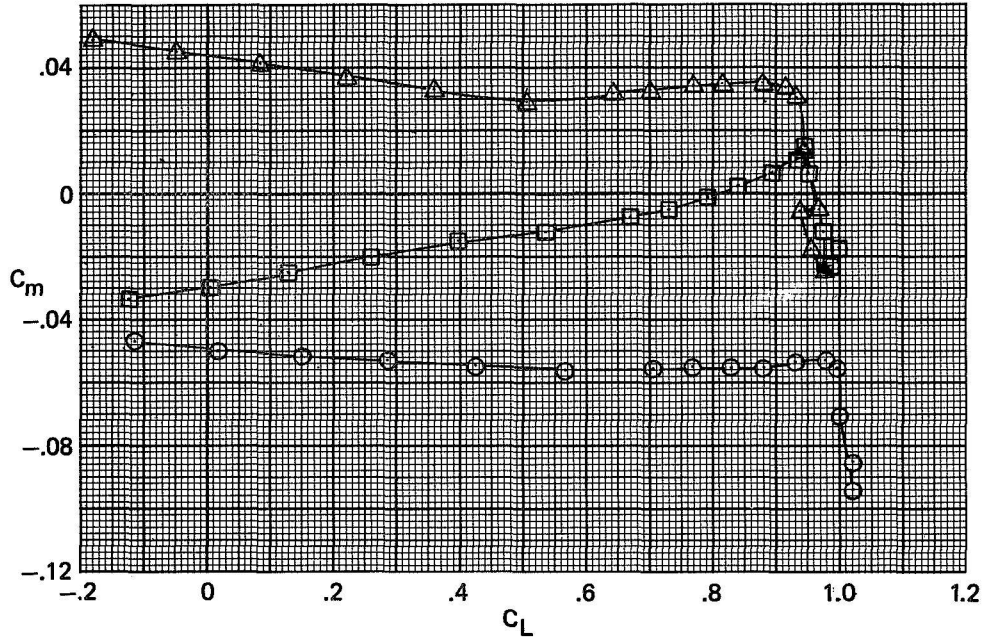
SYMBOL	CONFIGURATION	$i_t$	$\delta F_{K_3}$	$\delta F_{K_4}$
○	BASIC + $F_{K_3} F_{K_4}$	$0^\circ$	$20^\circ$	$20^\circ$
△	BASIC + $F_{K_3} F_{K_4}$	$-8^\circ$	$20^\circ$	$20^\circ$
□	BASIC + $F_{K_3} F_{K_4}$ TAIL OFF		$20^\circ$	$20^\circ$



(a)  $C_A$  and  $C_L$  plotted against  $\alpha$ .

Figure 16.- Effect of horizontal-tail incidence on the longitudinal characteristics of the basic configuration with the  $F_{K_3} F_{K_4}$  Krueger flaps ( $\delta F_{K_3}, \delta F_{K_4} = 20^\circ$ ).  $M = 0.60$ .

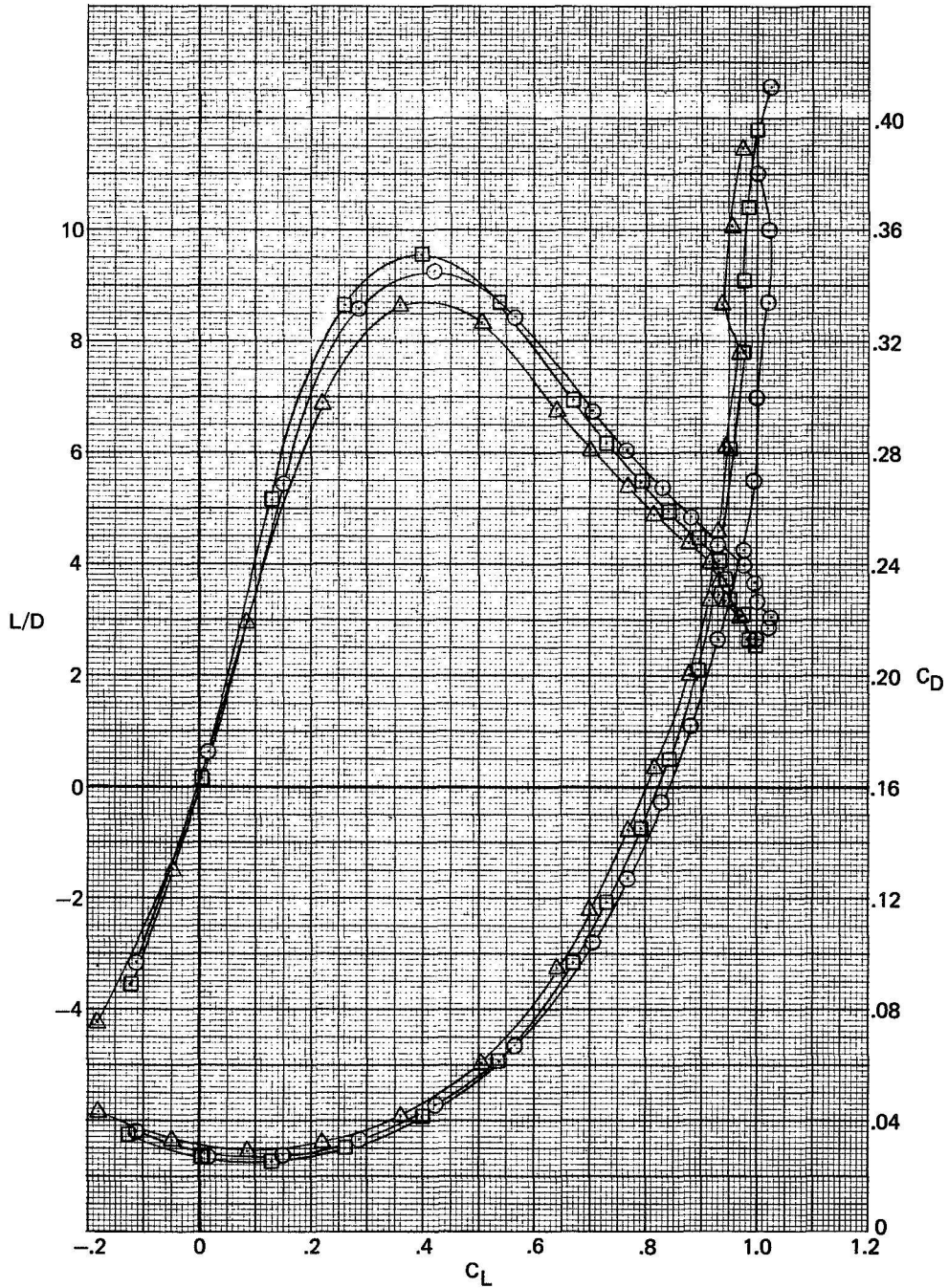
<u>SYMBOL</u>	<u>CONFIGURATION</u>	$i_t$	$\delta F_{K_3}$	$\delta F_{K_4}$
○	BASIC + $F_{K_3} F_{K_4}$	$0^\circ$	$20^\circ$	$20^\circ$
△	BASIC + $F_{K_3} F_{K_4}$	$-8^\circ$	$20^\circ$	$20^\circ$
□	BASIC + $F_{K_3} F_{K_4}$ TAIL OFF		$20^\circ$	$20^\circ$



(b)  $C_m$  plotted against  $C_L$  and  $\alpha$ .

Figure 16.- Continued.

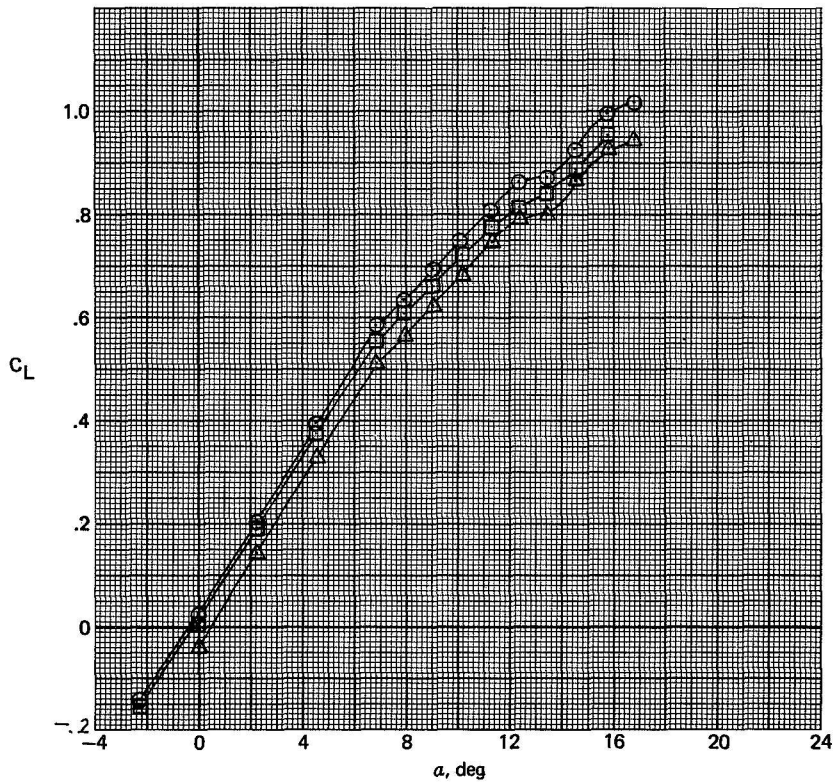
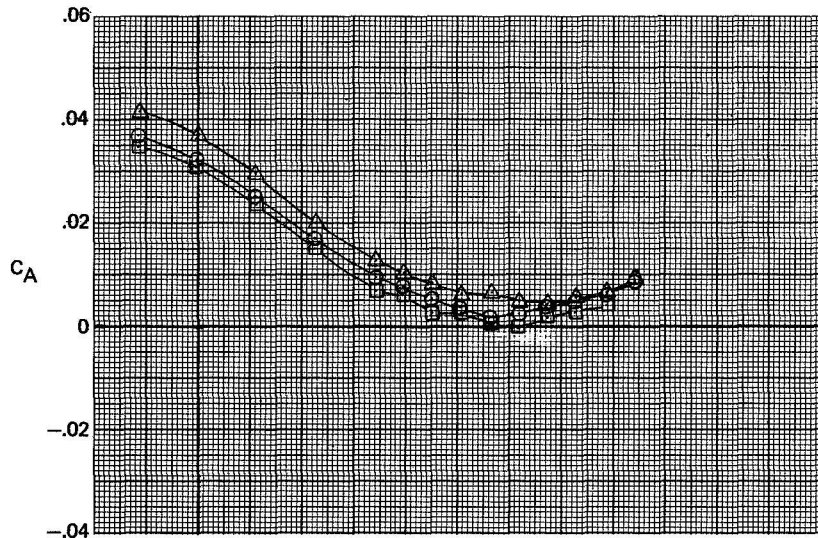
<u>SYMBOL</u>	<u>CONFIGURATION</u>	$i_t$	$\frac{\delta F_{K_3}}{20^\circ}$	$\frac{\delta F_{K_4}}{20^\circ}$
○	BASIC + F <sub>K<sub>3</sub></sub> F <sub>K<sub>4</sub></sub>	0°	20°	20°
△	BASIC + F <sub>K<sub>3</sub></sub> F <sub>K<sub>4</sub></sub>	-8°	20°	20°
□	BASIC + F <sub>K<sub>3</sub></sub> F <sub>K<sub>4</sub></sub> TAIL OFF	20°	20°	20°



(c) L/D and C<sub>D</sub> plotted against C<sub>L</sub>.

Figure 16.- Concluded.

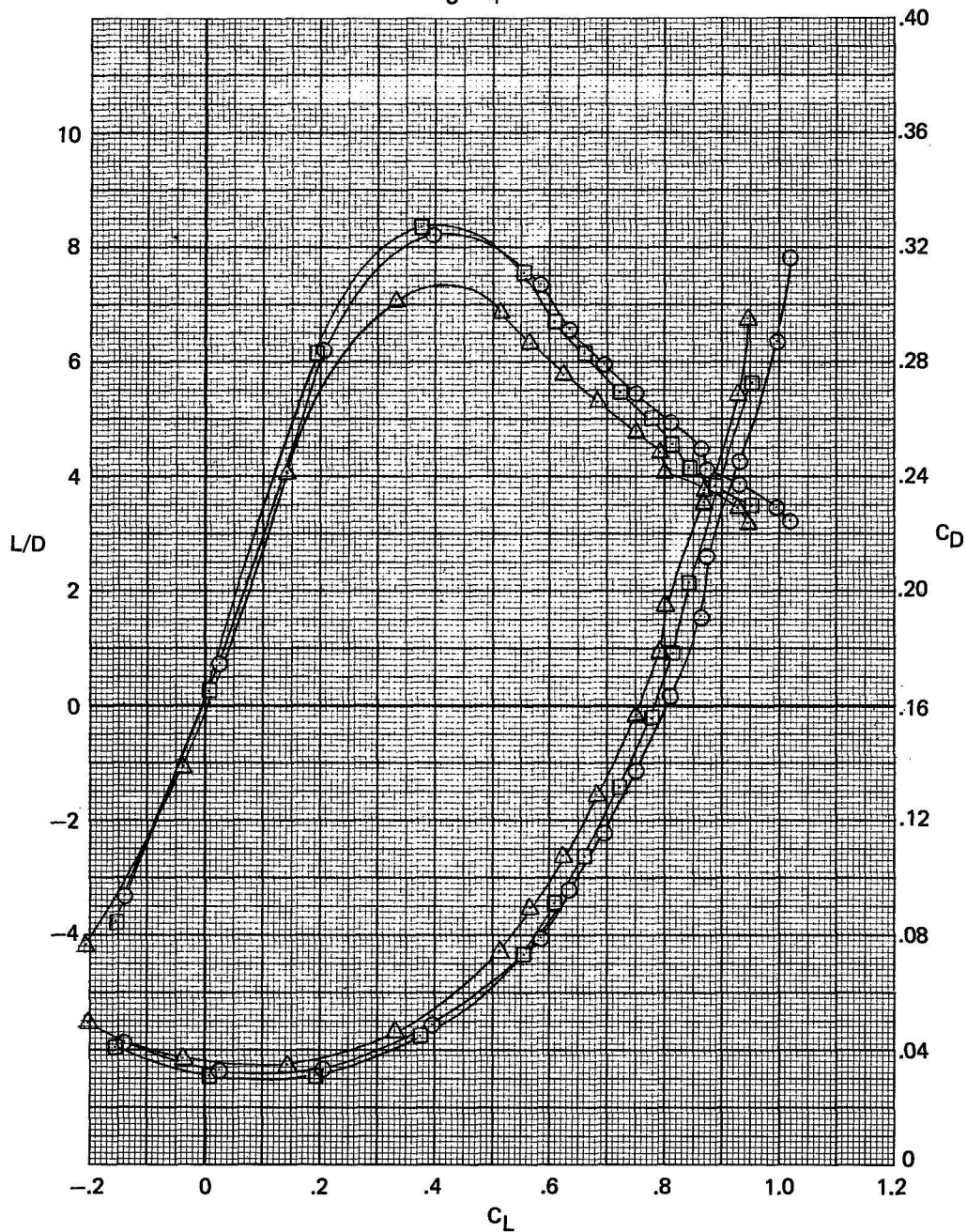
SYMBOL	CONFIGURATION	$i_t$	$\delta F_{K_3}$	$\delta F_{K_4}$
○	BASIC + $F_{K_3} F_{K_4}$	$0^\circ$	$20^\circ$	$20^\circ$
△	BASIC + $F_{K_3} F_{K_4}$	$-8^\circ$	$20^\circ$	$20^\circ$
□	BASIC + $F_{K_3} F_{K_4}$ TAIL OFF		$20^\circ$	$20^\circ$



(a)  $C_A$  and  $C_L$  plotted against  $\alpha$ .

Figure 17.- Effect of horizontal-tail incidence on the longitudinal characteristics of the basic configuration with the  $F_{K_3} F_{K_4}$  Krueger flaps ( $\delta F_{K_3}, \delta F_{K_4} = 20^\circ$ ).  $M = 0.90$ .

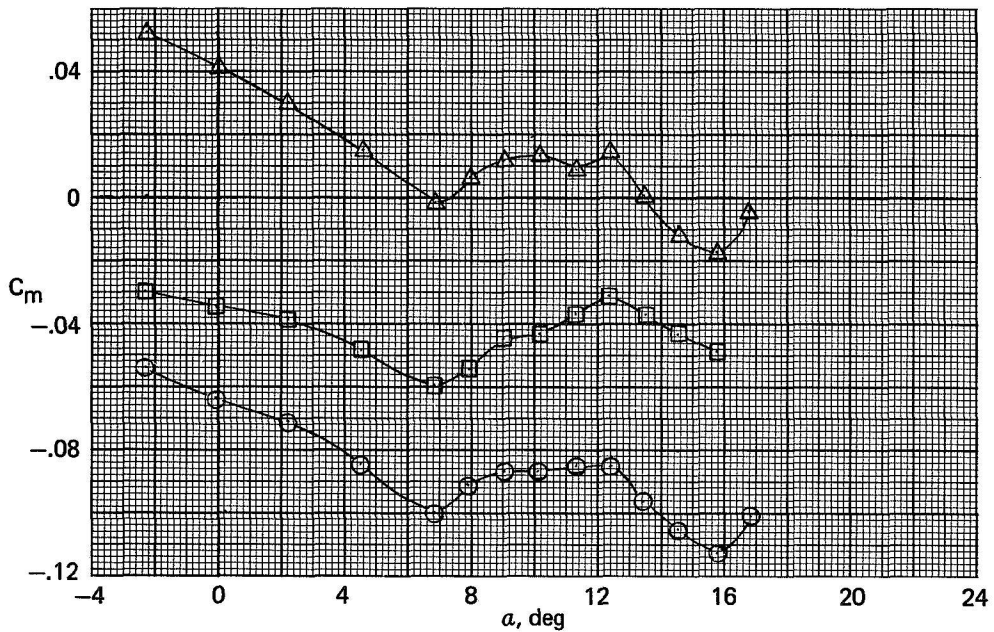
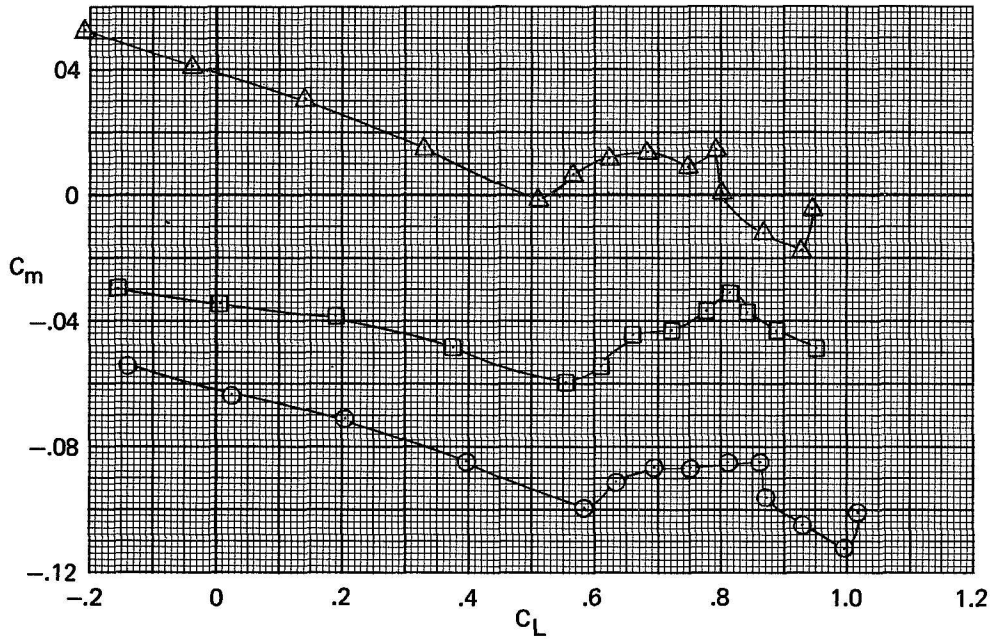
SYMBOL	CONFIGURATION	$i_t$	$\delta F_{K_3}$	$\delta F_{K_4}$
○	BASIC + $F_{K_3} F_{K_4}$	$0^\circ$	$20^\circ$	$20^\circ$
△	BASIC + $F_{K_3} F_{K_4}$	$-8^\circ$	$20^\circ$	$20^\circ$
□	BASIC + $F_{K_3} F_{K_4}$ TAIL OFF	$20^\circ$	$20^\circ$	$20^\circ$



(b)  $L/D$  and  $C_D$  plotted against  $C_L$ .

Figure 17.- Continued.

SYMBOL	CONFIGURATION	$i_t$	$\delta F_{K_3}$	$\delta F_{K_4}$
○	BASIC + $F_{K_3} F_{K_4}$	$0^\circ$	$20^\circ$	$20^\circ$
△	BASIC + $F_{K_3} F_{K_4}$	$-8^\circ$	$20^\circ$	$20^\circ$
□	BASIC + $F_{K_3} F_{K_4}$ TAIL OFF		$20^\circ$	$20^\circ$



(c)  $C_m$  plotted against  $C_L$  and  $\alpha$ .

Figure 17.- Concluded.



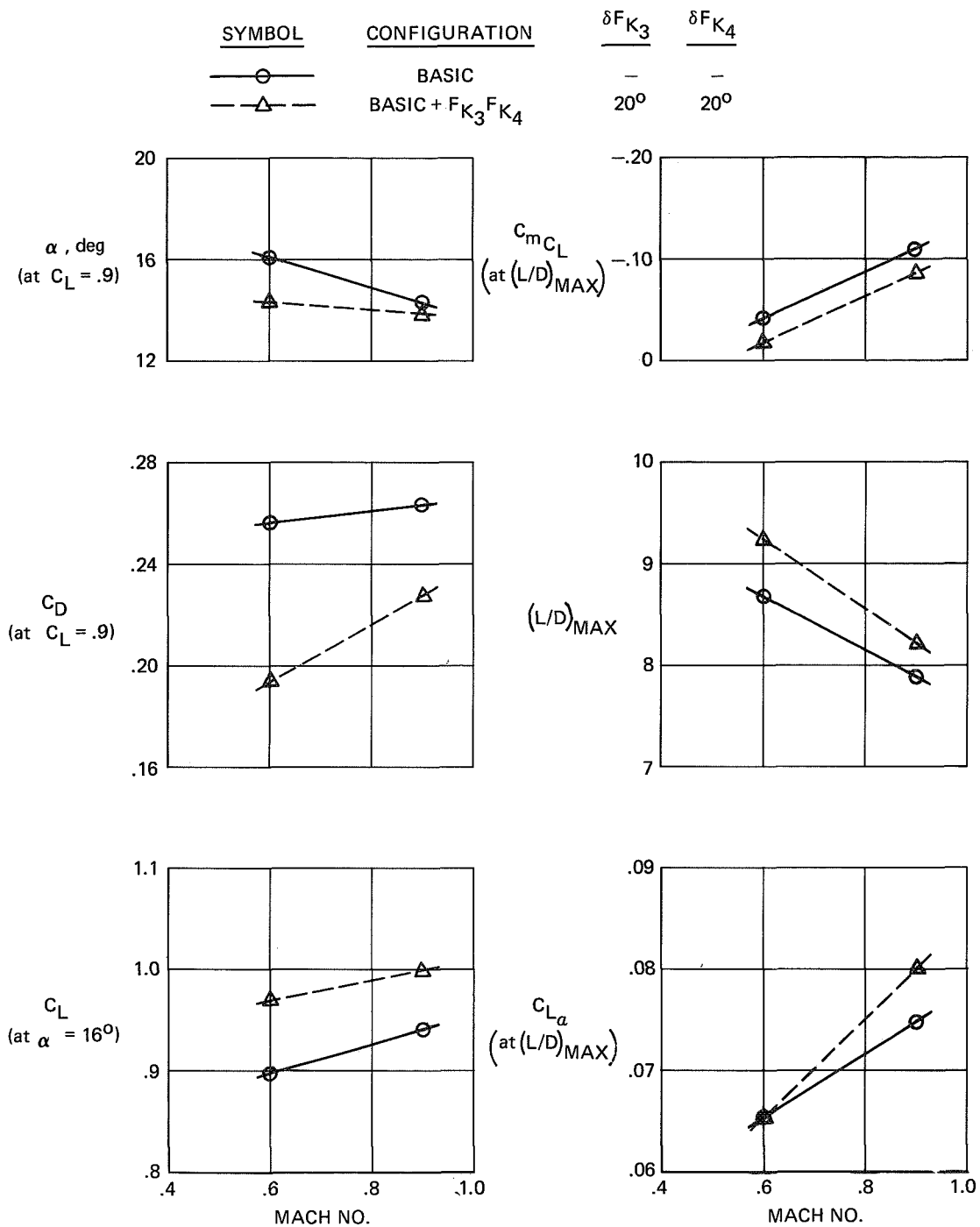
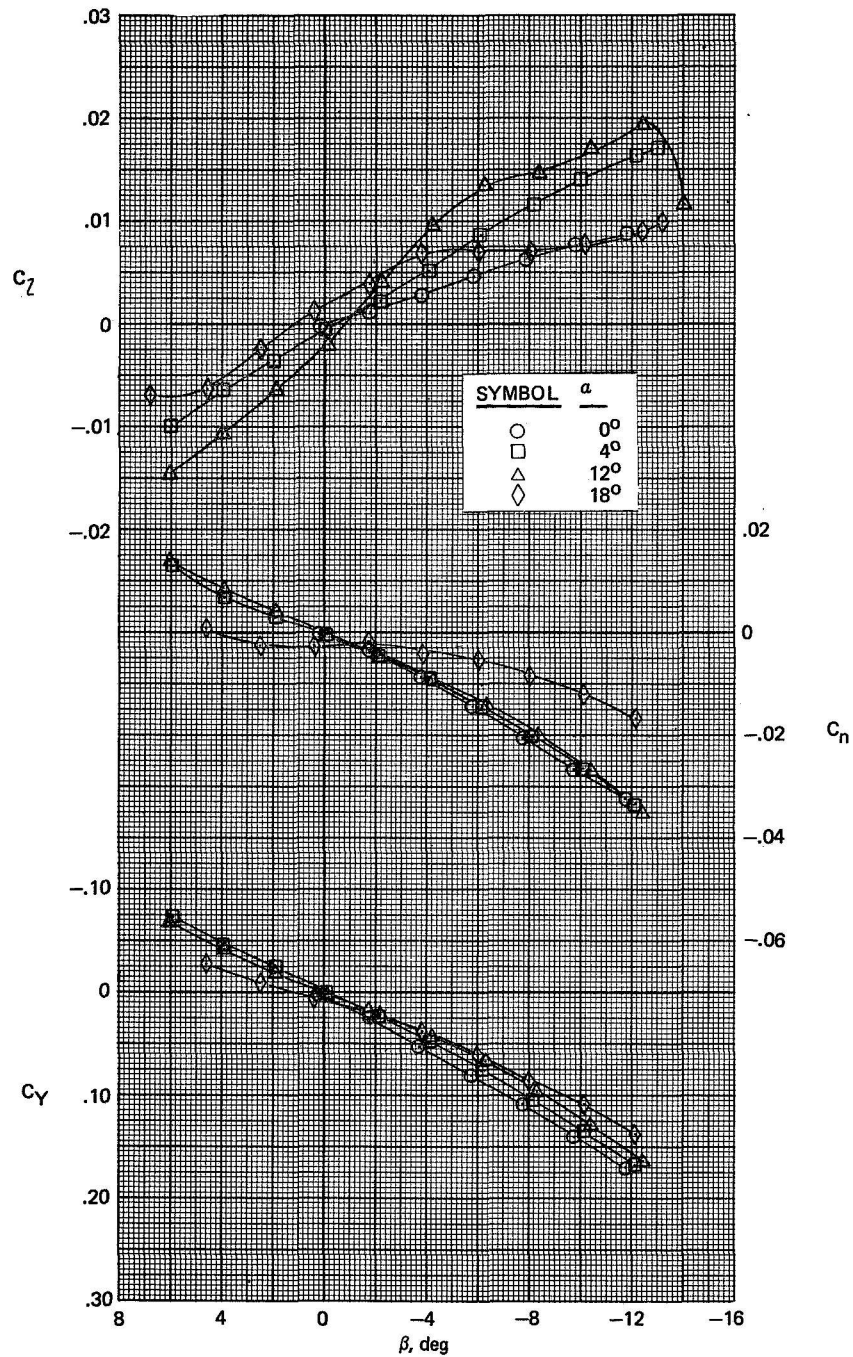
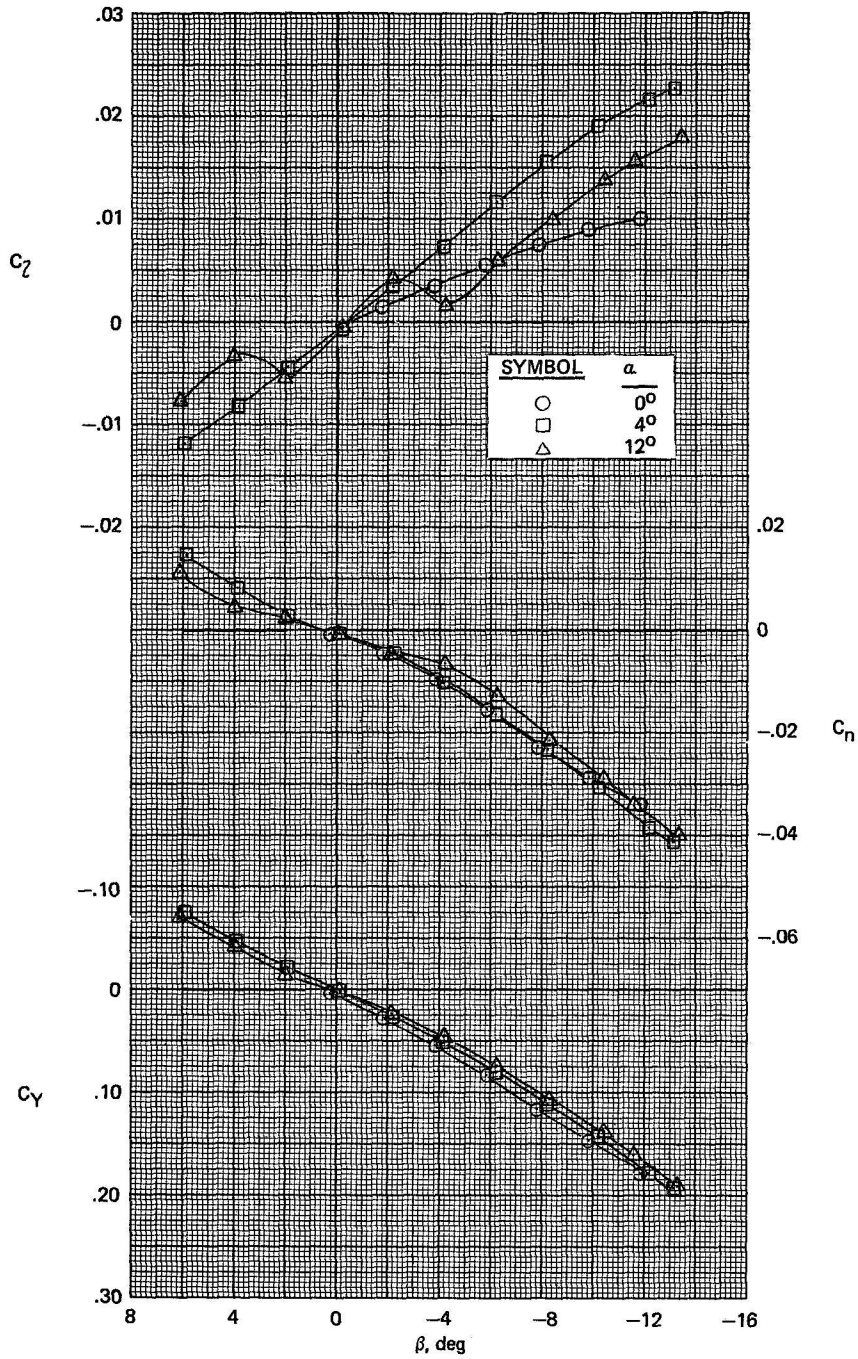


Figure 18.- Comparison of longitudinal characteristics of the basic configuration and the basic with  $F_{K3}$ - $F_{K4}$  Krueger flaps ( $\delta F_{K3}$ ,  $\delta F_{K4} = 20^\circ$ ).



(a)  $M = 0.60$ .

Figure 19.- Lateral-directional characteristics of the basic configuration.



(b)  $M = 0.90$ .

Figure 19.- Concluded.

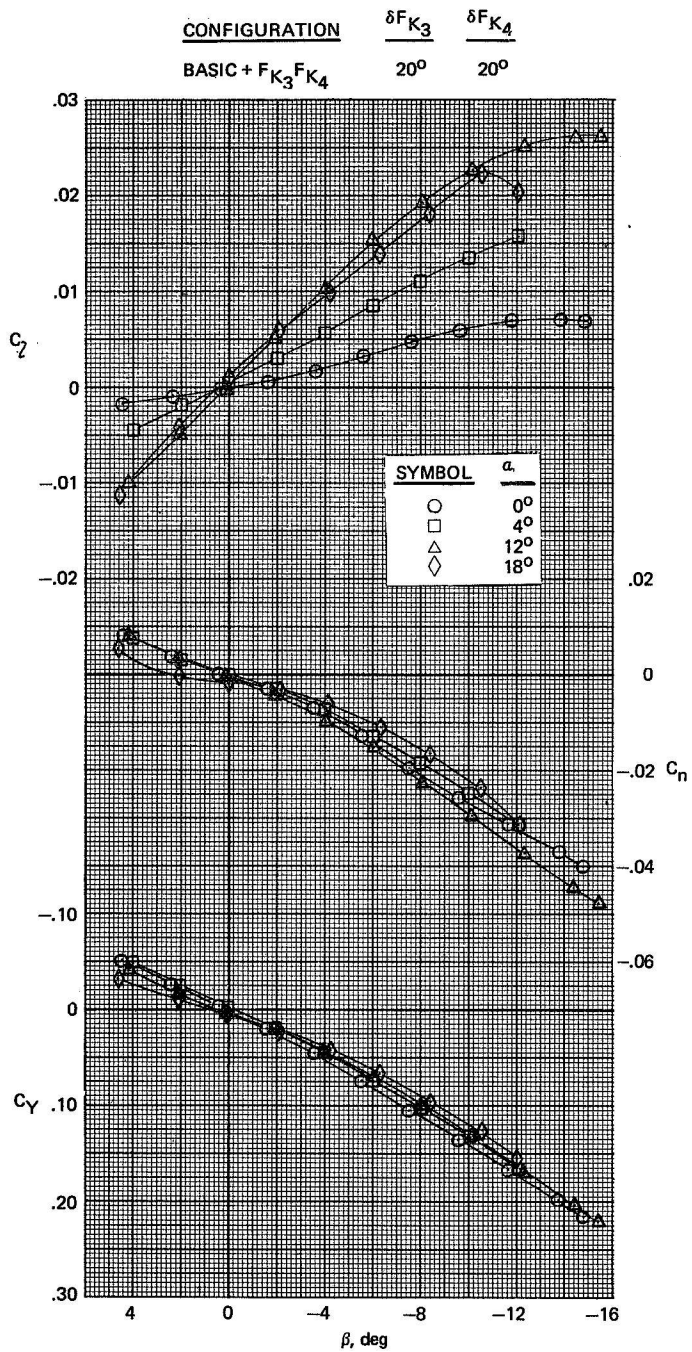
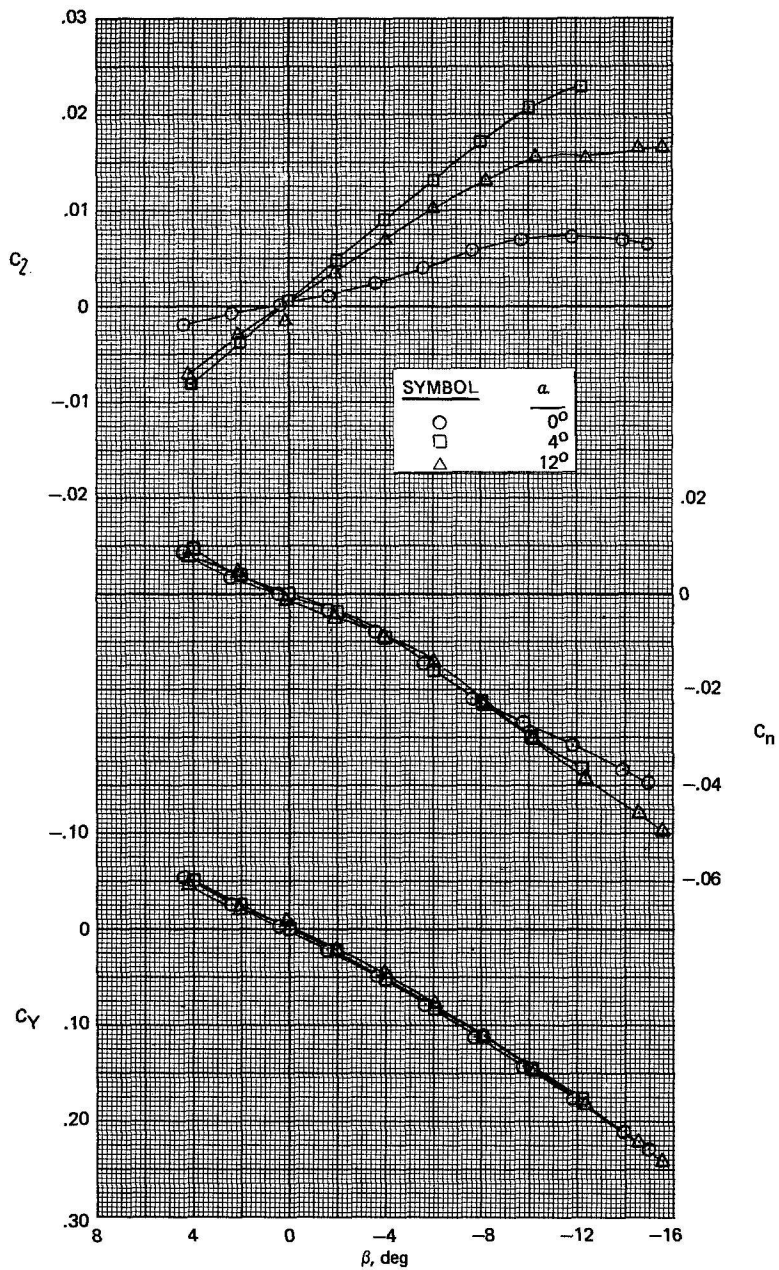


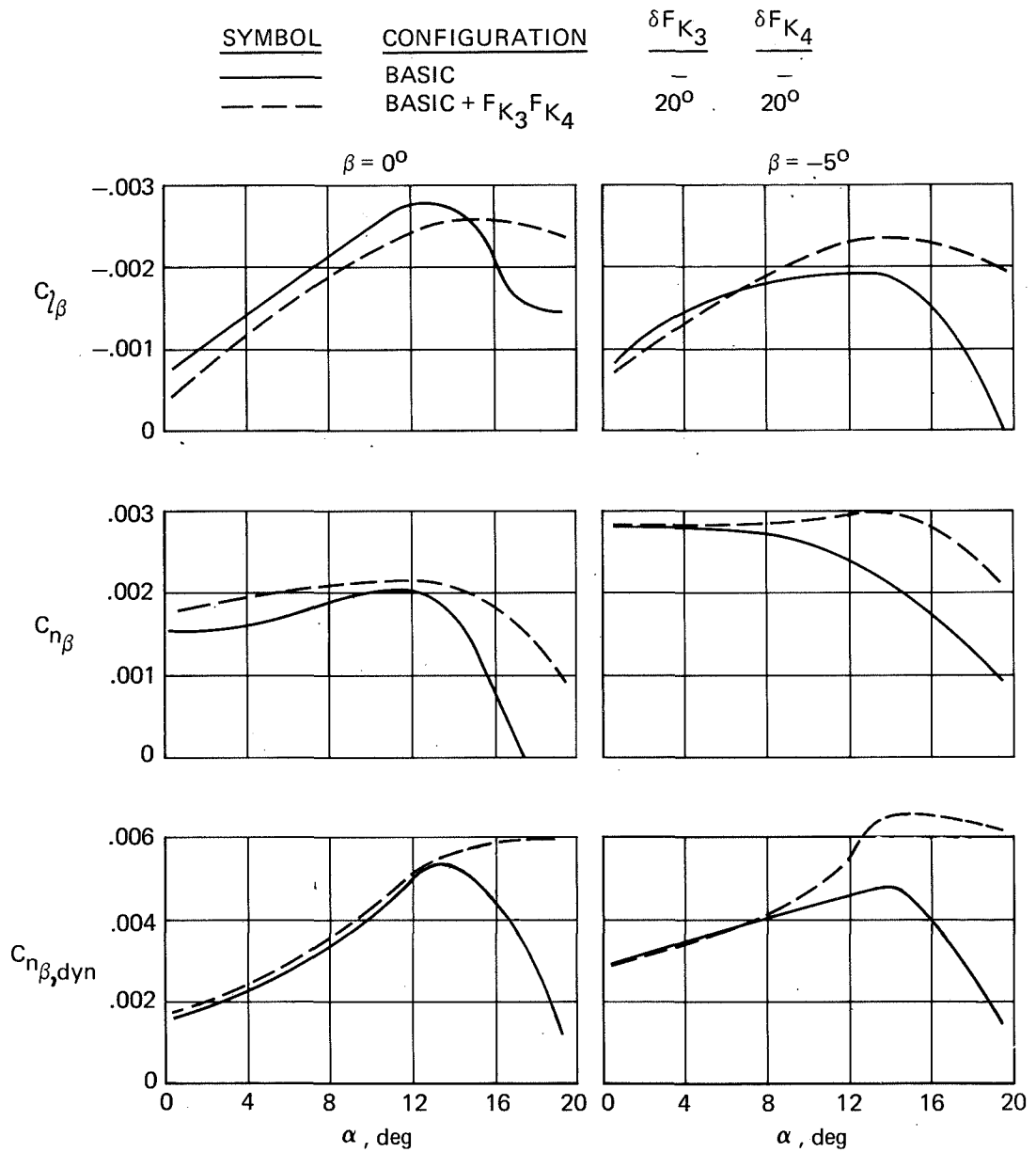
Figure 20.- Lateral-directional characteristics of the basic configuration with  $F_{K3}F_{K4}$  Krueger flaps ( $\delta F_{K3}, \delta F_{K4} = 20^\circ$ ).

<u>CONFIGURATION</u>	$\frac{\delta F_{K_3}}{\delta F_{K_4}}$	$\frac{\delta F_{K_4}}{\delta F_{K_3}}$
BASIC + F <sub>K<sub>3</sub></sub> F <sub>K<sub>4</sub></sub>	20°	20°



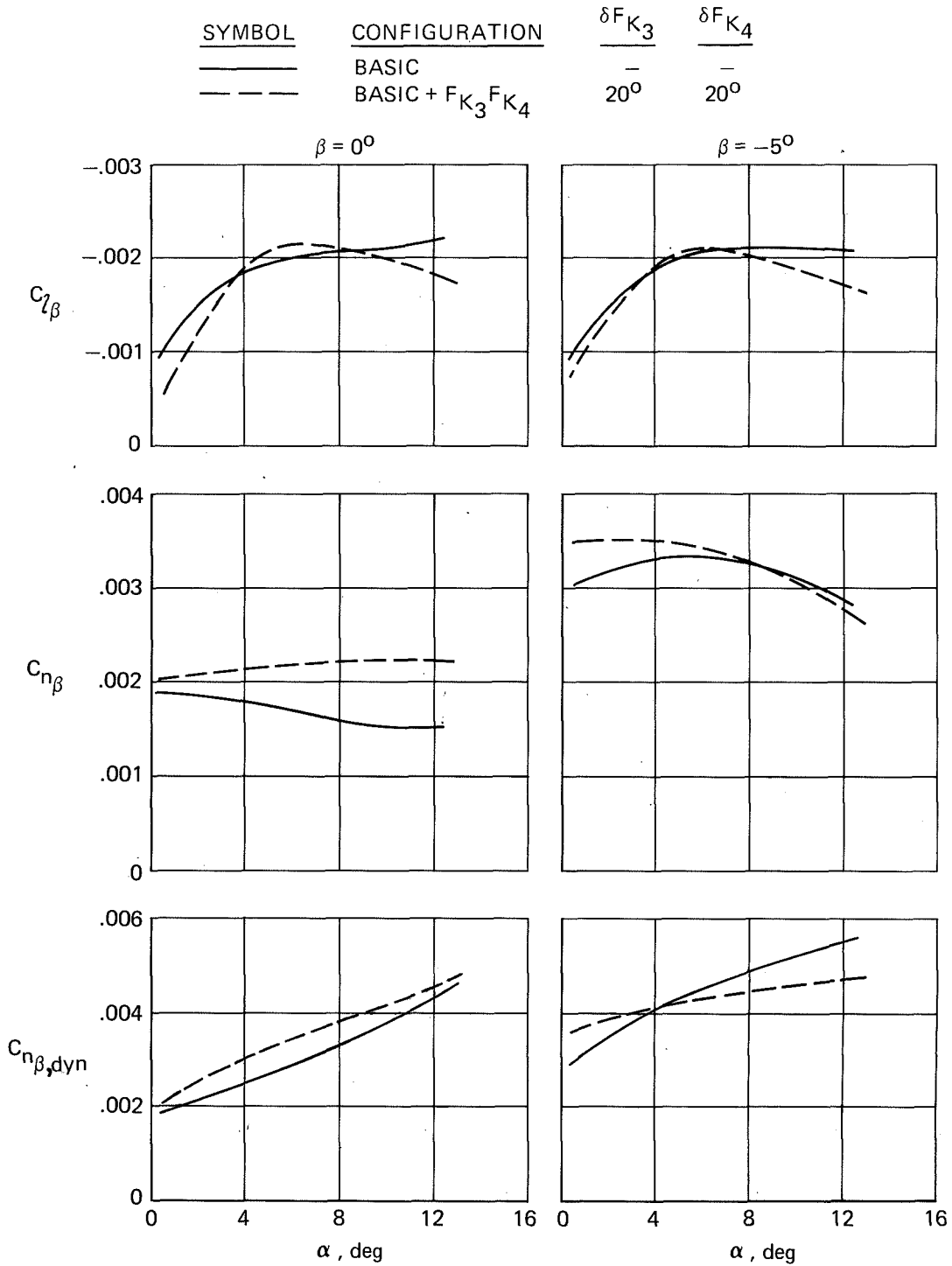
(b)  $M = 0.90$ .

Figure 20.- Concluded.



(a)  $M = 0.60$ .

Figure 21.- Comparison of lateral-directional characteristics of the basic configuration and the basic with  $F_{K3}$   $F_{K4}$  Krueger flaps ( $\delta F_{K3}, \delta F_{K4} = 20^\circ$ ).



(b)  $M = 0.90$ .

Figure 21.- Concluded.

NATIONAL AERONAUTICS AND SPACE ADMINISTRATION  
WASHINGTON, D.C. 20546

OFFICIAL BUSINESS  
PENALTY FOR PRIVATE USE \$300

FIRST CLASS MAIL

POSTAGE AND FEES PAID  
NATIONAL AERONAUTICS AND  
SPACE ADMINISTRATION



POSTMASTER: If Undeliverable (Section 158  
Postal Manual) Do Not Return

*"The aeronautical and space activities of the United States shall be conducted so as to contribute . . . to the expansion of human knowledge of phenomena in the atmosphere and space. The Administration shall provide for the widest practicable and appropriate dissemination of information concerning its activities and the results thereof."*

— NATIONAL AERONAUTICS AND SPACE ACT OF 1958

## NASA SCIENTIFIC AND TECHNICAL PUBLICATIONS

**TECHNICAL REPORTS:** Scientific and technical information considered important, complete, and a lasting contribution to existing knowledge.

**TECHNICAL NOTES:** Information less broad in scope but nevertheless of importance as a contribution to existing knowledge.

**TECHNICAL MEMORANDUMS:** Information receiving limited distribution because of preliminary data, security classification, or other reasons.

**CONTRACTOR REPORTS:** Scientific and technical information generated under a NASA contract or grant and considered an important contribution to existing knowledge.

**TECHNICAL TRANSLATIONS:** Information published in a foreign language considered to merit NASA distribution in English.

**SPECIAL PUBLICATIONS:** Information derived from or of value to NASA activities. Publications include conference proceedings, monographs, data compilations, handbooks, sourcebooks, and special bibliographies.

**TECHNOLOGY UTILIZATION PUBLICATIONS:** Information on technology used by NASA that may be of particular interest in commercial and other non-aerospace applications. Publications include Tech Briefs, Technology Utilization Reports and Technology Surveys.

*Details on the availability of these publications may be obtained from:*

**SCIENTIFIC AND TECHNICAL INFORMATION OFFICE**

**NATIONAL AERONAUTICS AND SPACE ADMINISTRATION**

Washington, D.C. 20546